UNIVERSITÀ DEGLI STUDI DI PADOVA

DIPARTIMENTO DI INGEGNERIA INDUSTRIALE

CORSO DI LAUREA MAGISTRALE IN INGEGNERIA CHIMICA E DEI PROCESSI INDUSTRIALI

Tesi di Laurea Magistrale in
Ingegneria Chimica e dei Processi Industriali

COKING IN A TWO-STAGES CATALYTIC UPGRADING OF BIOGAS

Relatore: Prof. Paolo Canu

Correlatore: Ing. Mattia Pagin

Laureando: ANDREA PIZZATO

Matricola: 2018751

ANNO ACCADEMICO 2022-2023

Abstract

Biogas, essentially a mixture of CH_4 and CO_2, obtained from the fermentation of organic waste and a subsequent cleaning, is currently exploited selectively separating the methane from the carbon dioxide, through different technologies. In this thesis, the technique proposed for biogas upgrading is the application of the Sabatier reaction, where CO_2 is also converted to CH_4, without any preventive separation. The reaction consists in the catalytic heterogeneous hydrogenation of CO_2, a highly exothermic reaction limited by thermodynamic equilibrium that requires high pressure and low temperature. A Ni/Al_2O_3 industrial has been evaluated, from 1 to 6 bar to characterize the catalyst activity under long duration tests and the relevance of carbon formation. We focused on the second of a two-stage adiabatic biogas methanation process, after the excess steam has been removed to force the CO_2 conversion; here the high inlet partial pressure of methane and the lack of steam are likely to support carbon formation, via methane cracking.

The experimental campaign was divided into two main sections. First, the investigation of the aging of the catalysts and the carbon deposition rate, at different pressure conditions, by coke formation stress-tests (tests running continuously for several days). Then, we investigate the role of addition of water vapor in the feed mixture to a second stage reactor, thus simulating a partial interstage condensation, as an approach to limit carbon formation. Particularly, the capability of the catalysts of operating for 5 days without any activity loss has been proved, both at atmospheric pressure and at 6 bar, also with addition of water in the reactant mixture. Then, the effect of steam addition to the reactant mixture has been proved to limit the Sabatier reaction, reducing the CH_4 enrichment and CO_2 conversion. However, steam has a positive effect on the coking rate, reducing it by 80% with a 20% addition. The maximum production of methane is obtained during the stress test without water addition, and it is equal to 96.4%. The CO_2 and CO molar percentages obtained in all the stress-test fulfil the Italian grid injection requirements, being $y_{CO2} < 2.5\%$ and CO never detected within the product mixture. However, H_2 volumetric fraction always exceeds the limit of 1%, even though it is always in line with the experimentations performed by Snam (Società Nazionale Metanodotti) in April and December 2019, to allow respectively 5% and 10% of H_2 (on volume basis) in the biomethane.

Riassunto

Il biogas, essenzialmente una miscela di CH_4 e CO_2, ottenuto dalla fermentazione dei rifiuti organici e successivamente depurata, viene attualmente sfruttato mediante la separazione selettiva del metano dalla anidride carbonica, mediante diverse tecnologie. In questa tesi, la tecnica proposta per l'upgrading del biogas è l'utilizzo della reazione di Sabatier, in cui anche la CO_2 viene convertita in CH_4, senza alcuna separazione preventiva. La reazione consiste nell'idrogenazione eterogenea catalitica della CO_2, una reazione altamente esotermica limitata dall'equilibrio termodinamico che richiede alta pressione e bassa temperatura. Un catalizzatore industriale a base di Ni/Al_2O_3 è stato testato, da 1 a 6 bar, per verificare l'attività del catalizzatore durante test a lunga durata e l'importanza della deposizione di coke. Ci siamo concentrati sul secondo stadio di un processo di metanazione del biogas adiabatico a due stadi, dopo che il vapore in eccesso è stato rimosso per forzare la conversione della CO_2; qui l'alta pressione parziale in ingresso di metano e la mancanza di vapore sono favorevoli alla formazione di coke, tramite cracking del metano. La campagna sperimentale è stata suddivisa in due parti principali. Inizialmente, l'indagine dell'invecchiamento dei catalizzatori e la velocità di deposizione del carbonio, a diverse condizioni di pressione, mediante test di stress per la formazione di coke (test eseguiti in modo continuativo per diversi giorni). Successivamente, abbiamo indagato il ruolo dell'aggiunta di vapore acqueo nella miscela di alimentazione a un secondo reattore a stadi, simulando così una condensazione parziale interstadio, come approccio per limitare la formazione di carbonio. In particolare, è stata dimostrata la capacità dei catalizzatori di operare per 5 giorni senza alcuna perdita di attività, sia a 1 che a 6 bar, anche con l'aggiunta di acqua nella miscela reattiva. Successivamente, è stato dimostrato che l'aggiunta di vapore in alimetazione limita la reazione di Sabatier, riducendo l'arricchimento di CH_4 e la conversione di CO_2. Tuttavia ha un effetto positivo sulla velocità di formazione di coke, riducendola dell'80% con un'aggiunta del 20%. La produzione massima di metano si ottiene durante il test di stress senza aggiunta di acqua ed è pari al 96,4%. Le frazioni di CO2 e CO ottenute in tutti i test di stress soddisfano i requisiti di iniezione nella rete italiana. Tuttavia, la frazione volumetrica di H_2 supera sempre il limite dell'1%, anche se è sempre in linea con le sperimentazioni effettuate da Snam (Società Nazionale Metanodotti) nel 2019, per consentire rispettivamente il 5% e il 10% di H2 (in base al volume) nel biometano.

Index

Introduction

Biogas is a combustible mixture of gas mainly composed of CH_4 and CO_2 and is produced from the anaerobic bacterial decomposition of organic compounds. In addition to these main components other undesirable compounds are presents such as NH_3, H_2S, H_2O and silicon organic compounds which are removed before any applications. The purified biogas can be upgraded to biomethane, a high purity methane which can be used directly as fuel or can be injected into the natural gas grid, selectively separating the CO_2 from the CH_4. The CO_2 separated can be then reused in the food industry, chemical industry, and water treatment, but the market request could not be so high, and a greater part of this CO_2 is vent to the atmosphere, causing global warming due to the greenhouse effect. A technique to avoid CO_2 venting is biogas upgrading via methanation, based on the Sabatier reaction to directly convert CO_2 to CH_4. Lot of studies have been done on this technique, that is proved to be capable of producing biomethane satisfying the Italian natural gas grid injection requirements by means of a two-stage process with adiabatic reactors and intermediate water sequestration.

The main purposes of this work are:

- Understanding the capability of the catalysts to operate continuously for long times (in the order of days) without significant activity loss and to understand the role of solid carbon formation on the catalyst deactivation. This is done though equilibrium calculations and experimental campaigns.
- Understanding the effect of water vapor on the solid carbon formation rate and catalyst performance.

The thesis is based on 4 Chapters:

- Chapter 1: during the first period of the thesis, a literature study focused on the biogas and the biogas upgrading through the methanation reaction has been performed. This Chapter contains a description of the current technologies employed for the biogas purification and for the classical biogas upgrading, a study of the Sabatier reaction, with the possible side reactions (dry reforming, reverse water gas shift, methane cracking), economical and chemical considerations about the active metal particles and the supports which favor the

Sabatier reaction. The activation of the metal particles and the possible causes which could lead to the catalyst deactivation are then reported, with a particular focus on the mechanisms of different morphologies of solid carbon, their mechanism and rate of production and the removal techniques. Finally, a review regarding the different types of methanation reactors, also considering already existing two-staged biogas/CO_2 methanation plants (at different scales) and the current state of biomethane in Italy, including the standards for the grid injection, has been done.

- Chapter 2: in this chapter, the thermodynamics equilibrium of the methanation reaction has been analyzed at atmospheric pressure and up to 6bar (absolute pressure of the experimental tests). The possibility of solid carbon formation has also been included in the calculation, and the effect on chemical equilibrium of the water addition to the reference mixture has been considered. The equilibrium has been calculated through Cantera on Matlab® using a reference inlet composition.
- Chapter 3: a complete description of the experimental plant used to carry out the tests, the analytical instruments and the methods and protocols used are reported in this chapter.
- Chapter 4: all the results obtained from the validation of the procedures used for catalysts activation and coke removal, the preliminary atmospheric pressure tests, the test at high pressure are reported and deeply analyzed in this chapter. The results are presented and described as molar fractions, CO_2 conversions trend, and with industrial parameter as coking rate to evaluate the relevance of carbon deposition.

Chapter 1

Biogas and biogas methanation

Nowadays about 79% of the total energy used is produced through combustion of fossil fuels [33] leading to a continuous increase of CO_2 concentration in atmosphere [34] therefore to global warming due to greenhouse effect. To limit CO_2 emissions (thus large waste of carbon) due to the consumption of fossil fuels, relevant efforts are being made to replace them with renewable energy sources. Other techniques to decrease the greenhouse effect related to CO_2 are Carbon Capture and Sequestration (CCS) and Carbon Capture and Utilization (CCU) [3].

Considering the former, the captured carbon dioxide is transported and then stored in underground deposits whereas in CCU the captured carbon dioxide is used to produce syngas (CO and H_2 mixture) but also to produce methane (via methanation) or other compounds such as methanol and higher alcohols. Particularly, the methanation reaction (also named Sabatier reaction) has recently gained renewed interest because of its application in biomass upgrading and power-to-gas technologies [1].

Biogas, essentially a mixture of CO_2, CH_4, is a renewable secondary energy carrier [2]. Biogas upgrading is commonly achieved by selective separation of CO_2 and CH_4 and by the following reutilization of the former according to CCU techniques. In this thesis the methanation of biogas will be studied.

The process is developed following the Block Flow Diagram shown in Figure 1.1.

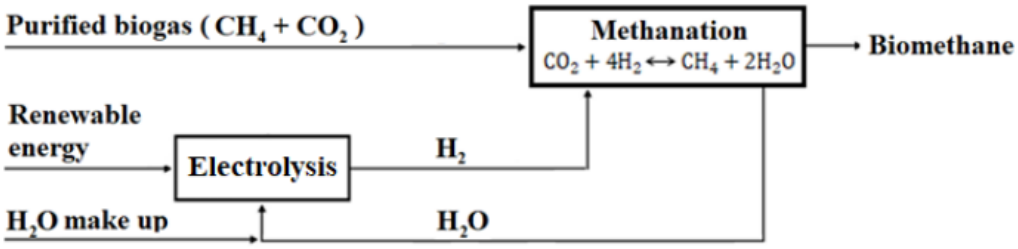

***Figure 1.1**: Block Flow Diagram of the biogas upgrading through Sabatier reaction.*

Through this technique the carbon dioxide of biogas is directly converted to methane by Sabatier reaction without any previous separation of the two. The hydrogen required as a reactant of methanation should be obtained through H_2O electrolysis using renewable electrical energy. A relevant quantity of H_2O is produced and should be recirculated from the reactor to the electrolyzer.

This process aims at the production of high purity methane to use as fuel or to introduce directly in the natural gas line, according to the Power-to-Gas (PtG) technology [3].

1.1 Biogas purification and upgrading

Biogas is a gaseous mixture of mainly CH_4 and CO_2 produced from organic compounds through anaerobic bacterial decomposition. Its composition varies depending on the feedstock, particularly [3]:

- CH_4 varies from 55% to 70% and CO_2 varies from 30% to 45%bfor biogas from anaerobic digestion of agro-industrial biowaste, livestock manure and sewage sludge;
- CH_4 can vary between 35% and 65% and CO_2 between 15 and 45% for biogas from landfill.

Other compounds exist in the biogas mixture, such as H_2S, NH_3, silicon organic compounds (for instance siloxanes) but also CO, H_2O, O_2, H_2 [2,9], whose quantities depend on the feedstock. Table 1.1 reports an example of composition of biogas obtained from different feedstocks.

Table 1.1: *Biogas composition for two different feedstocks. [2,9]*

Component	Unit of measure	Biogas from anaerobic digestion	Biogas from landfill
CH_4	vol%	55-70	35-65
CO_2	vol%	30-45	15-40
H_2O	vol%	1-5	1-5
N_2	vol%	0-0.5	15
H_2	vol%	0	0
O_2	vol%	0	1
H_2S	ppm	0-4000	0-100
NH_3	ppm	0-100	0-5
Siloxanes	mg Si Nm^{-3}	0-41	0-50
Chlorine as Cl^-	mg m^{-3}	0-5	20-200

1.1.1 Biogas purification

Among all the impurities, hydrogen sulfide (H_2S) is the most common, with a quantity varying from 100 to 1000 ppm. Since it is a poison for the methanation catalyst and corrosive for all metal pieces of equipment, it is necessary to remove it from the biogas. Another issue related to the presence of H_2S is the formation of SO_2 and consequently, in presence of water, to H_2SO_4, both highly corrosive, toxic and environmentally hazardous [2,9,10].

It is often removed in an early state of the upgrading process, either after or during (in-situ) the bacteria decomposition [9]. The most relevant techniques for H_2S separation from biogas are reported below [2,9,10]:

- Addition of Air/O_2 during digestion, leading to aerobic oxidation of H_2S to elemental sulfur by means of a group of specialized micro-organisms. For safety reasons a composition within the flammability range must be avoided. In this case the biogas upgrading through methanation is not possible since the oxygen introduced in the system could lead to catalyst deactivation, due to the oxidation of the active metal particles, and the presence of an inert (nitrogen) dilutes the energy released by the reaction;
- Addition of $FeCl_2$, $FeCl_3$ or $FeSO_4$ during digestion, to form solid FeS particles whose precipitate and are easily removed from the digestion tank. This technique cannot achieve the required hydrogen sulfide separation;
- Reaction with iron oxide or iron hydroxide, whose easily react with H_2S to form iron sulfide. This technique is carried out in a packed bed made of wood chips impregnated with the oxide or the hydroxide, to ensure a large surface-to-volume ratio;
- Absorption (either physical or chemical) with water or organic liquids. This process takes place in gas-liquid contactors such as packed beds or spray towers. The liquids most used for chemical absorption are diluted NaOH solutions, $FeCl_2$ solutions and $Fe(OH)_2$ solutions, capable of reacting with H_2S to form elemental sulfur or metal sulfides;
- Biological filters where hydrogen sulfide is absorbed in a liquid and then oxidated to elemental sulfur by specific bacteria, after addition of small quantities of air. The principle is similar to that of in situ addition of Air/O_2, thus it is not appropriate when the biogas is upgraded with methanation;
- Adsorption on activated carbon, performed with pressure swing adsorption upon a small addiction of oxygen, which allows the oxidation of adsorbed H_2S to elemental sulfur and the consequent formation of stronger bonds with the solid surface. This technique must not be used in case of successive upgrading via Sabatier reaction, since O_2 acts as a poison for the methanation catalyst leading to its deactivation. In this case carbon material impregnated with KI or $KMnO_4$ are preferred;

- Membrane separation, based on the selective permeation of biogas components across the membrane. The methane is preferentially retained at the retentate side whereas the hydrogen sulfide permeates preferentially across the membrane to the permeate side.

Untreated and raw biogas is generally saturated with water; therefore, the water content depends on biogas temperature [9]. This contaminant must be removed when biogas is used for grid injection or as vehicle fuel, but also before the upgrading via-methanation, since it is a Sabatier reaction product and has a negative effect on the equilibrium. It is also a cause of corrosion. The techniques for biogas drying are distinguished in physical and chemical [2,9]:

- Physical water separation is based on water condensation, followed by a system to capture and remove liquid droplets, such as demisters, cyclone separators, moisture traps and water taps in biogas pipelines.
- Chemical water separation is obtained with adsorption on silica or alumina traps, but also with absorption with glycols and absorption with hygroscopic salts.

An overview of advantages and drawbacks of these techniques is presented in Table 1.2.

Table 1.2: *Advantages and drawback of different water removal techniques [9]*

Method	Advantages	Disadvantages
Condensation methods Demister Cyclone Moister trap Water taps	- Higher HC's dust and oil are removed - Simple technique - Often used as pretreatment before other technologies	- Atmospheric pressure: dew point minimum 1°C - Gas at higher pressure to reach lower dew point (minimal -18°C) but freezing can occur
Adsorption dryer Silica Aluminum	- High removal: dew point -10 till -20°C - Low operational cost - Regeneration possible	- More expensive investment: pressure 6-10 bar - Dust and oil need to be removed in advance
Absorption with glycol	- High removal: dew point -5 till -15°C - Higher HC's and dust are removed - Not toxic or dangerous	- More expensive investment: high pressure and 200°C for regeneration - Higher gas volumes (>500 m^3/h) to be economical
Absorption with hygroscopic salts	- High removal efficiency - Not toxic or dangerous	- No regeneration done

Ammonia (NH_3) is another common contaminant of biogas which must be removed from the initial mixture because of its health risk and high corrosion potential. From its combustion toxic nitrogen oxides (NO_x) are produced, however their emissions are less relevant than that of the sulfur oxides therefore ammonia is not considered as hazardous as H_2S. Ammonia is generally removed with humidity, thanks to their high affinity, with one of the techniques previously mentioned. Other NH_3 separation techniques are washing process with diluted nitric acid or sulfuric acid solutions and separation with activated carbons [9].

Silicon organic compounds lead to deactivation of methanation catalyst by decomposition of siloxanes to oxides and silicates. These compounds may deposit on the catalyst and deactivate it but also form deposits damaging the pieces of equipment [12]. Possible techniques required to remove these compounds are [11]:

- Gas cooling and condensation of silicon organic compounds
- Adsorption on activated carbons, silica gel or aluminum
- Absorption with liquid mixtures of hydrocarbons

Other compound such as CO and O_2 may lead to catalyst deactivation (see §1.3.4 Catalyst deactivation) related to the oxidation of active metallic material [12]. They can be easily removed from biogas with pressure swing adsorption.

Finally, hydrogen is a reactant of the Sabatier, and it will be consumed during the methanation process. Thus, its separation from the raw biogas is not required.

1.1.2 Biogas Upgrading

The upgrading of biogas is required to produce biomethane, usually removing CO_2 from the biogas. Industrial techniques adopted for this separation are [2,9,10]:

- Physical absorption is based on scrubbing of biogas with a liquid toward which the biogas components have a different solubility, therefore achieving a selective separation. The process is carried out in packed columns to support the gas-liquid mass transfer, operating at about 6-10 bar. The liquid used, typically water or organic solvents such as methanol and dimethyl ether of polyethylene glycol (DMPEG) are regenerated in a desorption column operating at low pressure, with a counter-current flow of air or steam. Both water and organic solvent are also capable of removing H_2S, however it is advisable to remove the biogas impurities earlier than the carbon dioxide.
- Chemical absorption is based on reactive absorption of CO_2 with ammine solutions or alkali aqueous solutions (for instance KOH, K_2CO_3, $FeCl_2$ solutions). As in physical absorption the process is carried out in a packed column (either random or structured) in a counter-current flow configuration. A second column is required to regenerate the ammine/alkali solution. Differently from physical absorption, H_2S must be removed at an earlier stage since it is a poison for the ammine solution.

- Pressure swing adsorption is carried out in columns filled with adsorbents such as zeolites, synthetic resins, activated charcoal, activated carbon and silica gel. The separation is based on a sequence of adsorption, depressurization, desorption, and pressurization that allow to remove CO_2 from the biogas and release it regenerating the adsorbent material. It is advisable to remove H_2S at an earlier stage since it will irreversibly adsorb on the adsorbent, gradually decreasing the CO_2 separation capacity.
- Cryogenic separation of CO_2, based on the difference of condensation temperature of the gases involved. This technique is also useful to remove impurities such as N_2, O_2 and siloxanes (if still present in biogas), since liquid carbon dioxide acts as a solvent toward these components. Before cryogenic separation the biogas must be dried, to avoid water freezing.
- Membrane separation is based on difference in permeability of the gases through the membrane. Two different processes exist: gas-gas separation, where a gas phase is at both sides of the membrane, usually made of cellulose-acetate and gas-liquid separation with the liquid absorbing the component removed from the gas phase, therefore from the biogas. In this latter case, membrane usually employed are micro-porous hydrophobic materials.

Other upgrading methods are based on the conversion of carbon dioxide to methane via methanation, achieving a certain methane enrichment of biogas or producing biomethane without any previous CO_2 separation from biogas [2,5,6]:

- Biological methane enrichment is based on microalgae and micro-organisms capable of producing methane starting from hydrogen and carbon dioxide.
- Catalytic methanation is based on the catalytic conversion of CO_2 to CH_4 through the Sabatier reaction. This upgrading technique is the aim of this thesis work and will be discussed in a following section (see chapter §1.2).

A summary of the advantages and drawbacks of these techniques, except catalytic methanation, is presented in Table 1.3.

Table 1.3: *Summary of biogas upgrading techniques [9]*

Method	Advantages	Disadvantages
Absorption with water	- High efficiency (>97% CH_4) - Simultaneous removal of H_2S - Easy in operation - Capacity is adjustable by changing pressure or temperature - Regeneration possible - Low CH_4 losses - Tolerant for impurities	- Expensive investment and operation - Clogging due to bacteria growth - Possibility of foaming - Low flexibility toward variation of input gas
Absorption with polyethylene glycol	- High efficiency (>97% CH_4) - Simultaneous removal of organic S components, H_2S, NH_3, HCN and H_2O - Lower energy consumption than that of absorption with water - Low CH_4 losses	- Expensive investment and operation - Incomplete regeneration when stripping/vacuum (boiling required)
Chemical absorption with amines	- High efficiency (>99% CH_4) - Cheap operation - Regenerative - Low CH_4 losses	- Heat required for regeneration - Corrosion - Decomposition and poisoning - Precipitation of salts - Possible foaming
PSA Carbon molecular sieves Zeolites Alumina silicates	- High efficiency (95%-98% CH_4) - H_2S is removed - Low energy consumption - Regenerative - Used for small capacities also - Tolerant to impurities	- Expensive investment and operation - Expensive process control needed - CH_4 losses when malfunctioning of valves
Membrane technology Gas/gas Gas/liquid	- H_2S and H_2O are removed - Simple construction and operation - High reliability - Removal efficiency: gas/gas <92% CH_4 (1 step), >96% CH_4; gas/liquid >96% CH_4	- Compromise between purity of CH_4 and amount of upgraded biogas - Multiple steps required for high purity - CH_4 losses
Cryogenic separation	- Efficiency of 90%-98% CH_4 - CO_2 and CH_4 at high purity - Low extra energy costs to obtain liquid biomethane (LBM)	- Expensive investment and operation - CO_2 can remain in the CH_4
Biological removal	- Removal of CO_2 and H_2S and CH_4 enrichment - No unwanted end products	- Not developed at large scale - Requires addition of H_2

Figure 1.2 shows the evolution of the different biogas upgrading techniques from 554 facilities in the member countries of the International Energy Agency [21]. Nowadays the most used techniques are scrubbing (both chemical and with water), PSA and membrane separation technologies, particularly, in the last years the percentage of upgrading plants based on membrane separation as upgrading technology increased considerably.

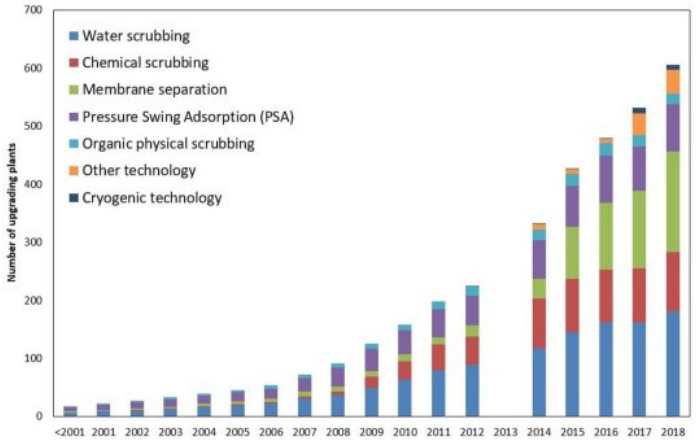

***Figure 1.1**: Evolution of different biogas upgrading technologies [21]*

1.2 Biogas catalytic methanation

A method to directly upgrade the biogas to biomethane, without any CO_2 separation, is the methanation reaction or, likewise, the Sabatier reaction to the purified biogas mixture. The reaction (1.1) represents the catalytic heterogeneous hydrogenation of CO to methane. It is exothermic and thermodynamically limited by equilibrium.

$$CO_2 + 4H_2 \rightleftarrows CH_4 + 2H_2O \qquad \Delta H_R^0 = -165 \text{ kJ/mol} \qquad (1.1)$$

The methanation mechanism should be seen as the combination of reverse water-gas-shift reaction (RWGS) and CO methanation or reverse steam reforming (RSR). The former (1.2) is endothermic whereas the latter (1.3) is strongly exothermic [5,7]:

$$CO_2 + H_2 \rightleftarrows CO + H_2O \qquad \Delta H_R^0 = +41 \text{ kJ/mol} \qquad (1.2)$$

$$CO + 3H_2 \rightleftarrows CH_4 + H_2O \qquad \Delta H_R^0 = -206 \text{ kJ/mol} \qquad (1.3)$$

$$CO_2 + CH_4 \rightleftarrows 2H_2 + 2CO \qquad \Delta H_R^0 = +247 \text{ kJ/mol} \qquad (1.4)$$

Among the possible side reactions, the most relevant are the RWGS and the dry reforming DR (1.4). Both these two reactions are endothermic and lead to consumption of methane and to formation of carbon monoxide which is a contaminant for the biomethane injection grid. Thus, to obtain high purity biomethane, these two side reactions must be strictly avoided.

Other side reactions are those related to carbon deposition and gasification:

$$CH_{4(g)} \rightleftarrows C_{(s)} + 2H_{2(g)} \qquad \Delta H_R^0 = +75 \text{ kJ/mol} \qquad (1.5)$$

$$2CO_{(g)} \rightleftarrows CO_{2(g)} + C_{(s)} \qquad \Delta H_R^0 = -173 \text{ kJ/mol} \qquad (1.6)$$

Particularly, methane cracking CRK (1.5) is endothermic and leads to additional unwanted methane consumption. The Boudouard reaction BOU (1.6) is responsible for carbon deposition related to the presence of carbon monoxide produced through DR and RWGS. It is of particular

interest also the reverse Boudouard, which is strongly endothermic and enlightens the possibility of formation of carbon monoxide from solid carbon deposits. Solid carbon also is a contaminant for the methanation catalysts, and its effect is described in detail in a following section (see chapter §1.2.3.1).

The Sabatier reaction (1.1) is characterized by a decreasing number of moles and by a strong exothermicity therefore it is thermodynamically favored by low temperatures and high pressures. The low temperatures also allow to reduce the effect of both side reactions, particularly the DR which is strongly endothermic. The high pressure also disadvantages the DR since it occurs with an increasing number of moles.

The inlet biogas contains a relevant quantity of methane, which is a product for the Sabatier reaction and a reactant for the dry reforming. Thus, it decreases the maximum CO_2 conversion due to Sabatier reaction and advantages the production of CO due to side reactions with respect to a gas feed made of CO_2 only.

A large amount of H_2 is required in the process (4:1 molar with respect to CO_2). The best option to produce it would be an electrolyzer, since it provides a constant and pure flowrate of hydrogen obtained by electrolysis of water, a by-product of the Sabatier reaction. To minimize waste and environmental impact should operate using excess renewable energy.

Surely not all the reactants are converted because of thermodynamic limitations, therefore there will be some CO_2 and H_2 in the outlet gas mixture. Thus, to obtain a product mixture suitable for the grid injection (see chapter §1.4) a two-staged methanation process is necessary, as shown in previous thesis work [21,22].

1.2.1 Methanation catalysts

According to Mills and Steffgen [8] the active materials toward the Sabatier reaction are metals mainly in groups 8-10. Particularly, the ranking in terms of activity and selectivity to methane (without any support for the catalyst) are the following [8,18]:

Activity: Ru > Fe > Ni > Co

Selectivity: Ni > Co > Fe > Ru

In Table 1.4 the prizes of these metals are listed:

Table 1.4: *Prizes of active metals [35]*

Metal	Prize ($/kg)
Ruthenium	19933.50
Iron	0.11
Nickel	24.45
Cobalt	34.93

Considering these four materials:

- Ruthenium (Ru): even if it is the most active material for Sabatier reaction its selectivity toward methane is low and it is much more expensive than the other metals considered. Thus, it is not used for biogas methanation [8].
- Nickel (Ni): it has the highest selectivity toward methane, a good activity and it is less expensive than Ru and Co, therefore it is the most used catalyst for methanation processes [1,8].
- Iron (Fe): even if it has a high activity, its selectivity to methane is poor. Thus, iron catalysts are not used for this process [8].
- Cobalt (Co): it has a similar activity and selectivity to those of Nickel but a larger cost, therefore it is not used for Sabatier reaction [8].

Besides the active material, support and promoters also influence the catalyst's performance. The preferred supports are those with large surface area such as titania (TiO_2), silica (SiO_2) and alumina (Al_2O_3). Particularly γ-Al_2O_3 is commonly used, given its high surface area and moderate cost [8]. However, recent studies focus on the microstructure of the support, particularly on the effect of the interparticle porosity and the related CO_2 diffusion within meso- and micro-pores, demonstrating how a higher carbon dioxide diffusion leads to enhanced Sabatier reaction rates [13]. According to this result, supports such as mesostructured silica nanoparticles (MSN) facilitate the transport of reactants and products allowing to obtain larger conversion than that obtained with Ni/γ-Al_2O_3 catalysts [13]. The main disadvantage of this type of support is its large cost (related to the catalyst preparation), therefore support such as alumina are still preferred.
Promoters are added to increase the performance of the catalyst under the methanation reaction conditions. Particularly for Ni/ γ-Al_2O_3 catalyst the promoters are [8,18]:

- MgO allows to increase the thermal stability of the catalyst but also enhances the coke resistance.

- La_2O_3 improves the Ni dispersion and the H_2 uptake on the catalyst, leading to an activity enhancement.
- V_2O_3 acts as MgO, leading to an increasing thermal stability and carbon resistance.
- CeO_2 facilitates the catalyst activation (so the reduction of Ni oxide species) and the long-term catalyst's stability.

For this thesis work Ni/γ-Al_2O_3 catalysts have been used, to continue previous studies of Pagin [21] and Scarpa [22], who had demonstrated experimentally the high activity of this catalyst toward biogas methanation, with the best performance in terms of methane enrichment and capability to avoid side reactions in the range of temperature of 280-400°C. From this paragraph on, all the consideration will be on this type of catalyst.

1.2.2 Catalyst activation

Nickel in the catalysts for methanation is present only in its oxidized form [8, 11], therefore, to activate it, a reduction step is required to convert the oxides to active metallic nickel, and it is achieved through a treatment at high temperature in a controlled reducing atmosphere, made of hydrogen and inert. Except for the reduction, other activation techniques are not required for nickel based methanation catalysts. Temperature and duration of the treatment are chosen according to the nature of the catalyst, and so to its surface area and nickel loading. Low temperature reduction favors the subsequent formation of higher hydrocarbons during the methanation process whereas higher temperatures lead to a larger reduction rate of the catalyst and to a larger activity and selectivity to methane. However, excessively high temperature may lead to catalyst deactivation by sintering of nickel particles negatively influencing the long-term stability of the catalyst [8,14]. It is also possible to alternate reaction and reduction of the catalyst (hydrogen bracketing technique) to inhibit catalyst deactivation and increase its long-term stability [8,15,16].
Detailed information on the catalyst behavior under reducing atmosphere are obtained with temperature programmed reduction (TPR), where the H_2 fraction is monitored continuously using a thermal conductivity detector (TCD) to understand whenever it is consumed. An example of results obtained for different catalysts is reported in Figure 1.3.
The number of peaks and the corresponding temperatures depend on the nickel loading.
Particularly, when nickel loading is lower than 10% only one peak appears, therefore only one

oxidized form (probably NiO) is present, whereas at larger nickel loading a second peak appears at lower temperatures.

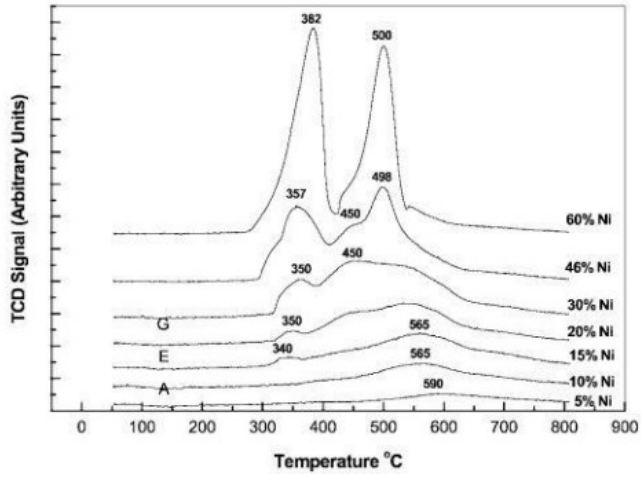

***Figure 1.3**: TPR of Ni/ γ-Al_2O_3 as a function of nickel loading [20]*

Previous thesis on the biogas methanation [21,22] shown that with a mixture of 5% H_2 and 95% inert, a complete activation Ni catalyst is achieved (see Figure 1.4); two peaks are highlighted: the first one at about 300°C is characteristics of the NiO_2 reduction while the second one at about 550-600°C of the NiO. This same activation procedure will be exploited for this work.

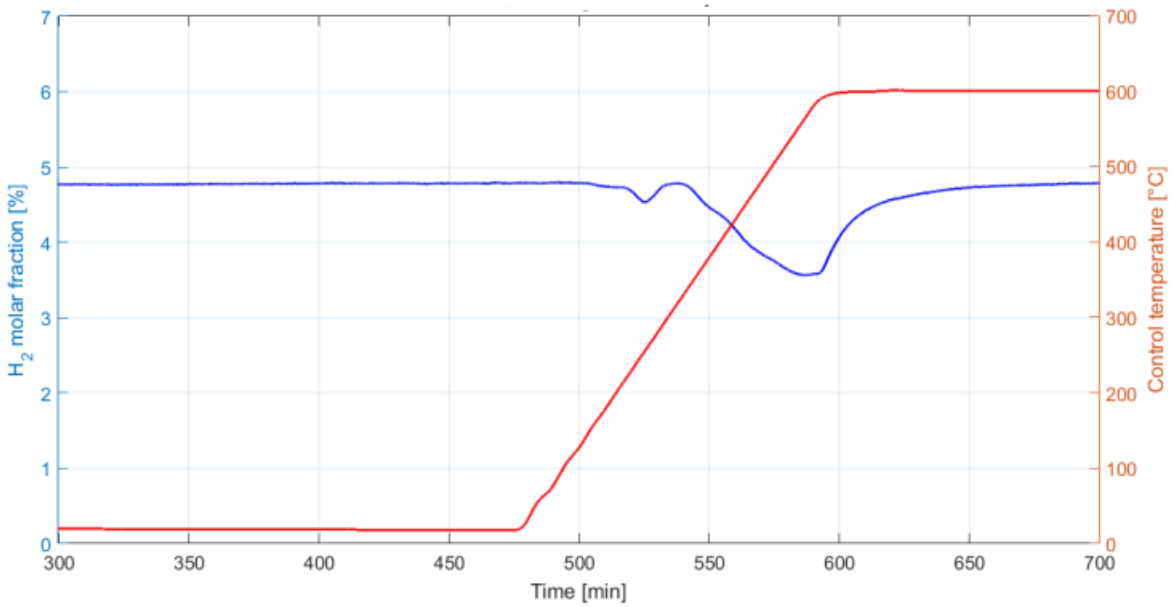

***Figure 1.4:** H_2 molar fraction during catalyst EX11914 activation [21]*

1.2.3 Catalyst deactivation

The possible categories of deactivation of nickel based methanation catalysts are chemical, thermal, and mechanical deactivation [8].

Two different phenomena lead to chemical deactivation:

- Poisoning: reactions of gas impurities with the catalyst's active material. An example is the poisoning due to H_2S which reacts with the nickel oxide (1.5) leading to an irreversible activity loss [8].
- Vapor-solid reaction: reaction between CO and Ni (1.7) leading to formation of nickel carbonyls at temperature lower than 230°C. This phenomenon is less relevant than poisoning since methanation catalysts are active at temperatures higher than 250°C and at this temperature the formation of carbon monoxide is avoided [8]. However, it should be an issue during the start-up when the biogas has not been well purified.

$$NiO_{(s)} + H_2S_{(g)} \rightleftarrows NiS_{(s)} + H_2O_{(g)} \qquad \Delta H_R^0 = +41 \text{ kJ/mol} \qquad (1.7)$$

Thermal deactivation due to high temperatures enhances solid diffusion of metallic nickel particles, causing sintering and the consequent decrease of the specific surface [8,14]. The more the temperature increases, the more sintering occurs, particularly for methanation catalysts it becomes relevant for temperatures larger than 500°C [1,8,23]. However, the absence of oxygen and the presence of hydrogen and steam produced by the reaction (1.1) in the reaction mixture allow to make the sintering less relevant [8,14,23]. Attrition, crushing, and fouling are the responsible of mechanical deactivation:

- Attrition leads to abrasion and consequently to losses of catalyst. It has relevant importance in fluidized bed reactors [8].
- Crushing means breakage of the particles of catalyst due to mechanical stress. Also, this phenomenon is relevant in fluidized bed or slurry reactors, and it is the result of collision of particles with the reactor wall or among themselves [8,23].
- Fouling is related to carbon deposition, and it is one of the main issues in the methanation process. Since it is the main purpose of this thesis work it is discussed in a sequent section (see chapter §1.2.3.1).

The mechanisms just described are summarized in Table 1.5.

Table 1.5: *Deactivation mechanisms for Ni/Al2O3 catalysts [8,19,23]*

Deactivation	Mechanism	Description
Chemical	Poisoning	Reaction of different gas impurities (especially sulfur compounds) on the catalytic surface therefore decreasing the active sites and the catalyst activity
	Vapor-solid reaction	Formation of nickel carbonyl with carbon monoxide when the temperature is below 230°C. Relevant during plant start-up and shutdown
Thermal	Thermal degradation	Nickel sintering and consequent surface area decrease at high temperatures (>600°C)
Mechanical	Attrition	Loss of catalytic material due to abrasion. Relevant in fluidized bed
	Crushing	Breaking of catalyst particles because of mechanical or thermal stress
	Fouling	Carbon and coke deposition on the catalyst active sites

1.2.3.1 Deactivation by carbon deposition

Carbon deposition over metallic catalysts can occur in all reactions involving hydrocarbons and carbon monoxide at high temperatures [23,30]. For the biogas methanation process the possible reactions involving solid carbon formation are methane cracking (1.5) and the Boudouard reaction (1.6) as enlighten in chapter §1.2.

Carbon formation is a relevant issue particularly for a second stage of biogas methanation, where the inlet mixture is rich in methane, larger than 70% with the best conditions tested in previous thesis [21,22], therefore enhancing the possibility of carbon formation due to reaction (1.5). This reaction is endothermic and occurs with increasing number of moles, hence it is favored at low pressure and high temperature. Also, the Boudouard reaction is considered since CO is an intermediate of Sabatier reaction mechanism but also a possible product of unwanted side reactions. Thus, carbon monoxide could be present in the mixture fed to the second stage but also produced within the reactor. However, for this thesis work the second stage inlet mixture is considered without any carbon monoxide and no CO is produced, due to the special velocity that allows to keep the first stage packed bed reactor below the 400°C required for the RWGS to activate [21]. Thus, the effect of reaction (1.6) can be neglected.

Possible effects of carbon deposition over Ni supported catalysts are:

- Chemisorption of carbon as a monolayer or physical adsorption as multilayers over catalyst surface, blocking the access of reactants to the active sites [8,23].
- Encapsulation of metal particles within carbon structures leading to complete deactivation of the active material [8,23].
- Plugging of micro-pores and meso-pores limiting the active specific surface and so the number of active sites the reactants can reach [23,32].
- Formation of strong carbon filaments whose may stress and, in extreme cases, fracture the support material but also block the interparticle voids increasing the upstream pressure, therefore leading to safety issues [23,32].

According to these four phenomena, carbon acts both as foulant and poison for Ni supported catalysts.

The mechanism of carbon deposition on Ni catalyst has been proved to involve the formation and the transformation of different carbon species. This is experimentally demonstrated [29,33] by temperature programmed surface reaction (TPSR). This treatment consists in exposing the fouled catalyst to H_2, under a specific temperature program (ramp of 1°C/sec from 25°C to 900°C). Hydrogen reacts at different temperatures with the different carbon species producing methane therefore depending on the signal related to methane detection those species are identified. In Table 1.6 a summary of the different carbon species, their formation temperature and of their TPSR results are reported.

***Table 1.6**: Possible carbon species formed by carbon deposition [29,32]*

	Type of carbon	Temperature of formation [°C]	Peak temperature for reaction with H_2 [°C]
C_α	Adsorbed atomic carbon	200-400	200 ± 20
C_β	Amorphous, polymeric carbon	250-500	400 ± 30
C_γ	Nickel carbide, Ni_3C	150-250	275 ± 20
C_V	Carbon fibers (whiskers)	300-1000	400 - 600
C_C	Crystalline or graphitic carbon	> 500	550 - 850

Particularly, polymeric carbon is mainly related to thermal decomposition of methane whereas filamentous and graphitic carbon are mainly due to catalytic decomposition. The mechanism of carbon filament formation has been deeply investigated [24] and undergoes to different steps:

i. Methane adsorption and dehydrogenation steps;
ii. Deposition of the remaining carbon over nickel leading to formation of carbon layers at the gas/metal interphase;
iii. Diffusion through Ni particles toward the metal/support interphase. The driving forces of this step are gradients of temperature and concentration between the metal/gas interphase and the metal/support interphase;
iv. Nucleation of filamentous carbon occurring because of carbon segregation behavior, to a high carbon coverage of nickel and the consequent high concentration of carbon in nickel particle.
v. Carbon filament growth. This consist in the Ni particle detachment from the support surface, now being supported by the carbon filament.

Figure 1.5 represents different steps of carbon filament nucleation and growth.

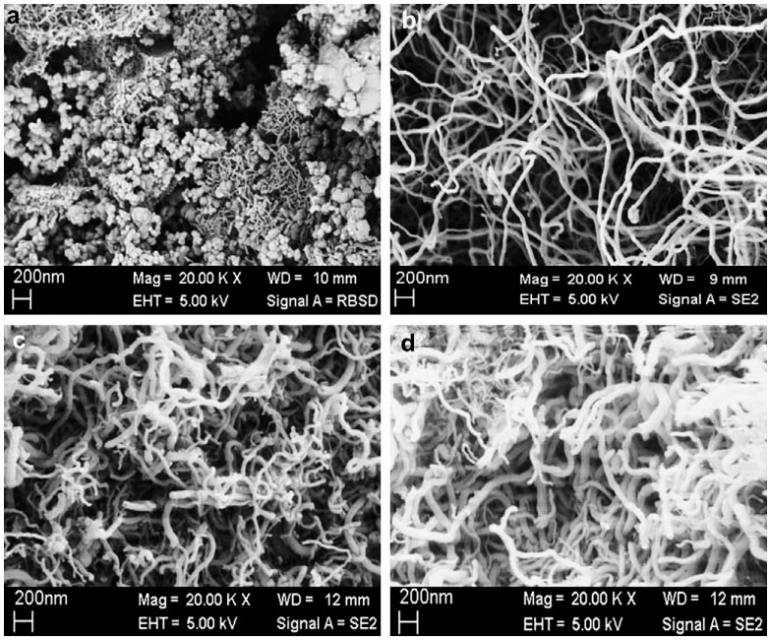

Figure 1.5: *SEM micrographs of nucleation and growth of carbon filaments over 5% Ni-Al_2O_3 [24]*

As anticipated with the concept of TPSR, carbon deposition can be removed from catalyst surface by means of specific treatments. The possible reactions involved are carbon hydrogenation (1.8), carbon gasification (1.9), reverse Boudouard reaction (1.5) and carbon oxidation (1.10, 1.11):

$$C_{(s)} + 2H_{2(g)} \rightleftarrows CH_{4(g)} \quad (1.8)$$

$$C_{(s)} + H_2O_{(g)} \rightleftarrows CO_{(g)} + H_{2(g)} \quad (1.9)$$

$$C_{(s)} + O_{2(g)} \rightleftarrows CO_{2(g)} \quad (1.10)$$

$$C_{(s)} + ½\ O_{2(g)} \rightleftarrows CO_{(g)} \quad (1.11)$$

Considering the rates of these four reactions [18,31]:

- The rate of carbon gasification with H_2 (1.8) increases with the temperature up to 700°C but then it is limited by thermodynamics.
- The rate of gasification with H_2O (1.9) or CO_2 (1.5) increases with temperature, and it is not limited by equilibrium. However, at temperatures larger than 700°C limitations due to mass transfer occurs. It is proved that gasification with steam gas has a higher rate than that with H_2 or CO [32].
- The rate of carbon oxidation is much larger than the previous ones and not limited by equilibrium. In this case special attention is required to avoid overheating and the related catalyst deactivation by sintering [8] due to the exothermicity of the reaction. This is the method used in this thesis work, according to the highest rate of carbon oxidation with respect to the other carbon removal techniques.

It is important to notice that, even if it is possible to regenerate the fouled catalyst, there should be a certain activity loss, probably related to the remotion of nickel crystallites from the support during the Sabatier reaction and their entrainment in the gas phase during the sequent carbon gasification or oxidation [18]. Also, the composition of the mixture used for catalyst regeneration is a relevant parameter: previous thesis demonstrated than using mixture of O_2 and inert with high oxygen content (e.g. 30% on molar basis) a certain activity loss occur, thus for the experimental test more conservative conditions are adopted (e.g. 5% O_2 on molar basis) avoiding activity loss due to catalyst reactivation treatment (see chapter §1.4.1 figure 4.4).

The reaction of carbon gasification, particularly (1.9), suggest the possibility of feeding $H_2O_{(v)}$ to the second methanation stage to avoid or limit the carbon deposition, taking advantage of the larger rate of gasification of C with H_2O than that with H_2 already present in the reactive mixture. This procedure has been studied at first with a thermodynamic approach [17] and it is the main purpose of this thesis work.

The most used index for the quantification of carbon is the carbon formation rate per unit mass of catalyst, expressed in $g_{carbon}/(g_{cat} \cdot h)$ [31,32]. This value is strongly dependent on temperature,

pressure, and methane and hydrogen partial pressure. Particularly, for methane cracking at 500°C, with $p_{H_2} = 0.2$ bar and $p_{CH_4} = 5$ bar, the carbon formation rate is equal to 2.4 $\frac{g_{carbon}}{g_{cat} \cdot h}$ [24].

1.3 Methanation reactors

Nowadays, the methanation process is industrially carried out using three types of reactors: fixed bed reactors, fluidized bed reactors and three phase reactors [8,19]. These applications do not refer to biogas methanation but to pure carbon dioxide methanation.

1.3.1 Fluidized bed methanation reactors

In fluidized bed reactors the gas flow allows to keep suspended the particles of catalyst leading to a uniform mixing within the unit. This, combined with the action of internal heat exchangers, ensures efficient temperature control, also achieving an almost isothermal operating condition, therefore those reactors will have a simple design and a single reactor will be sufficient instead of a cascade of reactors. Besides that, the fluidization of the catalyst leads to high mechanical stress of the particles and subsequently to a shorter reactor life related to catalyst losses and deactivation by attrition [8,19].

1.3.2 Three phase methanation reactors

The three phase methanation process was developed by Chem Systems Inc. and it is based on a single reactor operating at 70 bars with three phases: the solid catalyst, the gaseous reactant mixture, and an inert liquid with high heat capacity, usually a mineral oil, which ensure an effective temperature control [8,19]. In this process the catalyst powder is made of particles with diameter of 100μm. Drawbacks of these reactors are due to the additional mass transfer resistance related to mass exchange between gas and liquid, therefore resulting in a decrease of the single-pass conversion. This type of reactor is still under development and not used in industry.

1.3.3 Fixed bed methanation reactors

This type of reactor is packed with the size of particle of catalyst in the order of millimeters. The catalyst is active at 250-300°C and temperatures above 500°C must be prevented, to avoid sintering of catalyst particles [2,9,26] and the activation of side reactions leading to formation of CO, which is a contaminant for the biomethane injection grid. Fixed bed adiabatic reactors are generally

preferred, however thermal control is challenging, causing the formation of hot spots. To deal with this issue series of adiabatic packed bed with intermediate cooling are adopted, therefore leading to high values of pressure drops [10], and sometimes recirculation of the reacting mixture or steam addition are required for the temperature control [9].

Examples of plants working with adiabatic fixed bed reactors are [9,10]:

- Air Liquide (formerly Lurgi) plant works with a series of two adiabatic fixed bed reactors with intermediate cooling.
- Haldor Topsøe developed the Topsøe Recycle Energy-efficient Methanation (TREMP) based on a series of 3-4 adiabatic fixed-bed reactors and focusing on high temperature methanation.

Other solutions to overcome the issue of thermal control are cooled bed fixed bed reactors and structured reactors. Considering the former, an example is the plant developed by Linde [8,19], based on a two stage methanation where the first stage is carried out in a cooled reactor with integrated heat exchanger whereas the second stage consists of an adiabatic packed bed reactor. This application still does not exist at a commercial level. The main drawback of these reactors is the lower reaction rate than that of an adiabatic reactor, caused by lower temperature within the reactor. On the other hand, the internal structure of structured reactors allows a better heat transfer (by improving the radial heat transport), and lower pressure drops than that of adiabatic reactors [8].

Examples of this type of reactors are [8]:

- Honeycomb reactors with catalyst coating and cooling with thermal oil or water.
- Micro-structured reactor with high specific surface.
- Sorption enhanced reactors where the support of the catalyst can adsorb H_2O produced by Sabatier reaction, therefore, shifting the thermodynamic equilibrium toward the products.

It is important to notice that both structured and cooled packed bed reactors are polytropic and they are characterized by the formation of a hot spot close to the reactor entrance and by a moderate reactor outlet temperature (around 300°C). However, they are more expensive than adiabatic packed bed reactors [8].

A summary of the characteristics of the different reactors is reported in Table 1.7.

Table 1.7: Comparison between methanation reactors

	Adiabatic FB reactors	Cooled FB reactors	Micro-reactors	Fluidized-bed reactors	Three-phase reactors
Operation mode	Adiabatic	Polytropic	Polytropic	Almost isothermal	Isothermal
Reactor stages	2 - 7	1 - 2	1 - 2	1 - 2	1 - 2
Gas recycling	Usually	Sometimes	No	Sometimes	No
Temperature range	250 - 700	250 - 500	250 - 500	300 - 400	300 – 350
Arrangement/state of cat.	Packing	Packing	Coated	Fluidized	Fluidized or suspended
Particle size	Millimeters	Millimeters	<200 µm	100 - 500 µm	<100 µm
Mechanical stress of cat.	Low	Low	Low	High	Moderate
Thermal stress of cat.	High	Moderate	Moderate	Low	Low
Complexity of process set-up	High	Low	Low	Low	Low
Reactor costs	Medium	High	Very high	Low	Low-medium
GHSV	Medium-high	High	High	Medium-High	Low-medium
Technology readiness level (1-10 scale)	9	7	4 - 5	7	4 - 5

1.3.3.1 Two-staged methanation

To satisfy the Italian biomethane injection grid requirements (see chapter §1.4) a unique reaction stage is not enough, therefore a two-staged operation is required. Previous thesis work [21,22] demonstrated how a two-stage process with adiabatic reactors operating at atmospheric pressure with inter-stage water condensation can satisfy the grid requirements. However, the thermal control and coupling between the two reactors has become of critical importance. Previous studies [26] enlighten the presence of a temperature hot-spot close to the first-stage reactor entrance, leading to temperatures larger than 600°C in the first reaction stage (see Figure 1.6), therefore to the activation of undesired side reactions. This is not a critical issue in the second-stage reactor, where the heat released by the reaction is much smaller than that of the first stage.

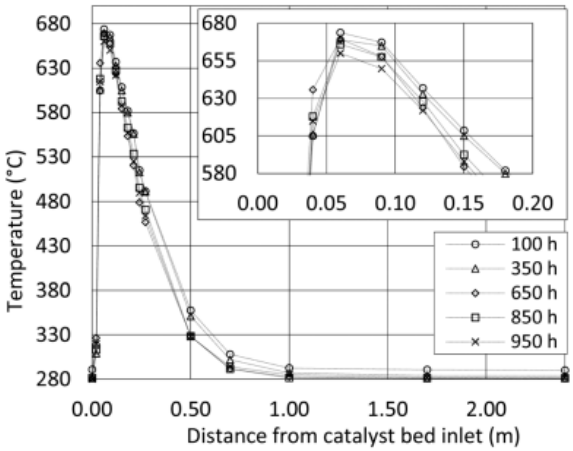

***Figure 1.6**: Example of temperature profile for a first-stage biogas methanation reactor [26]*

Different approaches have been developed to face this critical issue:

- Dannesboe, Hansen and Johannsen [26] propose a double-pass reaction section with intermediate water condensation, where the two packed bed reactors are within a bundle (as in a multitube reactor) where boiling water is used as coolant for temperature control (see Figure 1.7). The cooling water is pressurized at 65 bar to keep the boiling temperature at 280°C, which is the desired reactor temperature.

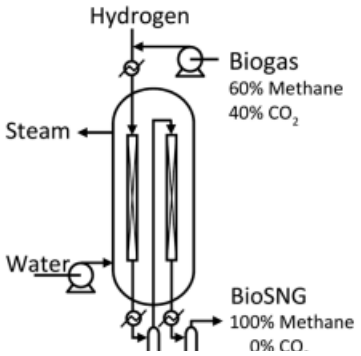

Figure 1.7: *Design of the reaction section [26]*

- Neubert and Hauser [25] propose an experimental set-up for CO_2 (not biogas) methanation, where the first stage is carried out in a structured reactor with feed gas preheating and a bundle of reaction channel cooled by means of a phase changing fluid flowing in channels named heat pipes. The second stage consists of an adiabatic packed bed reactor. Between the two stages an intermediate water removal is required. The process scheme is shown in Figure 1.8.

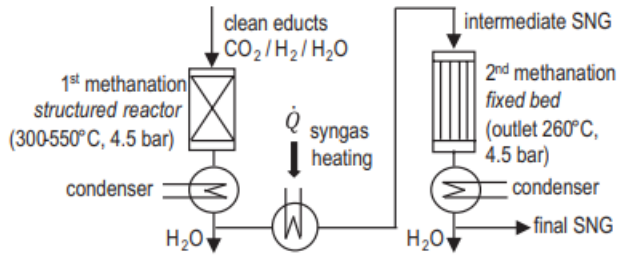

Figure 1.8: *Process scheme of a two-stage methanation with intermediate water sequestration [25]*

- Sayama and Yamamoto [27] CO_2 methanation with two cooled fixed bed reactors with intermediate water removal, operating at low pressure (2 bar_a). The cooling fluid is a diathermic oil. As shown in Figure 1.9 both hydrogen and the heat carrier flows are split between the two reactors. This process allows 70% of the generated heat to be recovered at 99% CO_2 conversion, with a Ru based catalyst.

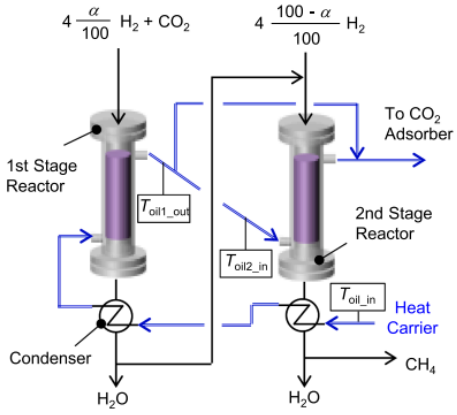

Figure 1.9: *Process scheme proposed by Sayama and Yamamoto [27]*

- Gruber and Weinbrecht [28] propose a CO_2 methanation module made of two reactors connected in series with intermediate water sequestration, as shown in Figure 1.10. The first reactor consists in six parallel reaction channels cooled by boiling water flowing in the outer bundle whereas the second stage reactor has only two reaction pipes, still cooled by means of boiling water.

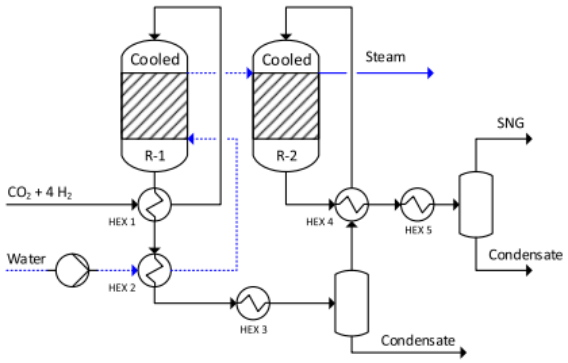

***Figure 1.10**: Reactor concept proposed by Gruber and Weinbrecht [28]*

1.4 Biomethane in Italy

Until 2015, Italy had only one active biogas upgrading plant at the Magrotta landfill, situated in Rome, where the biomethane obtained is utilized as biofuel for the garbage trucks. However, after the publication of the norm UNI EN 16732 of 16th December 2016, the first plant injecting the biomethane directly in the natural gas grid was inaugurated (Montello S.p.A plant in Montello, Bergamo) This is also the first "carbon negative" plant in Italy, since carbon dioxide is utilized to produce biomethane according to the biogas methanation process and the CO_2 non converted is separated from the product mixture and sold to the food industry or for technical use [36, 37].
As shown in Table 1.8 the acceptable values of S, Si, NH_3 and H_2O for the injection are very low so the biogas must be purified before the reaction section (see §1.1). High conversion of H_2 and CO_2 are required to keep their concentrations under 1% and 2.5% respectively. If it is not possible to reach these limits with the methanation, a separation section, maybe through membranes to exploit the high pressure, could be the solution. CO must be less than 0.1% so the side reactions must be avoided as much as possible (see chapter §1.3).

***Table 1.8**: Biomethane contaminants specification for gas grid injection [39]*

Contaminant/parameter	Unit of measure	Value
H_2O dew point	°C	≤ -5
CO_2	%mol	≤ 2.5
O_2	%mol	≤ 0.6
H_2S	mg/m^3	≤ 5
S (mercaptans)	mg/m^3	≤ 6
S (total)	mg/m^3	≤ 20
Si (total)	mg/m^3	$0.8 - 1$
CO	%mol	≤ 0.1
NH_3	mg/m^3	≤ 10
H_2	%vol	≤ 1
Chlorides	mg/m^3	< 1
Fluorides	mg/m^3	< 3

However, in April 2019, Snam (Società Nazionale Metanodotti) experimented with the grid injection of a mixture of methane and 5%vol of H_2. This mixture was supplied to two industrial companies situated in Conturi Terme, Salerno. Then, the experimentation was replicated in December 2019, using a mixture with 10%vol hydrogen content [41]. Applying this last mixture, instead of pure methane, to the total gas transported by Snam, a 5-ton CO_2 emission reduction should be achieved. Nowadays the company is verifying the compatibility of their infrastructures with an increasing content of hydrogen: only 70% of the methane pipelines are compatible with H_2. This movement towards H_2 gas grid limit increasing is of great interest for this project; we demonstrated in a previous thesis [21,22] that two atmospheric pressure stages in series are enough to keep H_2 below 5%.

In Italy, the biomethane is obtained separating CO_2 from the CH_4 through the techniques already described (see paragraph §1.1.2). 31% of it derives from the organic fraction of municipal solid waste treatment (OFMSW) (see Figure 1.11). Other important feedstocks are scraps of agri-food production (19%), agricultural biomass (22%) and zootechnical waste (18%). Of secondary importance are instead the biomass from forestry and forest maintenance and the sewage sludge which are used only for 3% and 7% respectively.

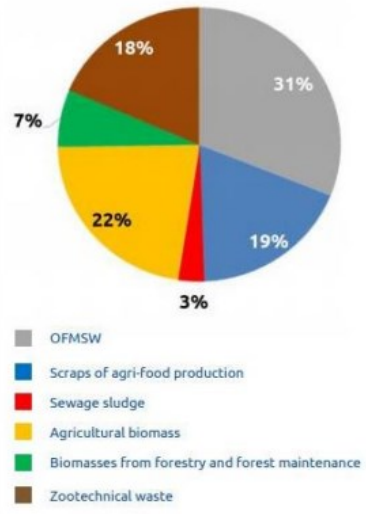

***Figure 1.11**: Type of biomasses as feedstock for biomethane production in Italy, year 2019 [37]*

Since 2017, the increasing interest in biomethane has been confirmed by data on connections to Snam's gas grid at the beginning of 2019 [37, 38], when 6 biomethane production plants were operating. In the last year the number of operating biomethane production plants has increased again, from 6 of 2019 to 27 of 2021. Their location, capacity and year of inauguration is shown in Figure 1.12.

***Figure 1.12:** Distribution of biomethane plants in Italy, year 2021 [40].*

1.4.1 Biomethane incentives

The Ministerial Decree of 15th September 2022, with validity from 30th January 2023 to 30th June 2026, PNRR (Piano Nazionale Ripresa e Resilienza) plans to invest 1.92 billion euros to enhance the utilization of biomethane, to reach the target planned for 2030. With the reimbursement of a grant in corporate budget at maximum equal to 40% of total expenses and with an incentive in energy account for 15 years related to the net biomethane production, the decree promotes [42]:

- Reconversion to biomethane of plants producing electric energy from biogas, for agricultural plants only.
- Development of new biomethane production plants both agricultural and from landfill.

So that the incentives are applied, plants must start operating before 30th June 2026 and the communication of the beginning of operation must be transmitted to the GSE (Gestione Servizi Energetici) before 30th July 2026.

The amount of incentives depends on the nature of the plant (agricultural or from landfill) but also on the productive capacity, as shown in Table 1.9.

***Table 1.9**: Maximum specific values in capital account with respect to the maximum expense expected.*

Plant type	Productivity [Scm/h]	Incentives for new plants [€/Sm³/h]	Incentives for reconversion of an existing plant [€/Sm³/h]
Agricultural	< 100	13200	5040
	100 – 500	11600	
	> 500	5200	4640
From organic waste	Any	20000	-

Chapter 2
Equilibrium study of coke production on second stage methanation reactor

The Sabatier reaction (2.1) consists in the catalytic heterogeneous hydrogenation of CO_2 to produce CH_4 and H_2O. It is exothermic and takes place decreasing the number of moles, so the equilibrium is favored by high pressures, low temperatures, and no inert addition.

$$CO_2 + 4H_2 \rightleftarrows CH_4 + 2H_2O \qquad \Delta H_R^0 = -165 \text{ kJ/mol} \qquad (2.1)$$

From previous experimental results [21,22] it has been observed that the side reactions responsible for CO production, dry reforming (DR, 2.2) and reverse water-gas shift (RWGS, 2.3) are active for temperatures larger than 400°C. Since the second methanation stage produces less heat than that produced in the first stage, temperatures as high as 400°C can be easily avoided. Thus, this will be the maximum temperature for chemical equilibrium calculations.

$$CO_2 + CH_4 \rightleftarrows 2H_2 + 2CO \qquad \Delta H_R^0 = +247 \text{ kJ/mol} \qquad (2.2)$$

$$CO_2 + H_2 \rightleftarrows CO + H_2O \qquad \Delta H_R^0 = +41 \text{ kJ/mol} \qquad (2.3)$$

Particularly, the reverse-water-gas-shift is considered as a first step of the CO_2 methanation mechanism, followed by CO methanation (2.4), which is a highly exothermic reaction occurring with decreasing number of moles, therefore favored by low temperatures, high pressures, and no inert addition.

$$CO + 3H_2 \rightleftarrows CH_4 + H_2O \qquad \Delta H_R^0 = -206 \text{ kJ/mol} \qquad (2.4)$$

As a consequence of the high CH_4 content, coke production and deposition on catalysts surface could occur in the second stage reactor. Particularly, two reactions can act as coke producers: methane cracking (MCK, 2.5) and Boudouard reaction (BOU, 2.6).

$$CH_{4(g)} \rightleftarrows C_{(s)} + 2H_{2(g)} \qquad \Delta H_R^0 = +75 \text{ kJ/mol} \qquad (2.5)$$

$$2CO_{(g)} \rightleftarrows CO_{2(g)} + C_{(s)} \qquad \Delta H_R^0 = -173 \text{ kJ/mol} \qquad (2.6)$$

Methane cracking is an endothermic reaction leading to an increase in the number of moles, therefore it is favored at high temperature and low pressure, but also by inert addition. Boudouard

reaction is highly exothermic and occurs with decreasing number of moles (considering the gas phase relevant for equilibrium calculation), hence it is favored at low temperature, high pressure, and no inert addition.

Then, also the possibility of solid carbon removal due to the presence of water vapor (carbon gasification) should be accounted for.

$$C_{(s)} + 2H_2O_{(g)} \rightleftarrows CO_{(g)} + H_{2(g)} \qquad \Delta H_R^0 = +140 \text{ kJ/mol} \qquad (2.7)$$

Carbon gasification with steam (CGS, 2.6) is strongly endothermic and leads to occurs with no variation of moles of the gas phase, therefore it is favored by high temperatures, whereas pressure and inert addition have no effect on the chemical equilibrium of this reaction.

The challenge of this work is the application of methanation to a mixture rich in methane, entering the second stage of reaction. The high inlet methane molar percentages (at least 70% on molar basis, depending on the first stage conditions) disadvantages the Sabatier reaction and favors other reactions where methane is as reactant, mainly MCK, leading to the need of studying the solid carbon formation, initially from a thermodynamic point of view.

The composition of the dry mixture (see Table 2.1) used for chemical equilibrium calculations is the same of that used for experimental test, corresponding to a second-stage of biogas catalytic methanation with intermediate water removal, where the first stage is carried out at a WHSV which allows to achieve an autothermal first stage, settling at a temperature where side reaction are only slightly active, therefore the presence of by-products, such as CO, entering the second-stage is not considered. The unique difference with inlet composition used for experimental tests is that the tracker is not considered for chemical equilibrium calculations, therefore molar percentages are rescaled on the tracker. Then, to evaluate the thermodynamic effect of the addition of water on the second stage, particularly the effect on solid carbon formation, a certain inlet molar percentage of water vapor has been considered, fixed the dry mixture composition specified in Table 2.1.

Table 2.1: *Inlet dry gas composition used for equilibrium calculation.*

y_{CH_4} [%]	y_{H_2} [%]	y_{CO_2} [%]
75.79	19.37	4.84

The equilibrium has been calculated varying the temperature and the pressure through Cantera on Matlab®. The program uses the GRI-Mech 3.0 thermodynamic database (available on

http://combustion.berkeley.edu/gri-mech/version30/files30/grimech30.dat) to calculate the equilibrium composition of a specified gas mixture. This mechanism includes 53 species, mostly radicals, with hydrocarbons up to C3. For the solid phase, graphitic carbon is considered.

In the next paragraphs, the results of these calculations are shown. The products composition profiles will be presented on dry basis, to compare the calculations with the experimental data, which will not contain quantification of water. Indeed, this is condensed before the analytical instruments (see Chapter 3 for details).

Then, also the moles (produced or consumed) of each species will be reported. For the calculation 100 moles has been considered as an initial condition. Once the number of moles of the different species at equilibrium are known, it is possible to calculate H_2 conversion (2.7) and CO_2 conversion (2.8).

$$X_{H_2} = 1 - \frac{\dot{n}_{H_2}^{EQ}}{\dot{n}_{H_2}^{IN}} = 1 - \frac{y_{Ar}^{IN} y_{H_2}^{EQ}}{y_{Ar}^{EQ} y_{H_2}^{IN}} \tag{2.7}$$

$$X_{CO_2} = 1 - \frac{\dot{n}_{CO_2}^{EQ}}{\dot{n}_{CO_2}^{IN}} = 1 - \frac{y_{Ar}^{IN} y_{CO_2}^{EQ}}{y_{Ar}^{EQ} y_{CO_2}^{IN}} \tag{2.8}$$

2.1 Effect of temperature

The temperature has varied from 20°C to 400°C whereas two pressures have been considered, 1 bar and 6 bar, hence the pressure of the experimental tests. The temperature range has been chosen according to results of previous thesis [21, 22], demonstrating that the optimal temperature range is between 250°C and 350°C and that the heat released by the reaction in the second stage reactor is not enough to rise the temperature to values outside the decided range.

From Figure 2.1 is possible to notice that up to 150°C the equilibrium of Sabatier reaction (2.1) is almost completely shifted towards the products (only 0.05% CO_2 left) and the side reactions such as RWGS, DR are not active, since no CO is produced. Above this temperature, the CH_4 molar percentage starts to decrease, because the Sabatier reaction is less favored but mainly for the effect of methane cracking (2.4). This is enlightened by the increasing molar percentage of hydrogen without any relevant increase on the CO_2 molar fraction. It is also possible to notice that the stoichiometric ratio H_2/CO_2 is not equal to 4 (as expected from the stoichiometric ratio of Sabatier

reaction) but it is much larger due to hydrogen production via methane cracking and also because of the contribution of the BOU reaction.

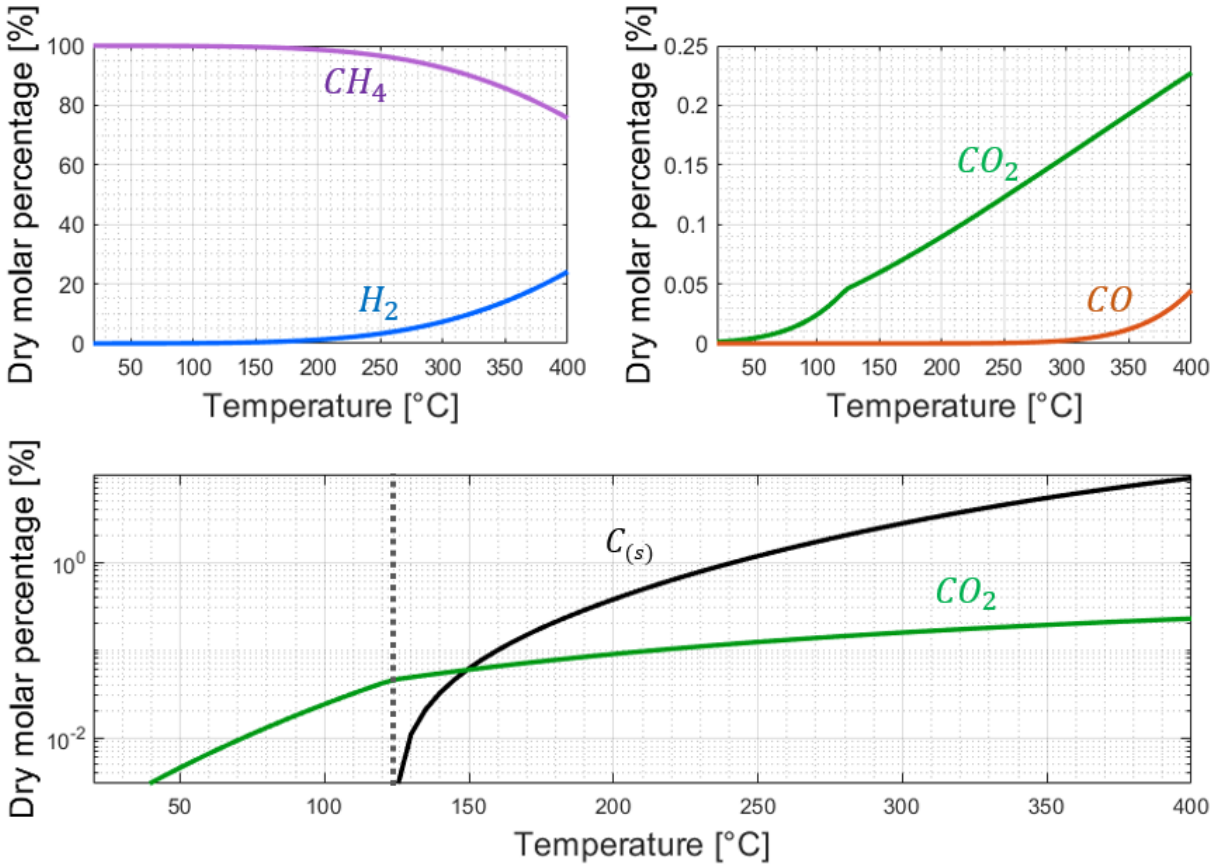

Figure 2.1: *Equilibrium molar percentages as a function of temperature. P = 1 bar and y^0 as in Table 2.1*

At temperatures below 250°C equilibrium trend shows that the maximum methane fraction is high, i.e., larger than 95%. Unfortunately, H_2 molar fraction is too high for the grid injection (see §1.5), and it is known that Nickel catalysts is not active in this temperature range. CO formation occurs for temperature exceeding 300°C, suggesting that DR (2.3) (favored by high methane inlet partial pressure) and reverse Boudouard (2.5) are only at high T (>300°C). Also, for temperatures larger than 330°C the methane and hydrogen molar percentages become, respectively, lower and larger than the initial ones (see Table 2.1), enlightening the effect of MCK (2.4) which becomes more relevant than the Sabatier reaction. For temperatures lower than 300°C, even though some CO is produced, it is consumed via CO methanation (2.4).

The inflection point at 130°C of the CO_2 profile should be related to the activation of side reactions consuming CO_2, since the slope of the curve decreases. It is also clear that the inflection point is

directly related to the beginning of solid carbon formation, therefore a possible explanation of this behavior of CO_2 profile is also due to the Boudouard reaction.

However, the identification of those side reactions is challenging: a possible method for their identification is based on the calculation of the moles of each species: Figure 2.2 shows the moles consumed or produced as a function of temperature.

As expected, the CO_2 consumption is almost constant for all the temperature range and leading to CO_2 molar fraction close to zero, as shown in Figure 2.1. On the other hand, methane is consumed at temperatures above 330°C whereas hydrogen is produced at temperatures larger than 380°C: this is possibly related to the effect of MCK but also to reverse CO_2 methanation, becoming the most relevant reaction at 330°C and of side reactions as RWGS (2.2) and DR, activating at these temperatures and leading to a small CO production.

Also, solid carbon formation is considered, confirming the activation of methane cracking at about 130°C and the importance of its effect at higher temperatures.

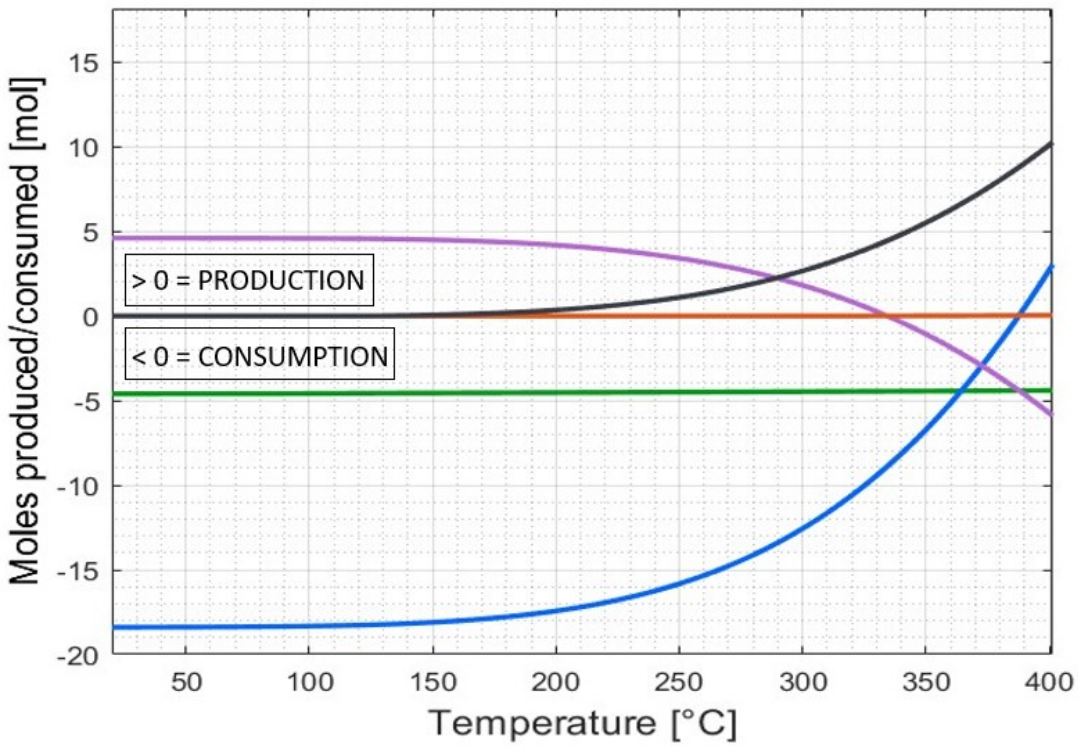

Figure 2.2: *Mole production and consumption at equilibrium considering 100 moles as an initial condition. P = 1 bar, y^0 as in Table 2.1. Positive values represent production of the species, negative values represent consumption of the species.*

H_2 and CO_2 conversion, represented in Figure 2.3, confirms that, for temperatures smaller than 150°C, the equilibrium of the Sabatier reaction is shifted towards the product, but also than at larger temperatures MCR activates, consuming CH_4 and producing H_2, therefore reducing H_2 conversion, up to 380°C when H_2 conversion drops to zero. Thus, hydrogen is produced, as already shown by Figure 2.2. Anyway, CO_2 conversion is larger than 94% for the whole temperature range: this is probably because of the effect of different reactions consuming carbon dioxide, particularly methanation at low temperatures and RWGS and reverse BOU higher temperatures.

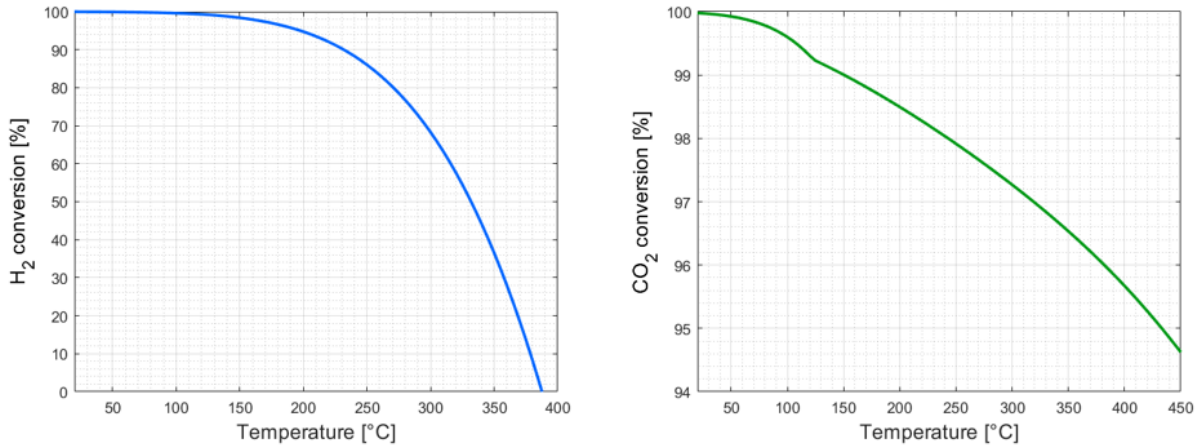

Figure 2.3: *CO_2 conversion at 1 bar on the left; H_2 conversion at 1 bar on the right. y^0 as in Table 2.1; n_{tot}^{in}=100 moles.*

2.2 Effect of pressure

For this study, the equilibrium has been calculated at 6 bar (absolute pressure of the experimental tests) for temperatures between 20°C and 450°C, as in the previous paragraph. As expected, the pressure has a positive effect on the methanation (see Figure 2.4): at the same temperature, the CH_4 fraction at 6 bar is higher than the one at 1 bar. In the catalyst activation range (250°C-300°C) the CH_4 molar fraction variation is: +2.5 percentage points (from 95% to 97.5%) at 250°C; + 3.5 percentage points (from 93% to 96.5%) at 300°C. This underlines the fact that a low temperature methanation (under 320°C, where the CH_4% is always above 90%), could be the best choice for a second stage reactor, to increase as much as possible the CH_4 production and, at the same time, to maximize H_2 conversion. This is related to a limited effect of MCK, which occurs with increasing number of moles, therefore it is disadvantaged by a higher pressure.

The pressure influences CO_2 molar fraction only at temperatures lower than 160°C, related to the effect on the Sabatier reaction. For temperatures larger than 160°C there is not any relevant difference because of the activation of side reactions leading to the production of carbon dioxide

already described. It is confirmed that, also increasing the pressure to 6 bar, the inflection point in the CO_2 profile is related to the production of solid carbon.

The production of CO is also limited, even though RWGS is not affected by the pressure, since, at higher pressures, DR is disadvantaged, CO methanation and BOU are enhanced. This also might be a consequence of the methanation favored at high pressure, that converts a larger amount of H_2 and CO_2 into H_2O and CH_4; H_2, CO_2 and H_2O are respectively the reagents and one product of the RWGS, so its equilibrium shifts to the left causing a reduction of the CO molar fraction at a given temperatures.

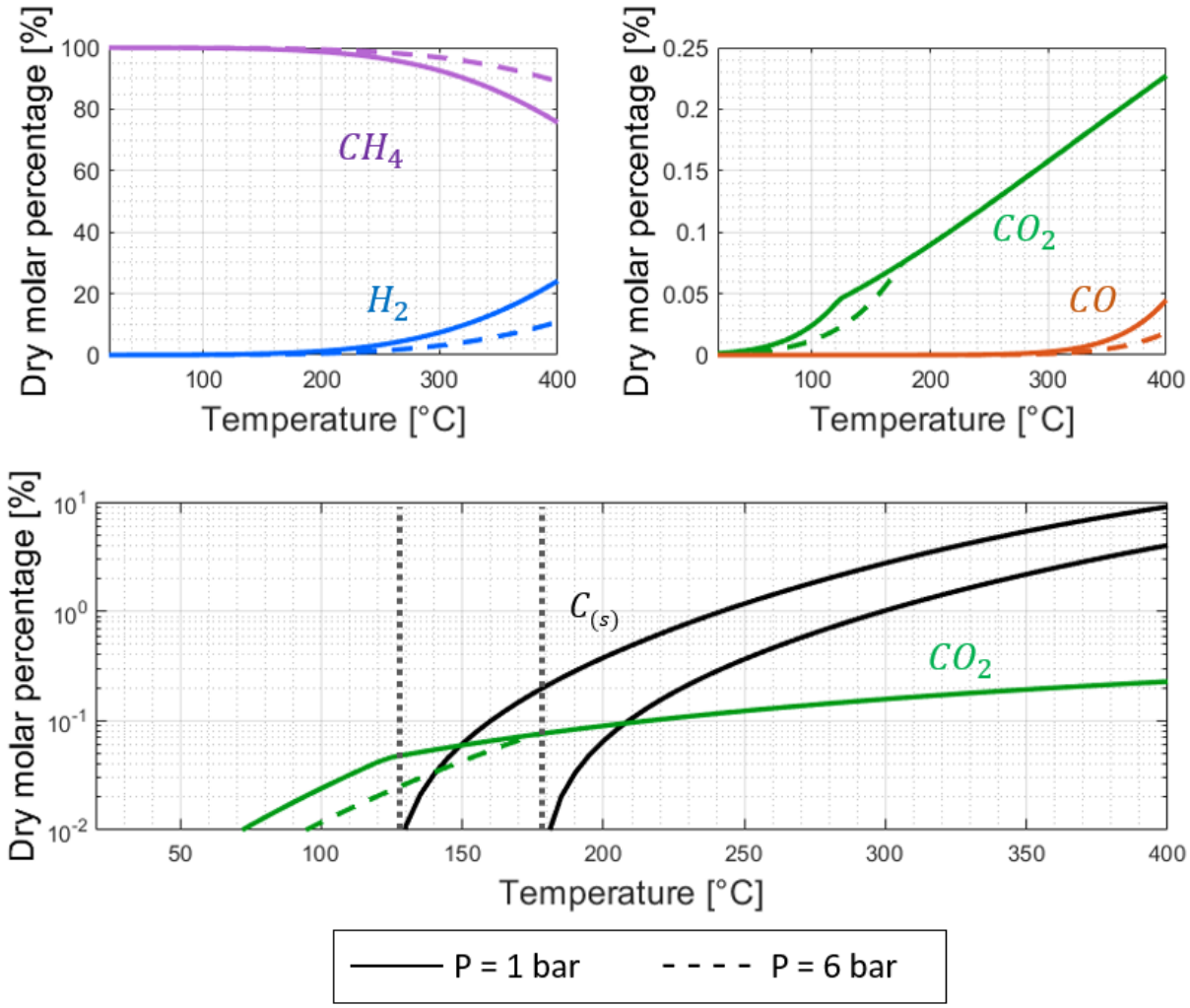

Figure 2.4: *Equilibrium molar percentages as a function of temperature. P = 1 bar and P = 6 bar; y^0 as in Table 2.1*

Figure 2.5, representing the moles of solid carbon formed at equilibrium, underlines how the methane cracking is limited by high pressures, particularly, carbon formation is shifted toward

higher temperatures (from 130°C at 1 bar to 175 °C at 6 bar) and the quantity decreases by more than 50% at any temperature, even though the trend is the same.

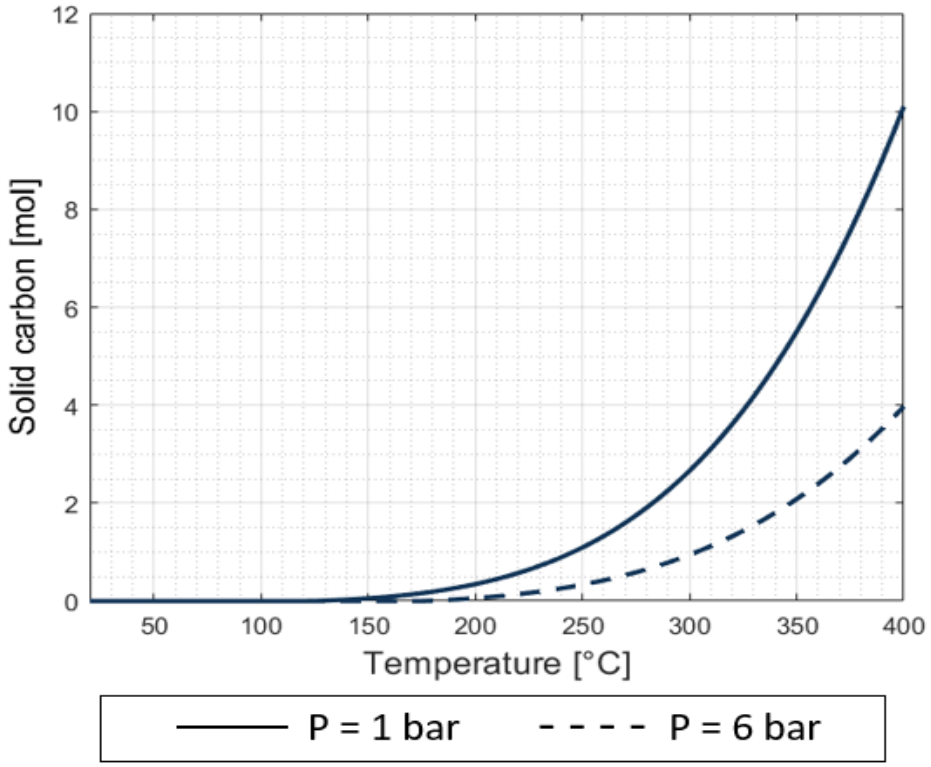

Figure 2.5: *Moles of carbon produced as a function of temperature. P = 1 bar, y^0 as in Table 2.1; n_{tot}^{in}=100 moles.*

Figure 2.6 compares the H_2 and CO_2 conversions trend at 1 bar and 6 bar. Particularly, in both cases the H_2 conversion is about 100% up to 140% and then starts decreasing, however, this decrease is much slower at high pressure. Moreover, at 6 bar and in the range of temperature considered, H_2 conversion never drops to zero, therefore no hydrogen no net hydrogen production due to side reaction occur. The CO_2 conversion at 6 bar, as expected, decreases with the temperature, showing a similar trend to that at 1 bar, particularly between 170°C and 270°C, where the values at different pressure are almost the same. However, the inflection point in the profile is shifted toward higher temperatures, confirming that, even though CO_2 consumption due to Sabatier reaction decreases with temperature, reactions consuming CO_2 (therefore reducing the decrease of its conversion) i.e., reverse Boudouard which activate at a larger temperature, since also the solid carbon formation is shifted to higher temperatures. Anyway, as expected from the values of molar percentage shown in Figure 2.4, the values of CO_2 conversion are larger than 94% in the whole range of temperature considered.

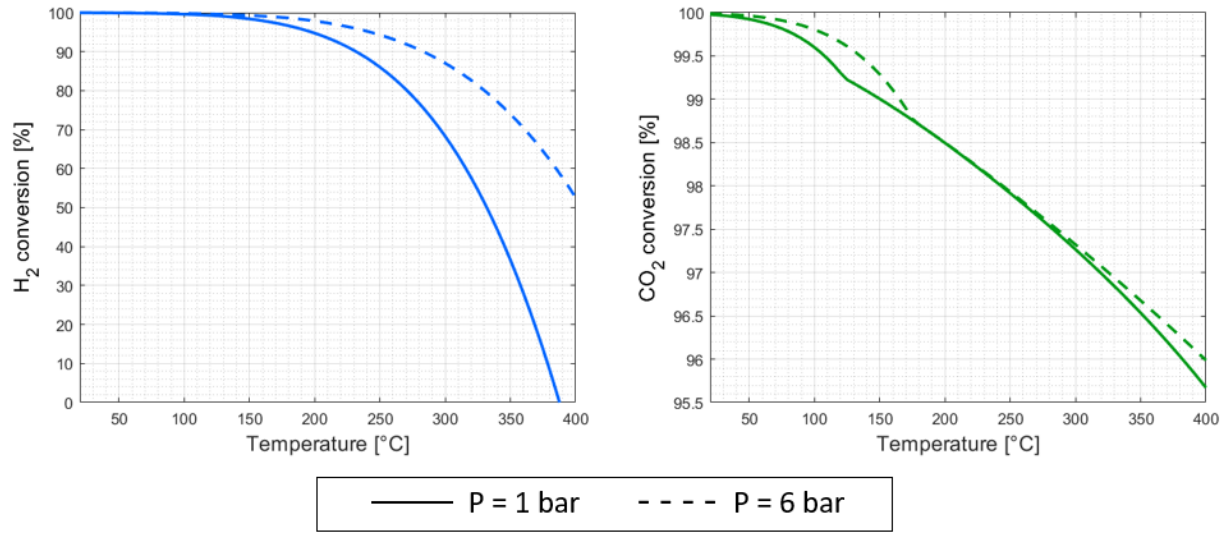

Figure 2.6: *CO_2 conversion at 1 bar and 6 bar on the left; H_2 conversion at 1 bar and 6 bar on the right. y^0 as in Table 2.1; n_{tot}^{in}=100 moles*

2.3 Comparison between equilibrium considering and not considering solid phase

In this section, the equilibrium without carbon formation is also accounted for. This means that reactions involving solid species (MCK, BOU, CGS) are neglected and the only database considered is GRI-Mech 3.0. The effect on the equilibrium composition is reported in Figure 2.7, representing the dry molar percentages as a function of temperature. Particularly, the CH_4 and H_2 percentage are, respectively, higher and lower than that obtained when carbon is considered: this is mainly related to the neglecting of methane cracking, which produces H_2 from CH_4. Consequently, the molar percentage of methane is about 100% up to 200°C (+50°C with respect to equilibrium considering solid carbon). Moreover, up to 300°C the ratio H_2/CO_2 equal to 4 is respected, therefore unwanted side reactions are not active. This is also confirmed by the absence of carbon monoxide, which starts forming at T > 300°C because of DR and RWGS. Also, the inflection point characteristic of the CO_2 profile in the case of carbon formation is absent, and the CO_2 molar percentage is much higher than that without considering solid carbon, underlining that the inflection point is related to reactions involving solid carbon and consuming CO_2: particularly, the Boudouard reaction respect these characteristics. However, no CO production is detected from 180°C (which is the temperature corresponding to the inflection point in the condition of Figure 2.7) to 250°C, probably because carbon monoxide is consumed by reactions such as CO methanation, a highly exothermic reaction favored at low temperature and high pressure.

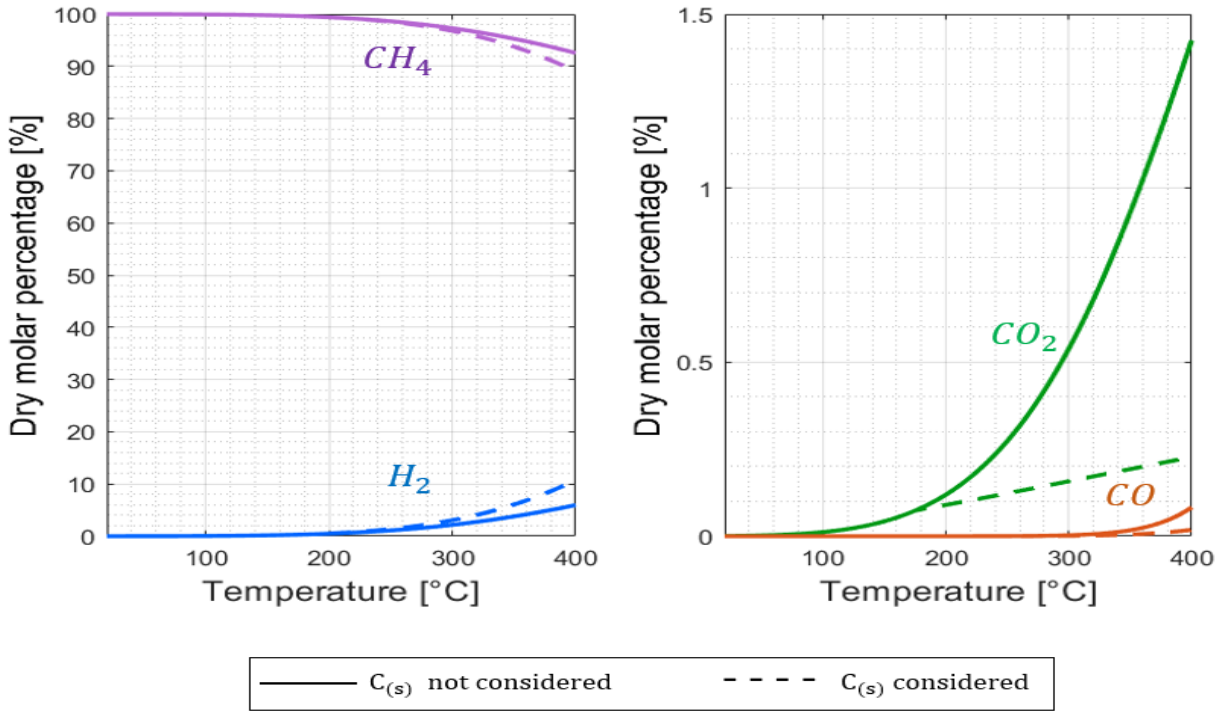

Figure 2.7: *Equilibrium molar percentages as a function of temperature. P = 6 bar and y^0 as in Table 2.1*

Figure 2.8 reports H_2 and CO_2 conversions. As expected, considering what has already been described for the molar percentages, the H_2 conversion is much higher when reactions involving solid carbon are not considered, since the effect of methane cracking is neglected. Differently, CO_2 conversion without considering solid carbon is smaller, since no carbon dioxide is consumed by reverse Boudouard at temperatures higher than 180°C.

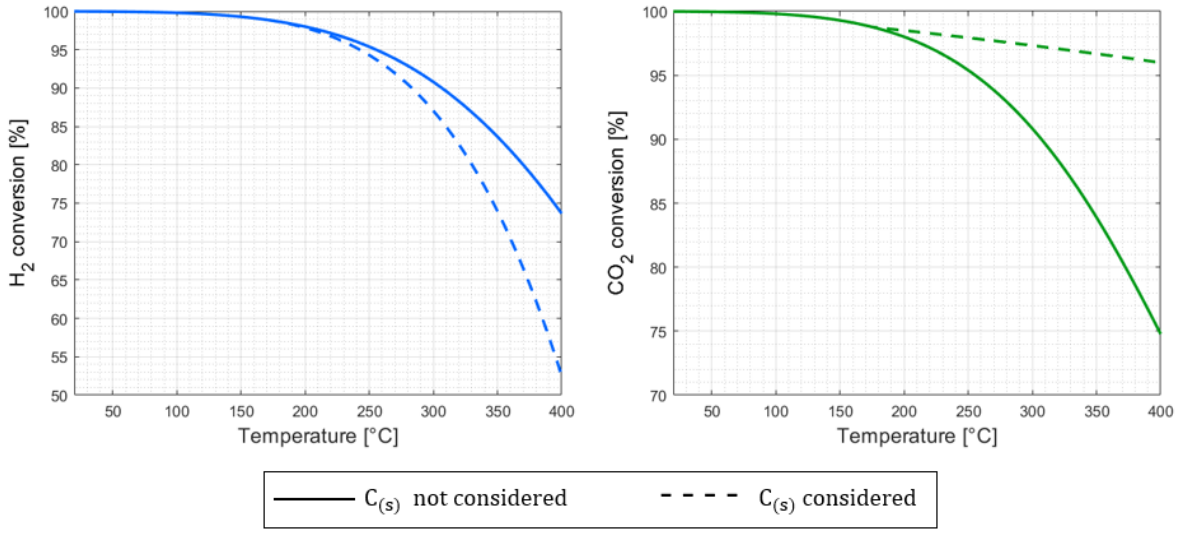

Figure 2.8: *CO_2 conversion at 6 bar on the left; H_2 conversion at 6 bar on the right. y^0 as in Table 2.1; n_{tot}^{in}=100 moles*

2.4 Effect of water vapor in the initial mixture

In this section, the effect of different inlet water vapor molar percentage is studied, particularly to evaluate its effect on carbon deposition. 100 moles of dry inlet mixture have been considered for the calculation. However, the real number of moles depends on the inlet water vapor molar percentage (see Table 2.2).

Table 2.2: Correspondence between water vapor molar fraction and the moles considered.

Inlet water vapor molar percentage [%]	Moles of inlet mixture [mol]
0	100
10	111.11
20	125
40	166.67

Figure 2.9, representing molar percentages of single components at equilibrium, underlines how increasing the water vapor inlet vapor molar percentage disadvantages the Sabatier reaction being a reaction product. Particularly, considering a 20% H_2O at 305°C the CH_4 molar percentage decreases by about 3%, CO_2 molar percentage increases by about 1%, whereas the effect on CO and H_2 molar percentages is not relevant, with only slight increase in their molar percentages, even if this is not true considering 40% H_2O at 305°C, where. Moreover, it also influences the temperature at which the inflection point in the CO_2 profile occurs, shifting it towards higher temperatures.

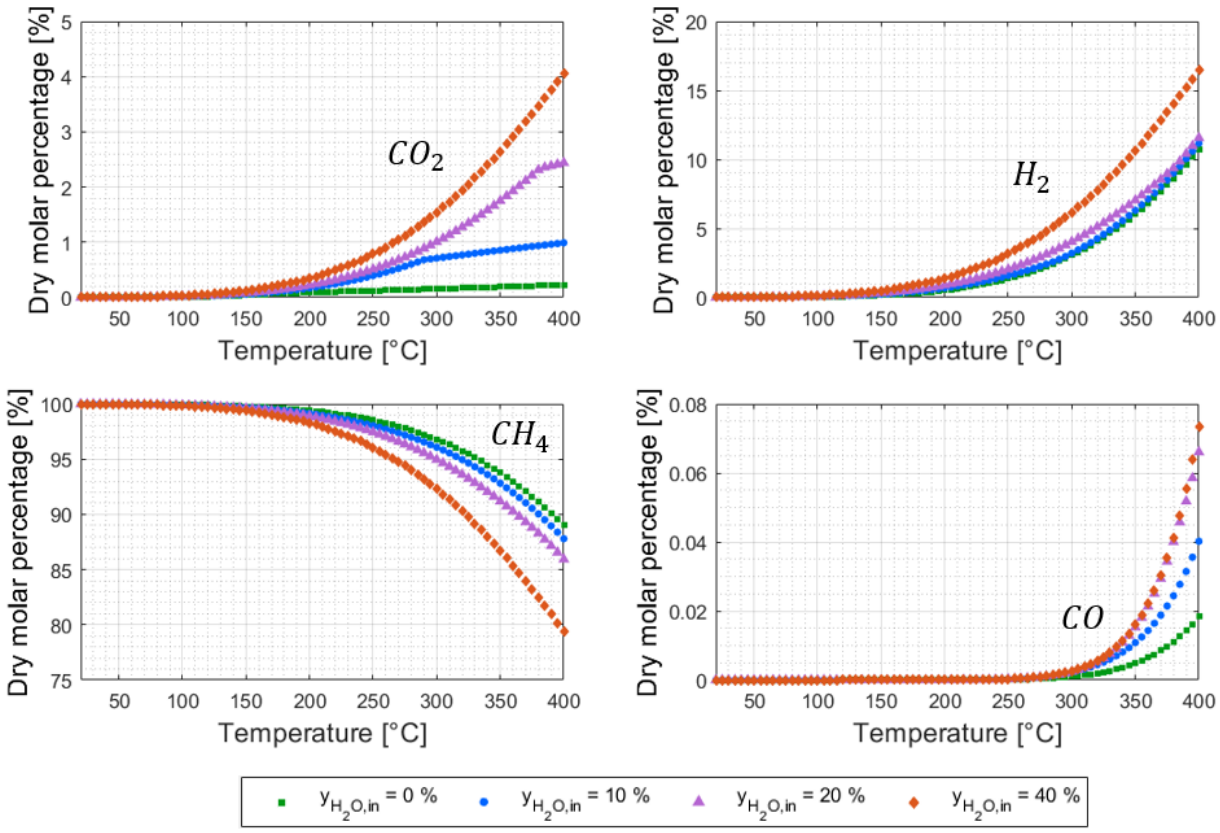

Figure 2.9 *Equilibrium molar percentages as a function of temperature. P = 6 bar; y^0_{dry} as in Table 2.1; y^0_{H2O} as in Table 2.2.*

More relevant is the effect of water vapor on solid carbon formation. Figure 2.10 underlines how increasing the inlet water vapor molar fraction the quantity of solid formed diminishes. Also, the temperature at which carbon produced via methane cracking is not consumed increases with respect to the case without any water addition to the feed (+100°C for 10% H_2O inlet molar percentage, +230°C for 20% H_2O inlet molar percentage). This effect is due to carbon gasification CGS (2.6) and should also explain the increase in CO and H_2 molar percentages, since they are product of this reaction. Particularly, with a 40% H_2O inlet molar fraction, no solid carbon is expected up to 400°C.

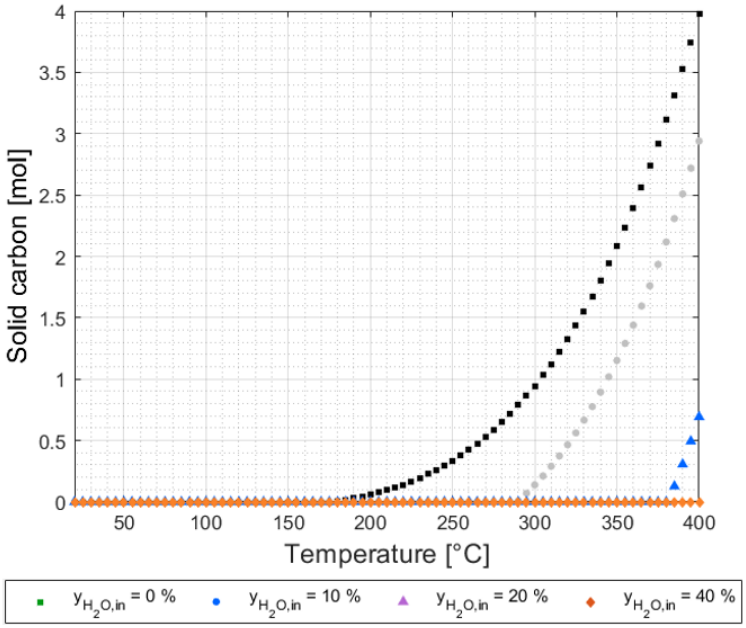

Figure 2.10: *Moles of carbon produced as a function of temperature. P = 6 bar; y^0_{dry} as in Table 2.1; y^0_{H2O} and n^{in}_{tot} as in Table 2.2.*

Figure 2.11 shows the H_2 and CO_2 conversions, particularly, as expected from the H_2 molar percentage, the addition of water vapor in the inlet mixture has only a scarce effect on its conversion, reducing it only by few percentage points at each temperature considered. Moreover, the effect on CO_2 conversion is much more relevant. However, both the conversions are about 100% up to 150°C because of the effect of Sabatier reaction and then starts decreasing when methane cracking and other side reactions activates.

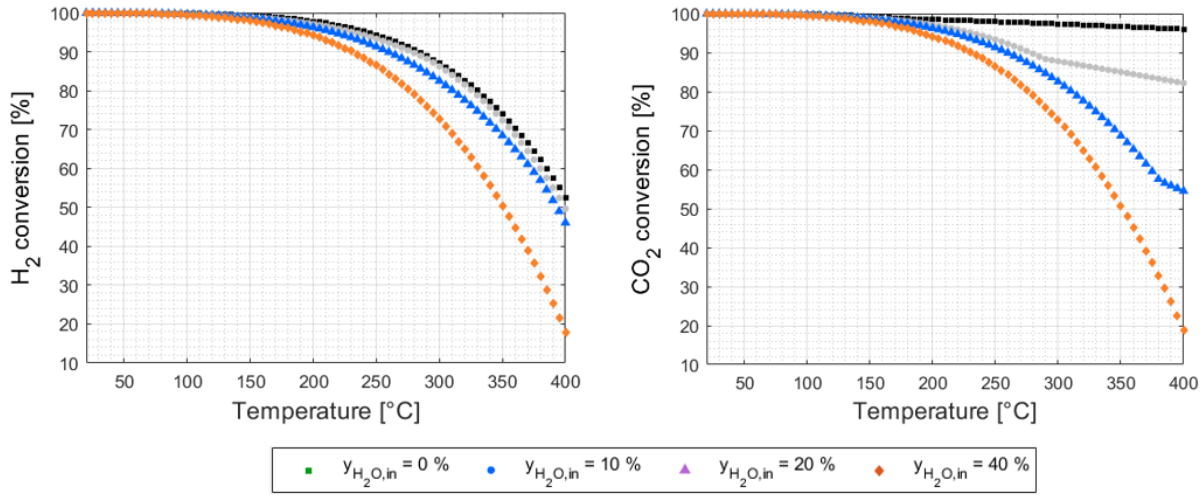

Figure 2.11: *CO_2 conversion at 6 bar on the left; H_2 conversion at 6 bar on the right. P = 6 bar; y^0_{dry} as in Table 2.1; y^0_{H2O} and n^{in}_{tot} as in Table 2.2.*

According to these results, the inlet water vapor molar percentage for the experimental tests is chosen to be 20%, since it offers a best compromise between the limitation on solid carbon formation and the effect on the dry outlet molar fraction. Particularly, the equilibrium molar percentage at 6 bar and 305°C (thus at the condition experimental tests are performed) are reported in Table 2.3. It is important to notice that the CO_2 and CO molar percentages respect the Italian grid injection requirements. However, H_2 molar percentage is higher than that allowed, but in line with the experimentation carried out by Snam (Società Nazionale Metanodotti) to allow 5% of H_2 in the biomethane pipelines (see Chapter 1.4).

Table 2.3: *Equilibrium dry gas composition at test conditions (305°C, 6 bar).*

y_{CH_4} [%]	y_{H_2} [%]	y_{CO_2} [%]	y_{CO} [%]
94.64	4.29	1.07	<0.01

Also, with this molar percentage, it is possible to use tower water as a refrigerant in the inter-stage condenser, since the condensation temperatures of water, required to have a 20% inlet molar percentage to the second methanation stage, are equal to 60°C and 109°C, respectively when condensation is performed at 1 bar and 6 bar.

Chapter 3

Experimental plant, procedures, methods

In this chapter, all the instruments and the methodologies used to carry out the experimental tests will be described. The entire experimental campaign has been carried out in a hood for safety reasons.

3.1 Experimental set-up

The experimental set-up used to carry out the experimental campaign is formed by:

- A gas feed section.
- A reaction section, where a fixed bed reactor has been assembled.
- An analytical section.

The pressure is regulated by a back-pressure manual regulator (BP) which throttles the gas upstream of the analytical section. The lines from the gas tanks to the mass flow controllers (MFCs) are made of stainless steel whereas all the other lines are made of polyamide 12 (PA12). All the seals have been tested up to 7 bar. The real plant used to carry out the experimental tests is reported in Figure 3.1 whereas the real plant used to carry out the tests is shown in Figure 3.2.

Figure 3.1: *Experimental set-up*

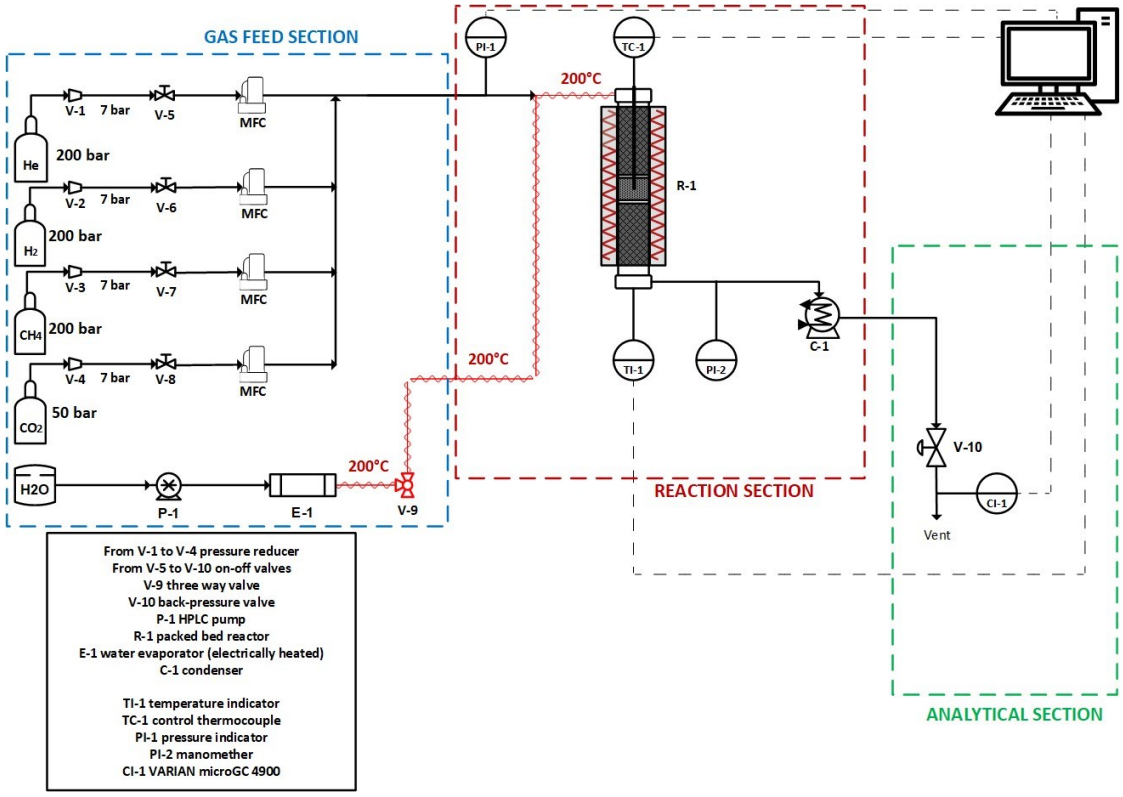

***Figure 3.2**: Scheme of the experimental setup*

3.1.1 Feed gas section

The mixtures used for the experimental tests are composed of synthetic gases coming from bottles at 200 bar or 50 bar. There are two steps of pressure reduction: the first one on the top of bottles themselves and the second one through the manual pressure reducer upstream the flow controllers. The on-off valves, before each MFC, can be closed, if necessary, to isolate the reactor from the reagent mixture.

The flowrate of each gas (CH_4, CO_2, H_2 and He) is controlled through a mass-flow controller (see Figure 3.1). A mass flow controller incorporates a sensor that measures the amount of mass flow and generates an electrical output signal directly proportional to the mass flow rate. Based on the intensity of the signal, the PID action implemented opens the valve to settle the flow at the required setpoint. The MFC's were calibrated periodically. N_2 was used as calibration gas for all MFC; then the corrective factors, specific for every gas and available in the manufacturer's instructions [43],

were applied. The flowrates were controlled with a bubble flowmeter before each TPR-catalytic activity test-TPO cycle. The gas flowrates from MFCs are mixed in a T fitting and then fed to the reactor.

Steam has been produced employing an evaporator. This consists in a series of steel pipes (OD = 1/8") electrically heated by means of OMEGALUX® FGR series electrical heating cables. Temperature is controlled by a thermoregulator; the value imposed was 200°C to ensure a complete water vaporization at 6 bar, considering a maximum steam percentage of 20% in the feed mixture (see §2.4 for details). The liquid water is sent to the evaporator using an HPLC Shimadzu LC-20AD. The instrument is capable of feeding liquids with a high precision from 1 μl/min to 10 ml/min with a pression between 1 and 70 bar, and the flowrate of liquid water to have a 20% in the feed mixture is of 43 μl/min.

3.1.2 Reaction section

The catalytic tests at atmospheric pressure were carried out in a tubular plug-flow reactor consisting of quartz tube with an internal diameter of 8mm. The catalyst was loaded inside the tube in a fixed-bed configuration. The bed was supported by a layer of quartz wool and a second layer is placed above the bed, to uniform the flux of reactant achieving an almost plug flow configuration, before entering the catalytic bed.

The catalytic tests at high pressure were carried out in a tubular plug-flow reactor (see Figure 3.3) consisting of an Inconel tube (a steel alloy enriched in nickel) with an internal diameter of 12mm. The catalyst was loaded inside the tube in a fixed-bed configuration. The bed was supported by a layer of quartz wool placed from the bottom of the reactor to the catalyst bed and a second layer is required to uniform the flux of reactant achieving an almost plug flow configuration before entering the catalytic bed, as in the atmospheric tests.

The design of these two reactors is reported in Table 3.1.

The schemes of the two reactors are reported in Figure 3.3, where ID and OD indicate, respectively, the internal and external reactor diameters, h_{bed} is the height if the catalytic bed, h_{w1} and h_{w2} represent, respectively, the heigh of the quartz wool layer downstream and upstream the catalyst.

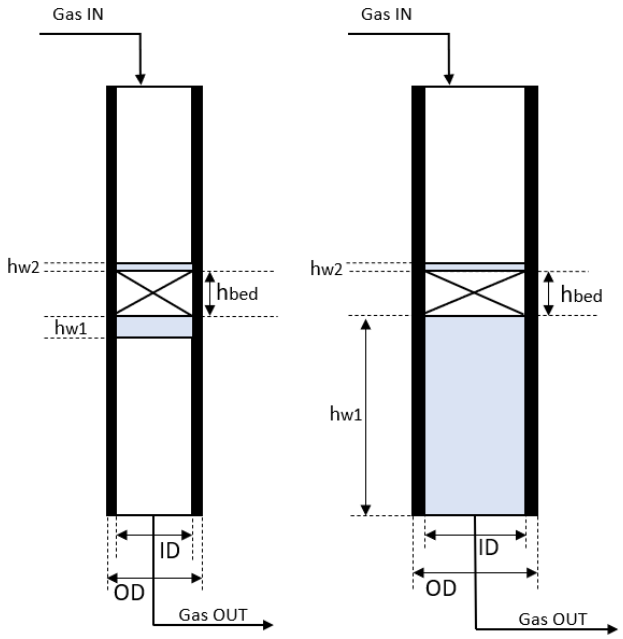

Figure 3.3: *Scheme of the quartz reactor (left) and of the Inconel reactor (right)*

Table 3.1*: Reactors design*

Reactor type [-]	ID [mm]	OD [mm]	h_{bed} [mm]	m_{cat} [mg]	h_{w1} [mm]	h_{w2} [mm]
Quartz	8	10	10	639.7	10	2
Inconel	12	16	7	993.4	60	2

The reactor was arranged into a tubular furnace (Watlow ceramic fiber heater) consisting of two ceramic heating elements which can supply a maximum power of 440W. Temperature is controlled by an OMRON E5CC thermoregulator (PID controller), through the software CX-Thermo, to establish the desired thermal profile inside the reactor. It allows to work with ramp up/down or through isotherms. Other temperatures have been collected during the tests, as described above, via a dedicated MATLAB® executable file. The monitoring and the control of the temperatures have been done with 2 configurations:

- For the atmospheric tests two K-type thermocouples have been mounted inside the reactor. The thermocouple for oven control (OD = 1/8”) was placed below the catalytic bed whereas a monitoring thermocouple (OD = 1/16”) was placed in the center of the packed bed to understand the thermal effect of the reaction;
- Also, for the high-pressure tests two K-type thermocouples have been employed. The control thermocouple (OD = 1/16”) was mounted in the center of the catalyst bed whereas

the monitoring thermocouple (OD = 1/8”) was placed within the quartz wool layer below the catalytic bed to obtain the gas temperature measurement.

Two different pressure transducers have been installed:

- A Sensor Technics CTE9020GN0 series for the pressure tests
- A Honeywell MPX5500 for the atmospheric tests

The first measures the pressure at the top of the reactor while the second measures the pressure drops between the reactor top and bottom. Both the transducers output signal is acquired by a Picolog data logger, and the sensors were calibrated before the beginning of the experimental campaign. The scheme used to calibrate the pressure transducer is shown in Figure 3.4. The first point of the calibration line, corresponding to the background electric signal was collected without flux, then a flux of air or nitrogen was used. From the manometer the value of the relative pressure was manually collected, whereas the electric signal generated by the pressure transducer was collected with Picolog data logger. Manually closing the back pressure valve (BKV) the pressure increase; when the electric signal became stable, also the value of the relative pressure was obtained. Thus, collecting couples of electric signal-relative pressure points the calibration line were built.

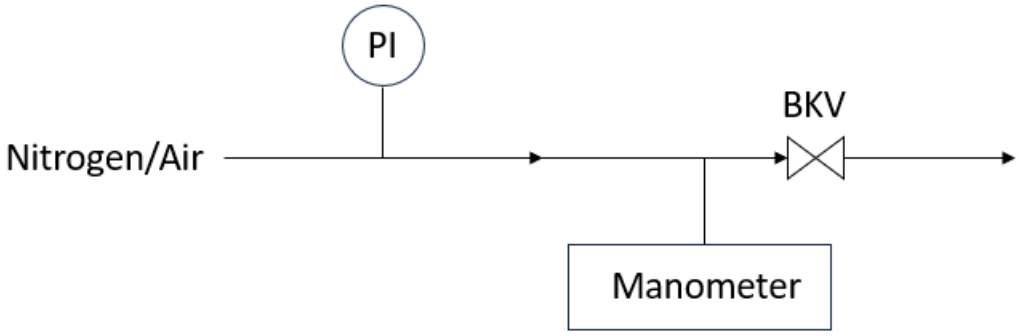

Figure 3.4: *Scheme for pressure transducers calibration.*

Methanation and RWGS lead to the formation of water, that for large quantities can be difficult to measure precisely (e.g., with gas-chromatograph) but also creates disturbances in the pressure regulation achieved with the back pressure valve. For these reasons, the water is separated through a condenser. In the external jacket, a refrigerating liquid (mixture of water and glycol) flows

continuously, whose temperature is maintained at 5°C by a chiller Desktip Low Temperature Circulator CCA-1111.

After the condenser the back-pressure manual regulator allows progressively to increase the pressure in the reactor throttling the gas upstream of the analytical section.

3.1.3 Analytical section

The gaseous mixture from the reactor output, after depressurization, is continuously analyzed through a micro-GC Varian CP-4900 (see Figure 3.5).

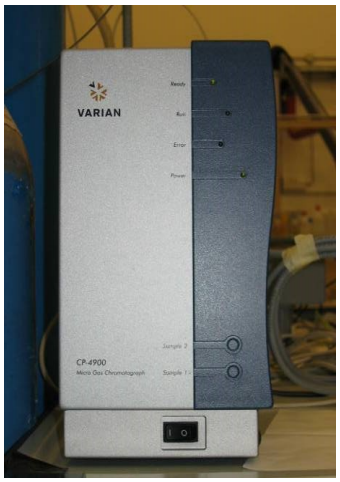

Figure 3.5: *Varian CP4900 micro-GC*

The sampling is performed by means of a membrane pump, inside the instrument, which sends part of the product mixture to the columns passing first from the injector, as enlightened in Figure 3.6.

Two columns, arranged in a parallel configuration, and preceded by a pre-column are installed:

- Capillary column Porapak Q (PPQ, on channel 1) used to separate and analyze light hydrocarbons and components such as H_2O and CO_2;
- Capillary column Molsieve 5Å (MS, on channel 2) capable of separating permanent gases such as H_2, O_2, Ar, He, N_2, CO but also CH_4. This column is irreversibly damaged by CO_2 and H_2O since they chemically interact with aluminum silicates acting as molecular sieves;
- The pre-column, a Parapak type, is required to achieve a first separation between the mixture components before the MS column, avoiding the presence of components such as H_2O and CO_2 in the MS column, according to the backflush system (BF). The BF consists in an inversion of the flux of carrier, as shown in Figure 3.7, occurring at a specific time

imposed by the user. This time is chosen to allow permanent gases (whose have lower residence time in the pre-column) to enter the MS column and to avoid the entrance of H_2O and CO_2, that will be entrained within the backflush flow, since they have larger residence time in the pre-column than that of permanent gases and methane.

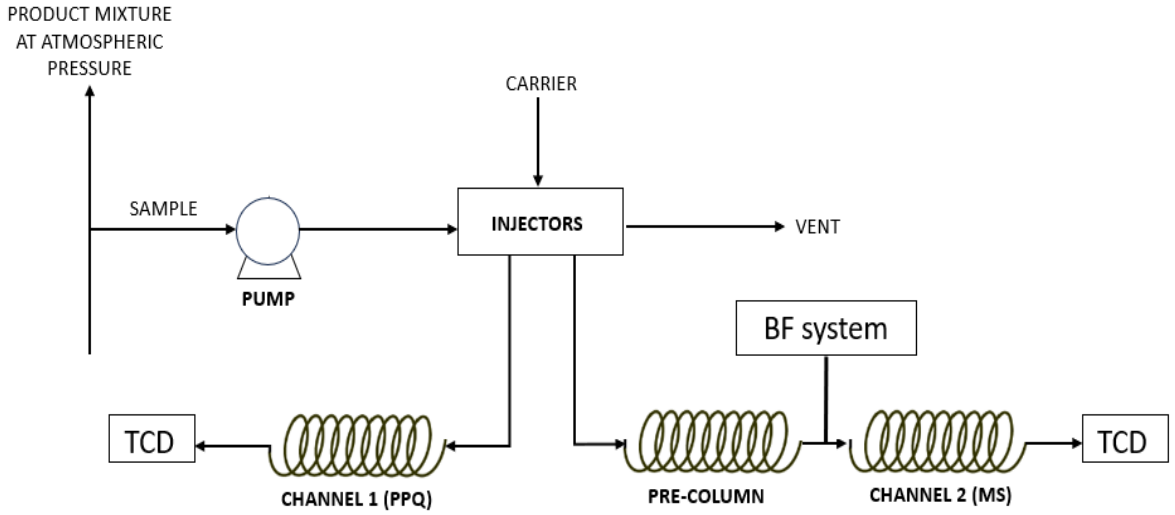

Figure 3.6: *Scheme of Varian CP4900 micro-GC*

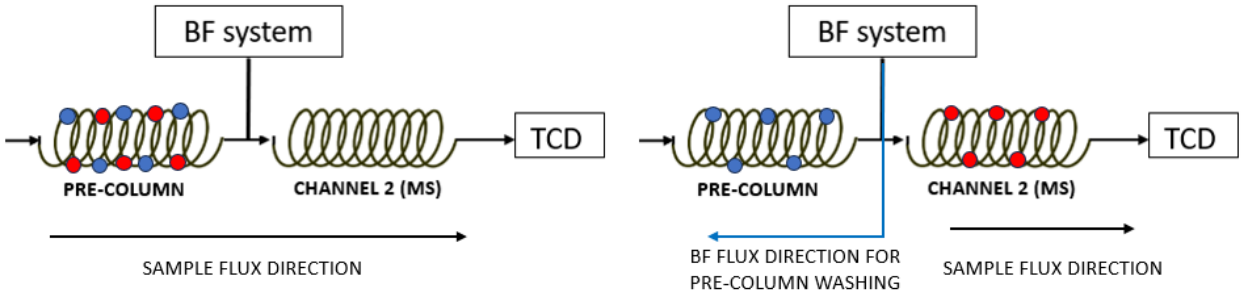

Figure 3.7: *Scheme of the backflush system. BF not activated (left) and BF activated (right)*

Finally, at the end of each column (MS and PPQ), a thermal conductivity detector (TCD) is installed and maintained at 180°C, to produce the chromatogram corresponding to the sample mixture composition. The TCD produces a signal proportional to the difference in thermal conductivity between the carrier and the species contained in the sample that have been separated within the columns.

The choice of the carrier is very important with the TCD: even though from Table 3.2 the best choice seems to be Helium (since it has a large difference in thermal conductivity with CH_4, CO_2 and CO), Argon has been chosen as carrier, to avoid issues related to H_2 peak integration due to the micro-GC software. Particularly, the software is not able to integrate peaks negative peaks, as in the case of mixture with H_2 content lower than 7.5% and using He as gas carrier.

Table 3.2: *Thermal conductivities at 180°C [44]*

Species	Thermal conductivity [W/m/K]
He	0.23588
H_2	0.24654
Ar	0.02463
CH_4	0.05816
CO	0.03194
CO_2	0.02896

To be sure to detect also small concentrations of CO_2 and to be capable of detecting variation in CH_4 concentrations, a specific sensibility analysis has been performed, considering the range of CH_4 and CO_2 molar percentages involved in the experimental tests (see Figure 3.8). Particularly, also with Argon employed as a carrier, small molar percentages of CO_2 are detected, also below the limit for the injection grid (see Chapter 1.5).

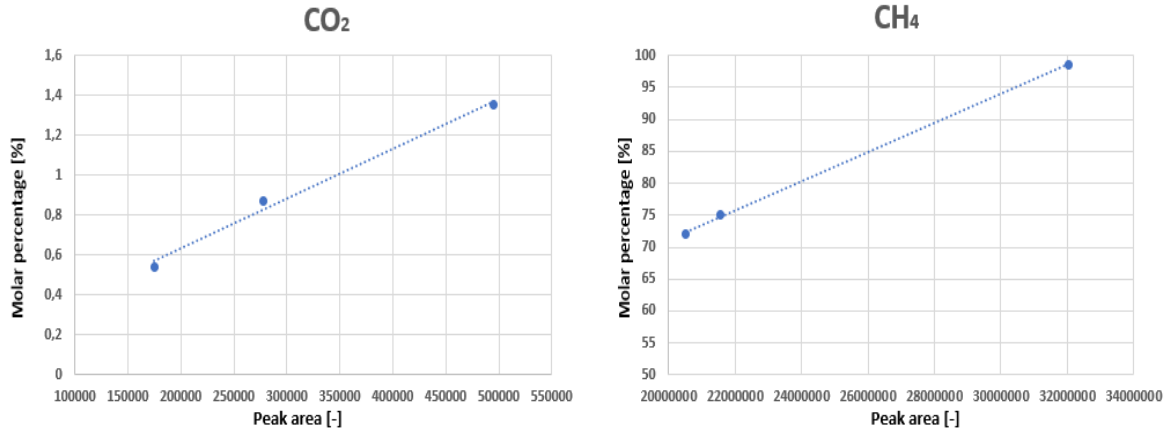

Figure 3.8: *results of the sensitivity analysis for CH_4 and CO_2*

The species which have been separated and quantified are CH_4, He, CO_2, H_2 and CO. The analytical method optimized for the gas mixtures compositions is reported in Table 3.3.

Table 3.3: *GC method for methanation mixture*

Parameter	Value, column MS	Value, column PPQ	Unit
Temperature	40	40	°C
Injection Temperature	40	40	°C
Pressure	200	50	kPa
Sampling time	20	20	sec
Injection time	20	20	msec
Stabilization time	5	5	sec
Backflush time	5	-	sec

These parameters influence the separation between the mixture components but also the aging of the columns. The method is the same for all the types of tests, the only varying parameter is the duration of the measurement, therefore the sampling frequency, reported in Table 3.4.

Table 3.4: *Sampling frequency for different type of tests*

Test type	Measurement time [min]	Sampling frequency x10^3 [Hz]
Temperature Programmed Reduction (TPR)	1.417	11.76
Temperature Programmed Oxidation (TPO)	3.417	4.878
Catalyst Activity Test	3.417	4.878
Coke formation stress-Test	10.417	1.176

The calibrations of the instrument have been performed periodically. An example of a typical chromatogram obtained during the calibrations, simulating a products mixture, done before starting with the experimental tests, is shown in Figure 3.9. The values in mV are referred to the TCD signal. The composition corresponding to the chromatogram represented in Figure 3.7 is reported in Table 3.5.

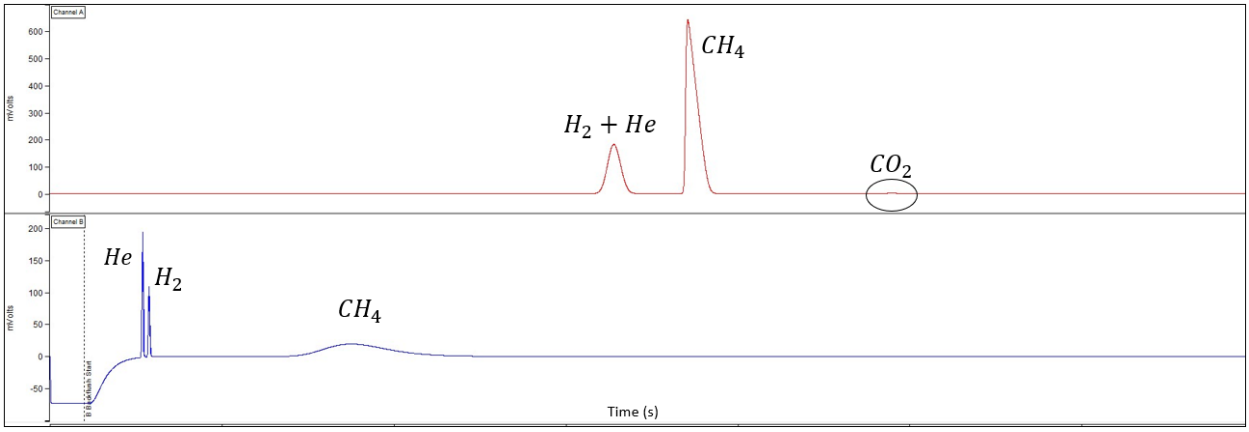

Figure 3.9: *Example of chromatogram representing a product mixture, with composition show in Table 3.5.*

	CH_4	CO_2	H_2	He
Molar fraction [%]	90.36	1.01	2.43	6.20

The main issue of the micro-GC is related to the aging of MS column: the separation capability of the instrument decreases with time, starting from the last conditioning, which is a treatment at maximum pressure and temperature (180°C, 250kPa), maintained for 6-8 hours, to clean the columns. Particularly, as the number of measurement increases, the retention time of He and H_2 become progressively closer to each other, thus not respecting the calibration anymore. Therefore,

to avoid this, frequent GC conditionings are required. It has been proved that the GC calibration is still effective after a conditioning treatment (see Figure 3.10). It is also possible to notice that after 5 measurements, the TCD signal is stable for all the species of the mixture considered, corresponding in terms of molar percentages to the dry mixture fed to the reactor (see Chapter 3.2, Table 3.6).

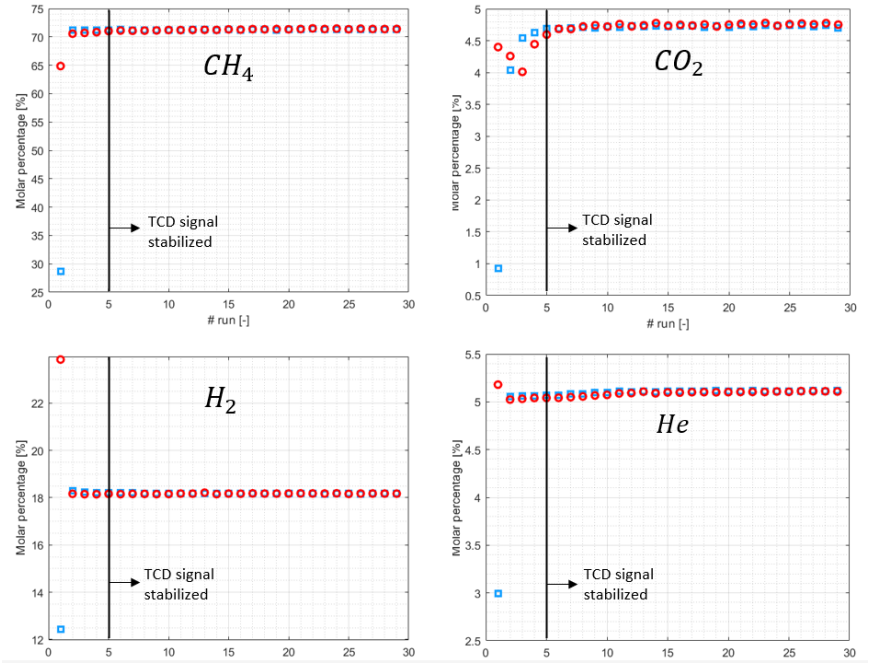

Figure 3.10: *Molar percentages before and after micro-GC conditioning, calculated using the same calibration curves.*

For each of the four components, after signal stabilization is achieved, the relative error, defined as in Equation (3.1), thus considering the difference in molar fractions between those obtained pre-conditioning and post-conditioning, has been calculated and reported in Table 3.5.

$$Er = 100 \cdot \left| \frac{y_i^{pre\_cond} - y_i^{post\_cond}}{y_i^{pre\_cond}} \right| \quad [\%] \qquad (3.1)$$

It is important to underline that molar fractions were used instead of molar percentages, to avoid misunderstanding related to the unit use to express them: while fractions are dimensionless number, the relative error is multiplied by a factor of 100, to obtain a percentage value.

Table 3.6: *Relative error for the mixture components as expressed in equation 3.1.*

	CH_4	CO_2	H_2	He
Relative error [%]	0.0667	0.5166	0.0199	0.1949

3.2 Experimental procedures

The experimental tests performed in this work are the following:

A. TPR on fresh catalyst or after TPO.
B. Coke formation long-duration test, at atmospheric and high pressure, with and without water in the inlet mixture to the second-stage reactor.
C. TPO on catalysts bed, after each catalysts aging test.

To simulate a real second stage industrial process, the composition of the inlet mixture is chosen starting from previous thesis results [21,22], particularly obtained from a first stage carried out at 1 atm and 300°C with the same catalyst used for experimental tests, therefore avoiding any relevant by-product (e.g., CO) formation. Depending on the test, total or partial water condensation before the second-stage reactor is assumed. Besides these main components, a small quantity of He or Ar (5% in the mixture) has been added as tracer, for the calculation of the total outlet molar flowrate (3.4), expected to be lower compared to the inlet total flowrate. The experimental dry feed mixture composition always used for the catalyst activity tests is reported on Table 3.7.

***Table 3.7**: Reagent dry mixture composition*

y_{CH_4} [%]	y_{CO_2} [%]	y_{H_2} [%]	y_{He} [%]
72.0	4.6	18.4	5.0

A summary of all the tests performed with their respective conditions is shown in Table 3.8.

***Table 3.8:** Summary of the tests performed with the respective conditions.*

Test	Reactor type	Catalyst tested	Dry mixture composition	Pressure [bar]	WHSH tested $\left[\frac{ml}{mg_{cat}h}\right]$	Temperature program
Blank Test	Inconel	-	72.0% CH_4 18.4% H_2 4.6% CO_2 5% Ar	6	Not defined (no catalyst)	Heating 10°C/min up to 305°C
TPR	Inconel Quartz	EX11914	5% H_2 95% Ar	1	12.08	Heating 5°C/min up to 600°C
Atmospheric pressure tests	Quartz	EX11914	72.0% CH_4 18.4% H_2 4.6% CO_2 5% Ar	1	14.27	Heating 10°C/min up to 280°C

High pressure tests	Inconel	EX11914	72.0% CH_4 18.4% H_2 4.6% CO_2 5% Ar	6	14.27	Heating 10°C/min up to 305°C
High pressure tests with water vapor	Inconel	EX11914	72.0% CH_4 18.4% H_2 4.6% CO_2 5% Ar	6	12.08	Heating 10°C/min up to 305°C
TPO	Inconel Quartz	EX11914	5% O_2 95% Ar	1	Not calculated	Heating 5°C/min up to 700°C

3.2.1 Catalysts and WHSV

The same commercial Ni/Al_2O_3 catalysts (EX11914) provided by Clariant employed in [21,22] was used for all the experimental campaign. The actual chemical composition and the density of both the catalysts have not been provided. A specific granulometric class between 112μm and 150μm has been selected to have comparable results with those of previous work done by [21,22].

A typical parameter used in literature, related to the total inlet gas flowrate, is the gas hourly space velocity (GHSV, equation 3.2). From the industrial point of view, high values of GHSV could be preferred to use less catalysts and operate at large flowrates; however, in this process, where the biogas is produced from the anaerobic digestion of some feedstock, also low GHSV could be of interest, since the inlet flowrates can be quite low.

$$\text{GHSV} = \frac{\dot{V}_{standard\ conditions}}{V_{bed}}\ [h^{-1}] \tag{3.2}$$

However, to compare tests done in different setups and/or with different pressures, the usage of WHSV, which is based on the mass of catalysts, is preferred, since the volume of catalyst is not easy to reproduce, being dependent on the reactor mounting but also on the pressure. Thus, GHSV is an unreliable parameter and cannot be used to compare tests made at different operating conditions. Thus, weight hourly space velocity (WHSV) has been used instead. This measure is related to the catalyst mass instead of packed bed volume, making the tests at different pressure and with different reactors comparable.

$$\text{WHSV} = \frac{\dot{V}_{standard\ conditions}}{m_{catalyst}}\ \left[\frac{ml}{mg_{cat}h}\right] \tag{3.3}$$

All the experiments were performed at WHSV = 14.27 $\frac{\text{ml}}{\text{mg}_{\text{cat}}\text{h}}$; the corresponding GHSV, as a function of reactor used (quartz or Inconel), are shown in Table 3.9.

Table 3.9: Correspondence between GHSV and WHSV for different reactor design

Reactor type [-]	WHSV $\left[\frac{\text{ml}}{\text{mg}_{\text{cat}}\text{h}}\right]$	Bed apparent density [kg/m^3]	GHSV [h^{-1}]
Quartz	14.27	1273	18160
Inconel	14.27	1255	17906

3.2.2 Processing of experimental data

The experimental data obtained by the analytical instruments were processed with tailored scripts written with MATLAB®, that allows to easily obtain the match between the compositions, the temperatures, the time and the pressure, the quantification of conversions, selectivities and atomic balances, such as other variables as reported in Chapter 4. The script for the methanation tests used on MATLAB® can open the files .txt from Varian micro-GC and read the values of each area associated to a single component; open and read files .dat from the MATLAB® executable for the monitored temperature, files .txt from CX-thermo for the control temperature and file .csv from Picolog for the pressure measurements. The total molar flowrate exiting from the reactor has been calculated through the steady state He balance (3.4 and 3.5). The inlet and the outlet He molar fraction are obtained from Varian micro-GC; the measure is done at atmospheric pressure and at the same temperature, therefore, under the assumption of ideal gas mixture, there are no difference between molar and volumetric fraction.

$$\dot{n}_{tot}^{IN} y_{He}^{IN} - \dot{n}_{tot}^{OUT} y_{He}^{OUT} = 0 \tag{3.4}$$

$$\dot{n}_{tot}^{OUT} = \frac{\dot{n}_{tot}^{IN} y_{He}^{IN}}{y_{He}^{OUT}} \tag{3.5}$$

Then, for each species except the tracker, the flowrate can be computed according to (3.5), where the species molar fraction are the result of the chromatographic analysis.

$$\dot{n}_{i}^{OUT} = y_i \cdot \dot{n}_{tot}^{OUT} \tag{3.5}$$

The CO_2 and H_2 conversion (3.6 and 3.7), can then be calculated as follows.

$$X_{CO_2} = 1 - \frac{\dot{n}_{CO_2}^{OUT}}{\dot{n}_{CO_2}^{IN}} \tag{3.6}$$

$$X_{H_2} = 1 - \frac{\dot{n}_{H_2}^{OUT}}{\dot{n}_{H_2}^{IN}} \tag{3.7}$$

The accuracy of the methanation tests results has been estimated calculating the error on the closure of the carbon balance (3.8).

$$errC = \frac{\dot{n}_C^{IN} - \dot{n}_C^{OUT}}{\dot{n}_C^{IN}} \cdot 100 = \frac{\dot{n}_{CH_4}^{IN} + \dot{n}_{CO_2}^{IN} - (\dot{n}_{CH_4}^{OUT} + \dot{n}_{CO_2}^{OUT} + \dot{n}_{CO}^{OUT})}{\dot{n}_{CH_4}^{IN} + \dot{n}_{CO_2}^{IN}} \cdot 100 \tag{3.8}$$

The experimental error depends on several factors such as: the accuracy of the calibrations of the gas chromatograph, the propagation of the error in the quantification of He used for the calculation of the partial molar flowrates, the presence of some species formed (i.e., solid carbon depositions) but not considered/measured. For instance, positive values of errC suggest that some C is missing in the outlet, possibly due to the formation of coke that is favored at high temperatures. Values of errC between 2% and 3% are considerable acceptable because the experimental error is minimum. To understand the variability of experimental data embedded in the error on the closure on carbon balance, some statistical parameters such as mean, standard deviation and coefficient of variation (defined as the ratio between the standard deviation and the mean) will be computed. A better solution would have been the error on the closure of oxygen or hydrogen atomic balances. However, the water produced is condensed after the reactor to avoid its presence in the microGC columns, therefore a balance on these two atoms is not possible.

Temperature programmed oxidation (TPO) is used to quantify the solid carbon produced in the long duration activity tests. The C produced is calculated from the total moles of CO and CO_2 produced during the oxidation (see equations 3.9 and 3.10). Since no CO and CO_2 are fed to the reactor during the TPO, the molar flowrates produced are equal to the molar flowrates leaving the reactor itself.

$$n_C = \int \left(\dot{n}_{CO_2}^{PROD} + \dot{n}_{CO}^{PROD}\right) dt \qquad [mol] \tag{3.9}$$

$$n_C = \int \left(\dot{n}_{CO_2}^{OUT} + \dot{n}_{CO}^{OUT}\right) dt \qquad [mol] \tag{3.10}$$

Chapter 4
Results and discussion

In this Chapter the tests executed at atmospheric pressure and all the tests at high pressure, including the blank tests, will be reported and analyzed. For all the methanation tests, the reagent dry mixture composition reported in Table 3.6 has been used i.e., with a H_2/CO_2 ratio equal to 4 and with the large fraction of CH_4 (>70%) produced in the first stage The products composition profiles will be presented in two forms:

- On dry basis, since all the water must be removed after the reactor, in the laboratory to avoid issues in the analytic section of the experimental plant, as already discussed in Chapter 3 but also in real-scale plants, since its presence in the biomethane pipeline must be avoided (as shown in Chapter 1.5, Table 1.16).
- Re-scaled on He that finally is subtracted readjusting the other compounds fractions, to align the results with the real-scale process, where the tracer is not used.

4.1 Experimental campaign at atmospheric pressure

For the atmospheric tests the reactor used is the quartz reactor. Its design has already been reported in Chapter 3, Table 3.1. Two K-type thermocouples have been used: one placed within the catalyst bed for the temperature monitoring; the other placed below the bed for the temperature control but also acting as a support for the catalytic bed and the two quartz wool layers (see Figure 4.1). The catalyst is EX11914 type in powder form, provided by Clariant. Only the fraction with granulometry between 112μm and 150μm has been used, to allow a comparison with previous works [21,22]. To avoid ambiguities due to the bulk density, WHSV is used instead of GHSV, as discussed in Chapter 3.

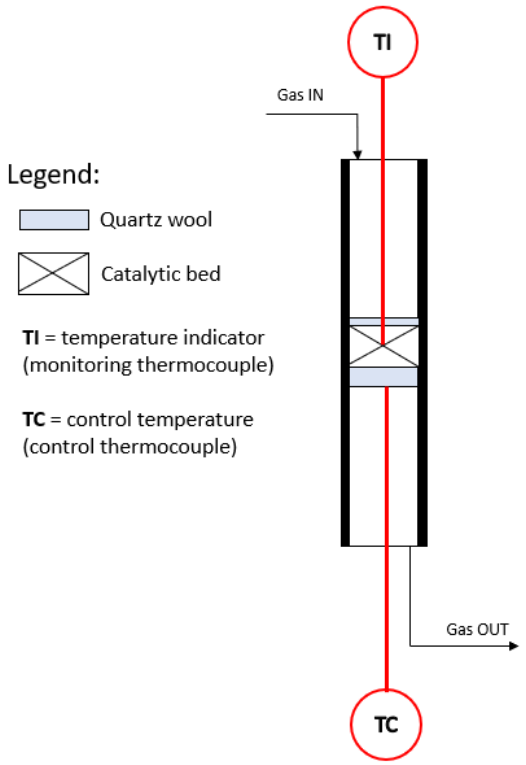

Figure 4.1: *Scheme of the reactor used for the atmospheric experimental tests. Catalyst EX11914.*

4.1.1 Procedures for TPR – coke formation stress test – TPO cycles

Before the beginning of the campaign to investigate coke deposition, two TRP-activity test-TPO cycles have been carried out, to verify the TPR capability of completely activate the catalysts, even after a full oxidation (TPO), to verify that the procedure adopted for the temperature programmed oxidation do not lead to irreversible catalyst deactivation.

The experimental conditions of catalyst activation by means of TPR are reported in Table 4.1.

Table 4.1: *Experimental condition of TPR*

y_{H2} [%]	y_{Ar} [%]	$\dot{V}$ [ml/min]	Temperature Range [°C]	Heating Rate [°C/min]
5	95	200	RT-600°C for 2 hours	5

The temperature program and the measured profile of H_2 molar percentage at the reactor outlet are reported in Figure 4.1. It is possible to notice two peaks due to a certain H_2 consumption, corresponding to the reduction of the two forms of nickel oxides. Particularly, the former,

between 180 and 400°C, should be associated to the reduction of Ni_2O_3 (the least stable among Nickel oxides), whereas the secondo one, between 300 and 600°C, is related to NiO.

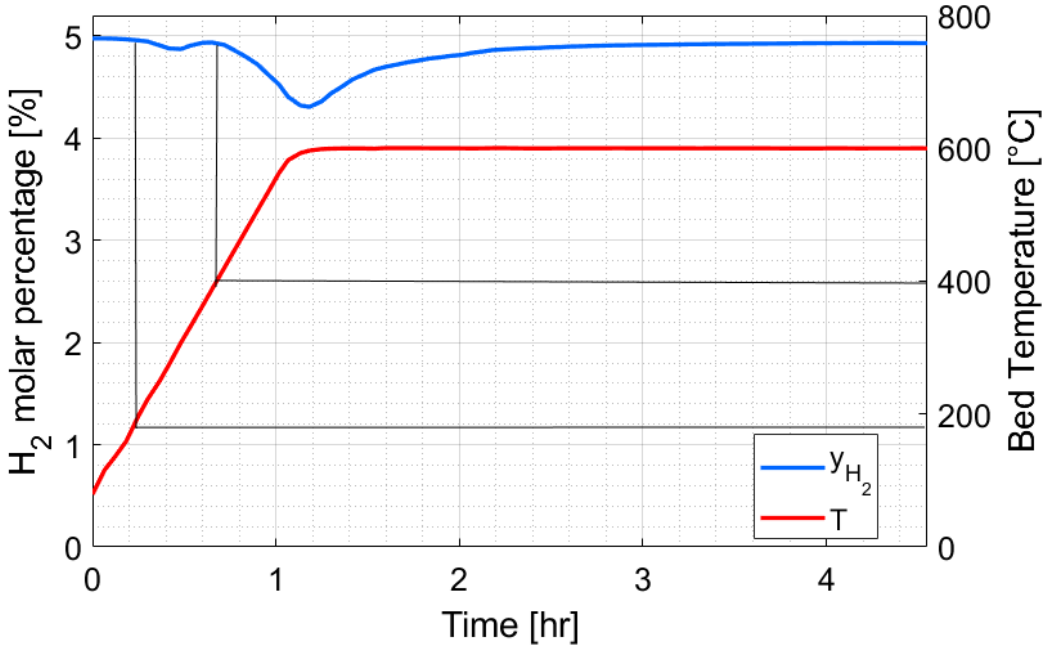

Figure 4.2: *H_2 molar percentage and bed temperature during catalyst activation. Reagent mixture composition as specified in Table 4.1*

The temperature programmed oxidation, as already specified in Chapter 1.2.3.1, is one of the possible techniques used to remove solid carbon likely formed during the coke formation stress tests. The experimental conditions for TPO are reported in Table 4.2.

Table 4.2: *Experimental conditions of TPO.*

y_{O2} [%]	y_{Ar} [%]	$\dot{V}$ [ml/min]	Temperature Range [°C]	Heating Rate [°C/min]
5	95	200	RT-700°C for 4 hours	5

The possible species formed by reaction with O_2 can only be CO and CO_2. A typical composition profile of a TPO, performed after carbon formation and deposition on catalyst surface, is reported in Figure 4.3; the temperature profile of the catalytic bed is also shown. It is possible to notice that the complete oxidation of carbon to CO_2 is favored with respect to the partial oxidation to CO, since the latter is not detected in the outlet. This means that, even if also CO is produced, its concentration is not high enough to be detected by the gas chromatograph. Moreover, two peaks are associated with O_2 consumption, the first, at 50-400°C, is due to

oxidation of the nickel present in the catalysts whereas the second, starting at about 500°C, is due to solid carbon oxidation, since CO_2 is produced. Therefore, only CO_2 profile will be considered for all the TPOs performed after coke formation stress tests and to evaluate the related quantity of solid carbon produced. Since CO is never produced during temperature programmed oxidations, its profile will not be included in the figures.

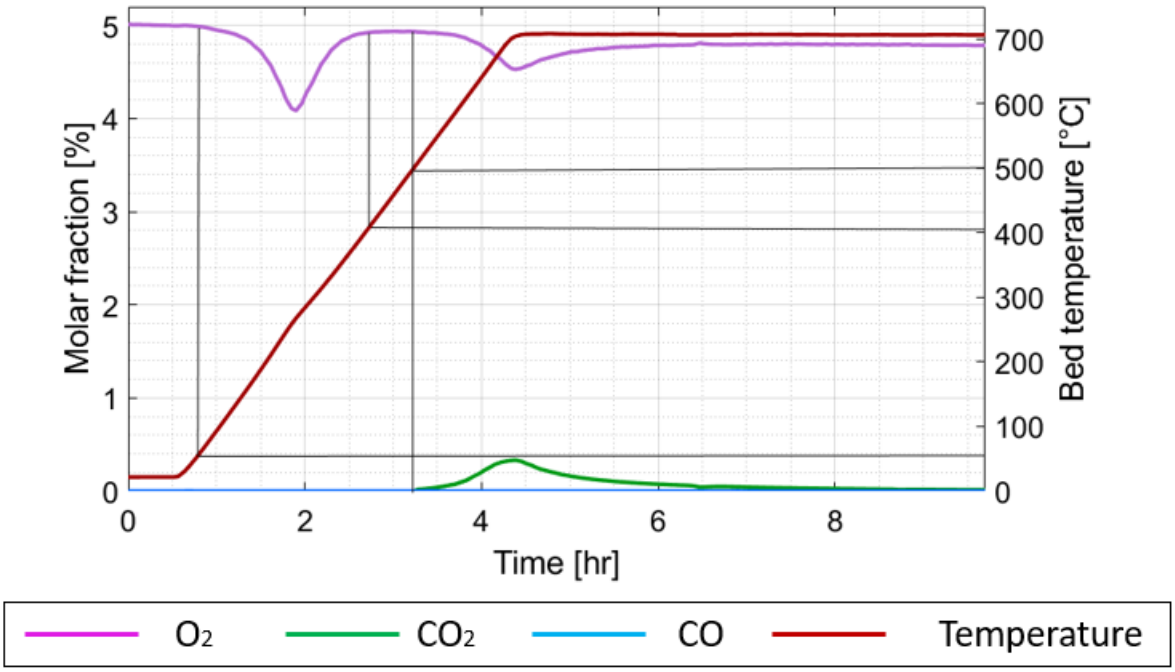

Figure 4.3: *Molar percentages and bed temperature during temperature programmed oxidation. Reagent mixture composition as specified in Table 4.2*

To verify the absence of any activity loss, the activity tests of the two subsequent TPR-methanation-TPO cycles are compared. The experimental conditions for both methanation steps are reported in table 4.3.

Table 4.3: *Experimental conditions of the activity tests. WHSV = 14.27 ml/mg/h. Inlet molar percentages as in Table 3.6.*

$\dot{V}$ [ml/min]	Temperature Range [°C]	Heating Rate [°C/min]
153	RT-300°C for 1 hour	10

In Figure 4.4 the results of the comparisons of dry molar percentages are reported. From this figure it is possible to notice that the catalysts activation toward methanation in the two tests present a difference of about 20°C, but always being within the expected temperature range. Moreover, at the steady state at 300°C the experimental compositions coincides, except for some

experimental error, thus the catalyst is not subjected to irreversible activity loss related to the TPO procedure and that the TPR procedure is capable of completely activate the catalysts even after the complete nickel oxidation that has occurred during solid carbon oxidation, according to the hydrogen bracketing technique explained in Chapter 1.2.2.

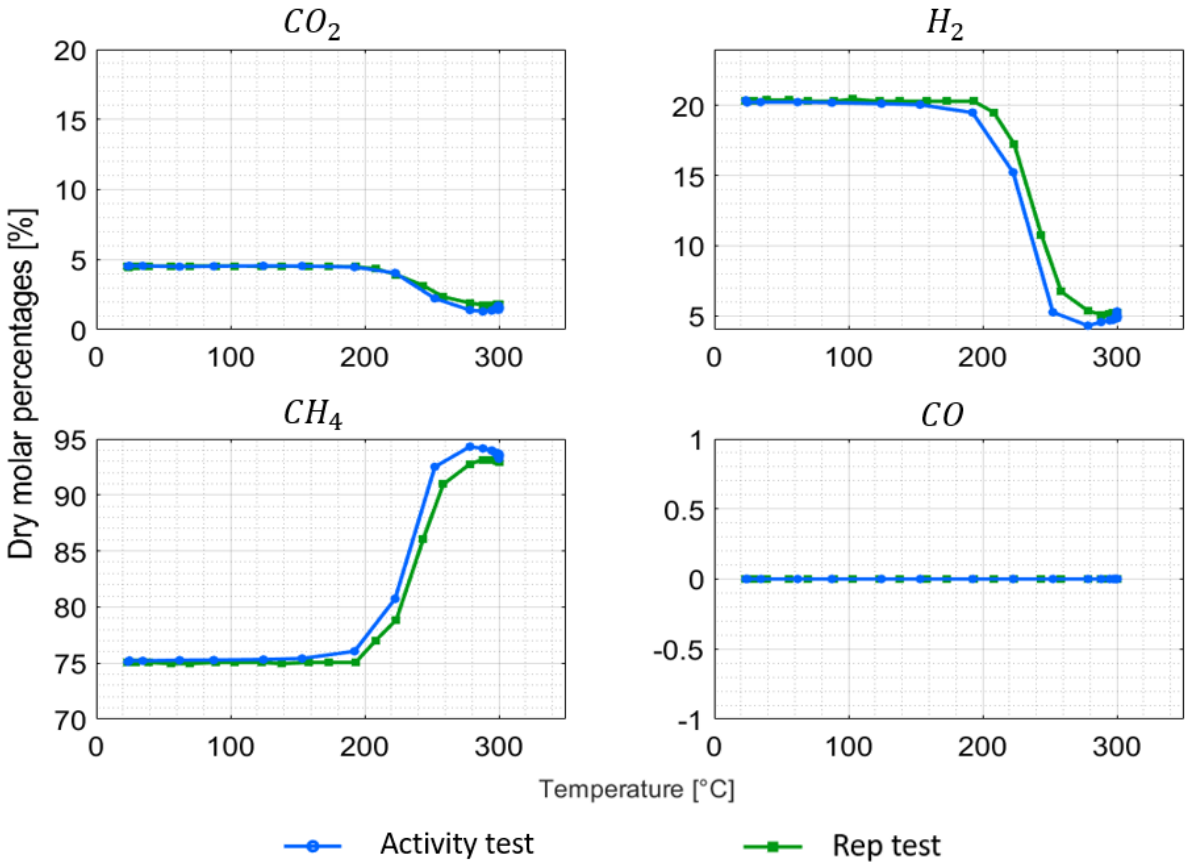

Figure 4.4: *Comparison between activity tests. Experimental conditions as reported in Table 4.3. Inlet molar percentages as reported in Table 3.6.*

Therefore, it is possible to conclude that the procedures used for TPR and TPO are acceptable, and they will be adopted for all the following TPR-coke formation stress tests-TPO cycles.

4.1.2 Coke formation stress test

The equilibrium calculation showed how the solid carbon formation plays a role of fundamental importance on the second stage methanation reactor, after H_2O was removed, leading to a significant reduction in the methane enrichment but also to catalyst deactivation, as explained in Chapter 1.2.3.1. This test has the purpose of verifying coke production, but it also provides a

reference for the experimental campaign carried out at 6 bar. Moreover, it allows to understand the behavior of the catalysts under several days of continuous operation, to verify its stability.

The experimental conditions of the test are reported in Table 4.4.

Table 4.4: Experimental conditions of the activity tests. WHSV = 14.27 ml/mg/h. Inlet molar percentages as in Table 3.6.

$\dot{V}$ [ml/min]	Temperature Range [°C]	Heating Rate [°C/min]
153	RT-280°C, kept at 280°C for 5 days	10

The reactor is set to an isotherm of 280°C, however, the control thermocouple was placed below the catalytic bed and because of the exothermicity of the Sabatier reaction (2.1), the bed temperature was at about 305°C, as shown in Figure 4.5. Moreover, at other points of the catalytic bed the temperature should also be larger, due to the possible formation of hot spots. It is also possible to see that, throughout the whole steady state, no relevant variations of temperature are detected.

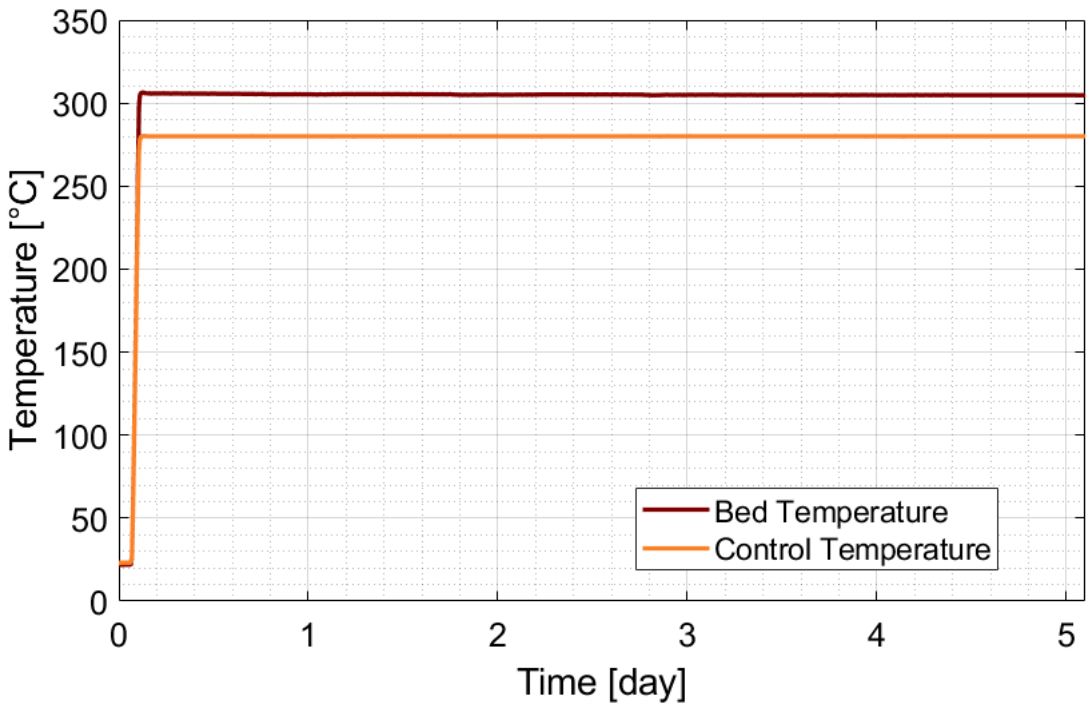

Figure 4.5: Test 136: trend of monitored and controlled temperatures. P = 1 bar. Catalysts EX11914.

Figure 4.6 shows the experimental dry molar percentages and a comparison to those obtained from chemical equilibrium, both considering and neglecting the possibility of solid carbon formation in the equilibrium calculation.

To avoid having a large number of points making the figures less significant and more confused, only a subsampling has been represented, considering one point every twenty. This is true also for all the following long duration methanation tests.

The measured H_2 profile is lower than that predicted by the equilibrium accounting for carbon formation. Therefore, the effect of methane cracking in practice is less relevant than expected, suggesting a higher activation energy. However, the dry molar fraction calculated from equilibrium neglecting coke formation are not reached, thus, at 305°C the kinetics limit the Sabatier reaction (2.1). This equilibrium represents a situation where the rate of carbon formation is much smaller than that of the methanation reaction.

The Italian grid injection requirements are not satisfied, since the H_2 molar percentage (assumed equal to the volumetric one, according to the ideal gas law) is larger than 1%, even though no CO production is observed, and the CO_2 molar percentage is below the limit of 2.5%. Furthermore, CO_2 molar percentage is closer to the equilibrium one than H_2 and CH_4, suggesting that, even at a slow rate, a contribution of methane cracking is present.

Still, a significant enrichment of CH_4 is achieved, from 75.8% of the feed mixture to 91.0% of the product mixture, even though the CH_4 actually produced is somehow lower than predicted by equilibrium, being 93.9%, without considering solid carbon in the calculation.

Furthermore, the catalytic activity does not show any relevant decrease even after 5 days of continuous operation, suggesting that coke, if present, does not accumulate enough to deactivate the catalysts.

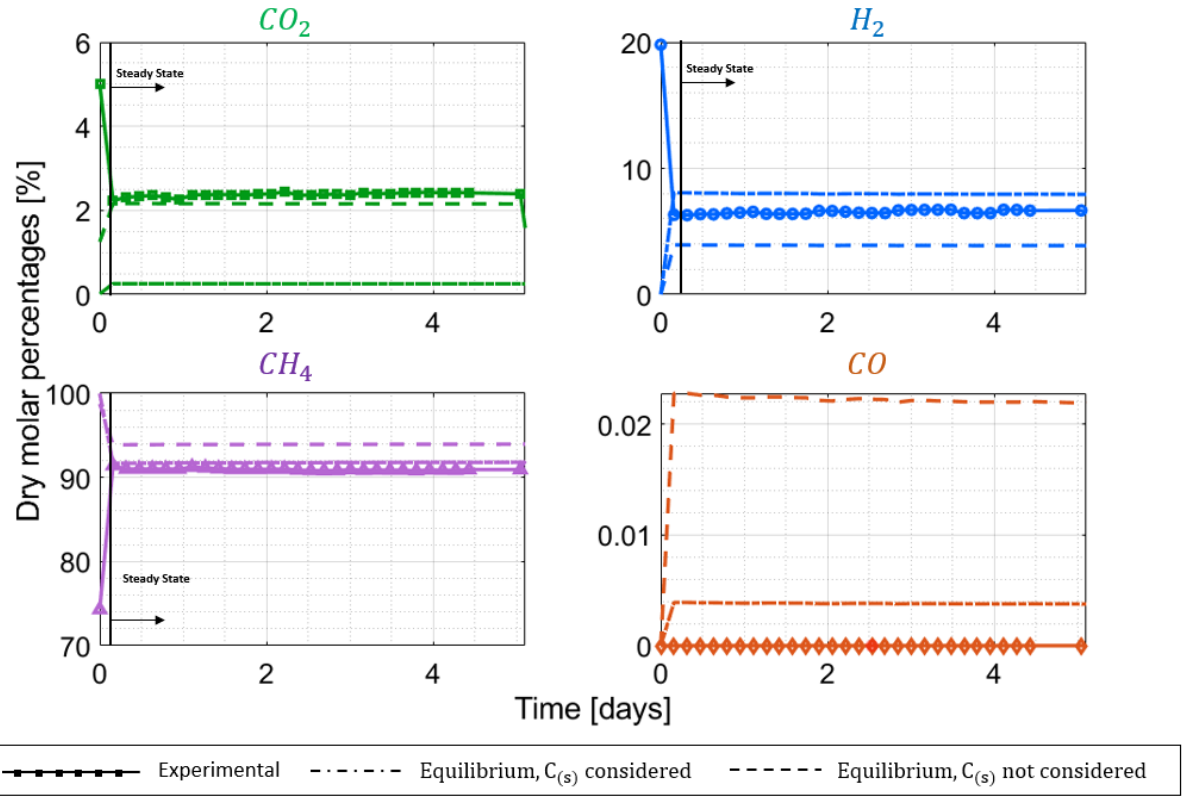

Figure 4.6: *Dry gas molar percentages as a function of time Measurements compared to equilibrium accounting and excluding solid carbon formation, both calculated at 1 bar with the experimental y^0. P = 1 bar. Catalysts EX11914. Experimental conditions reported in Table 4.4.*

The CO_2 conversion, shown in Figure 4.7, confirms that experimental points only approach the equilibrium predictions obtained without considering solid carbon: the average experimental CO_2 conversion achieved at steady state is equal to 67.6% against the 69.7% expected at equilibrium. Moreover, the variability on CO_2 conversion is due to an uncertainty in the mole calculation as a function of the dry molar percentage, related to the variability of the tracer peak integration performed by the micro-GC software. This issue is adjusted in the following tests by changing the carrier used in the micro-GC from helium to argon, and consequently the analytical and the integration method.

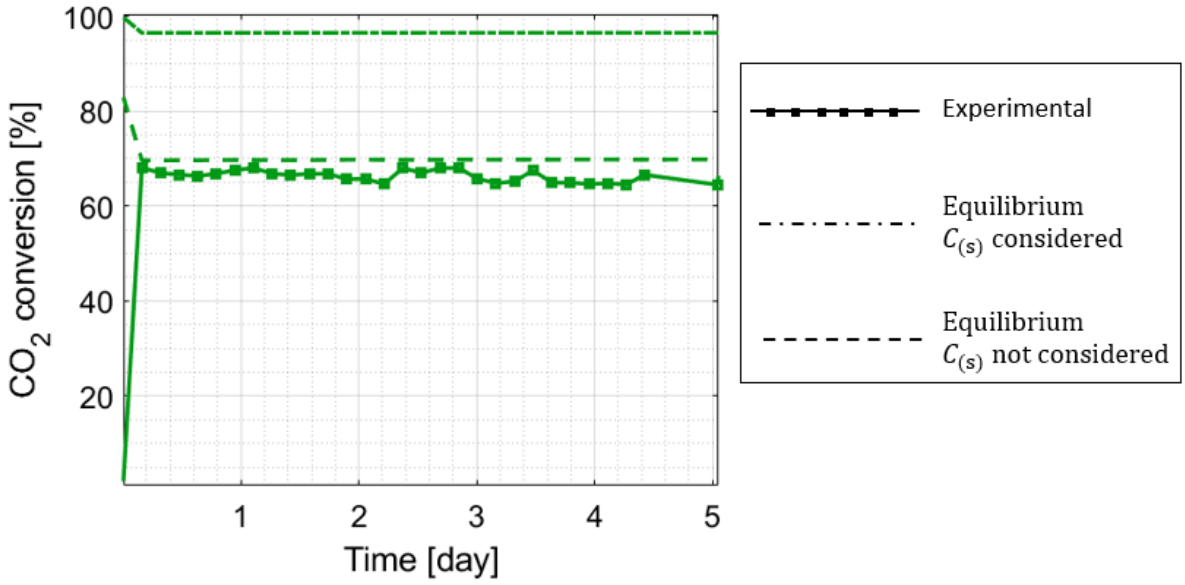

Figure 4.7: *CO_2 conversion as a function of time, compared to equilibrium where solid carbon formation is considered in the calculation and with equilibrium where solid carbon formation is not considered in the calculation, both calculated at 1 bar with the experimental y^0. P = 1 bar. Catalysts EX11914. Experimental conditions reported in Table 4.4.*

Figure 4.8 shows that no relevant increase of pressure drop along time is observed, strengthening the hypothesis of low or absent solid carbon production. However, pressure drops are an indicator of macropores clogging only, neglecting other deactivation mechanisms such as Ni particle encapsulation and detachment. Therefore, pressure drops are not a sensible indicator of solid carbon formation, even if they can enlighten macropores clogging when it occurs.

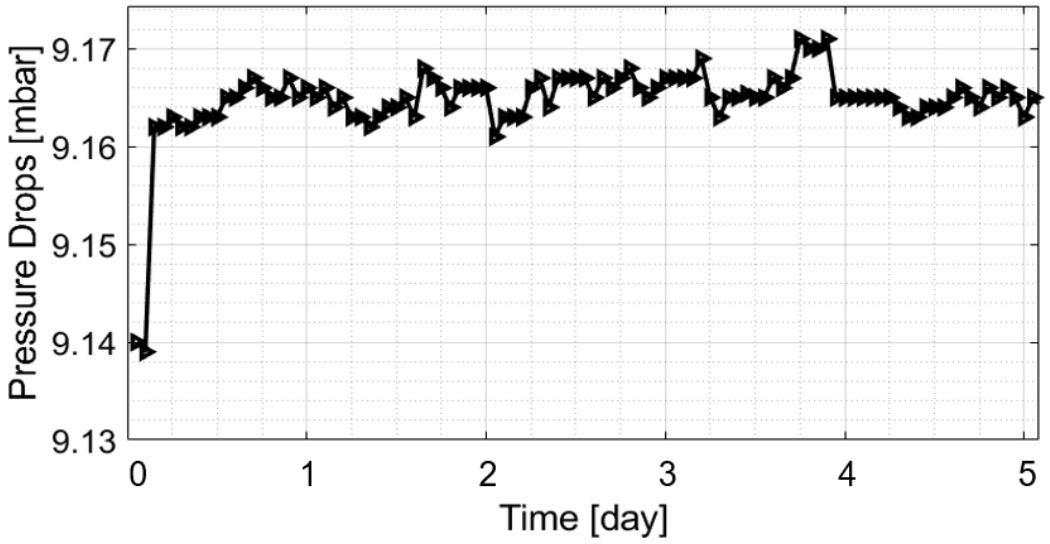

Figure 4.8: *Pressure drops across the reactor as a function of time. P = 1 bar. Catalyst EX11914. Experimental conditions as reported in Table 4.4.*

The error on the closure of carbon balance, represented in Figure 4.9, also does not highlight significant carbon formation, since it oscillates around 0%. Moreover, the experimental error is low, being always lower than 4% in absolute value, demonstrating that the experimental error is low and confirming the accuracy of the data. However, at about the 4^{th} day of continuous operation the variability of errC increases because of the variability of the tracer peak integration already cited.

The progressive mean μ on errC and the two confidence bands obtained as μ±σ, where σ is the progressive standard deviation, are also reported. Particularly, the progressive mean shows an increasing trend within the first 3 days, then stabilizes and decrease the last day, always being lower than 0.5%

The final value of the statistical parameters computed the end of the coke-formation stress test at atmospheric pressure, particularly the mean of the error on carbon balance, the standard deviation, and the coefficient of variation, (the ratio between the standard deviation and the mean), are shown in Table 4.5. It is important to notice that mean and standard deviation are expressed as percentage since it is also the unit of measure of the error on the closure on carbon balance. The very large value of the coefficient of variation is due to its inappropriate information when the mean value approaches 0%. Therefore, the coefficient of variation for this test is not representative of the data variability and standard deviation is considered instead. Particularly, σ value is lower than 1%, confirming that data are well distributed close to the mean.

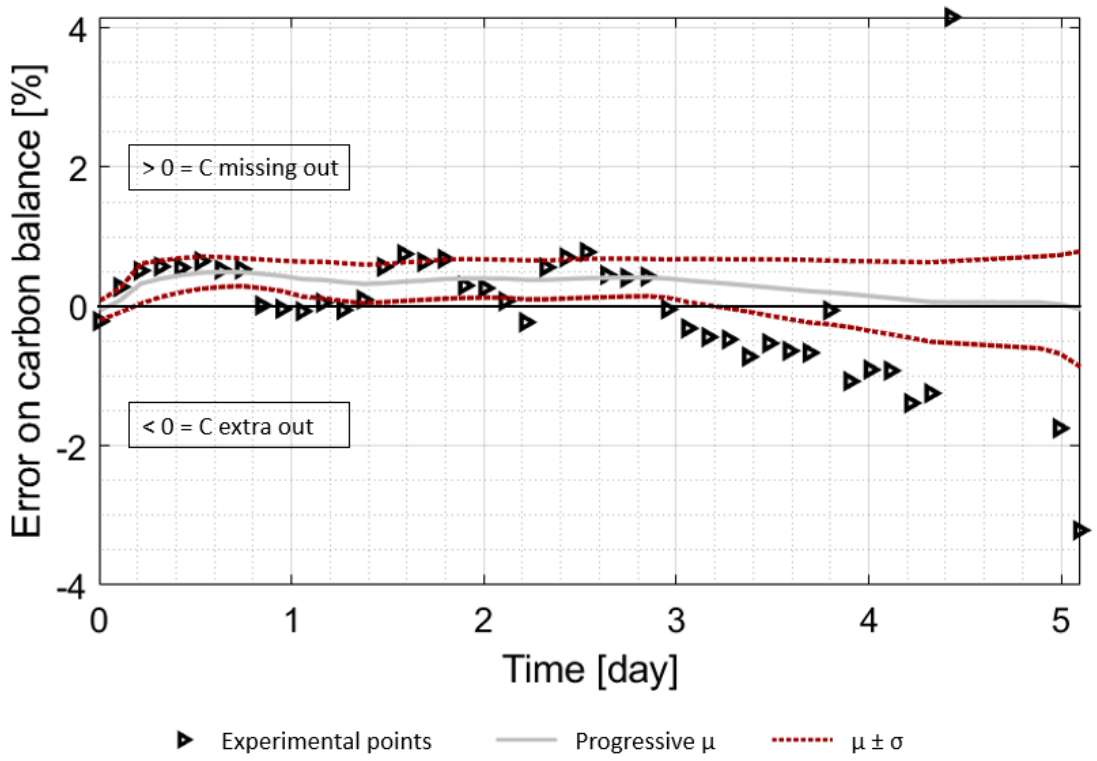

Figure 4.9: *Error on the closure of carbon balance (errC), progressive mean, and confidence intervals as a function of time. P = 1 bar. Catalyst EX11914. Experimental conditions as reported in Table 4.4.*

Table 4.5: *Statistical parameters for the coke-formation stress tests at 1 bar.*

Mean μ [%]	Standard Deviation σ [%]	Coefficient of Variation σ/μ [-]
-0.0383	0.7518	19.63

The molar percentage of CO_2 obtained during the following TPO, represented is Figure 4.10, is always 0% for all the control temperatures, confirming the fact that no solid carbon is produced during the coke-formation stress test at atmospheric pressure.

The quantity of carbon produced in the stress test and the coking rate are reported in Table 4.9, also with the mass of carbon expected at equilibrium. Particularly, the mass of coke expected at equilibrium is obtained according to (4.1):

$$m_{C,eq} = MW \cdot \dot{n}_{C,eq} \cdot t$$

Where MW is the atomic weight of carbon, t is the test duration and $\dot{n}_{C,eq}$ is the molar flowrate of carbon obtained from equilibrium calculations, obtained starting from the inlet volumetric flowrate given as input in the equilibrium calculation.

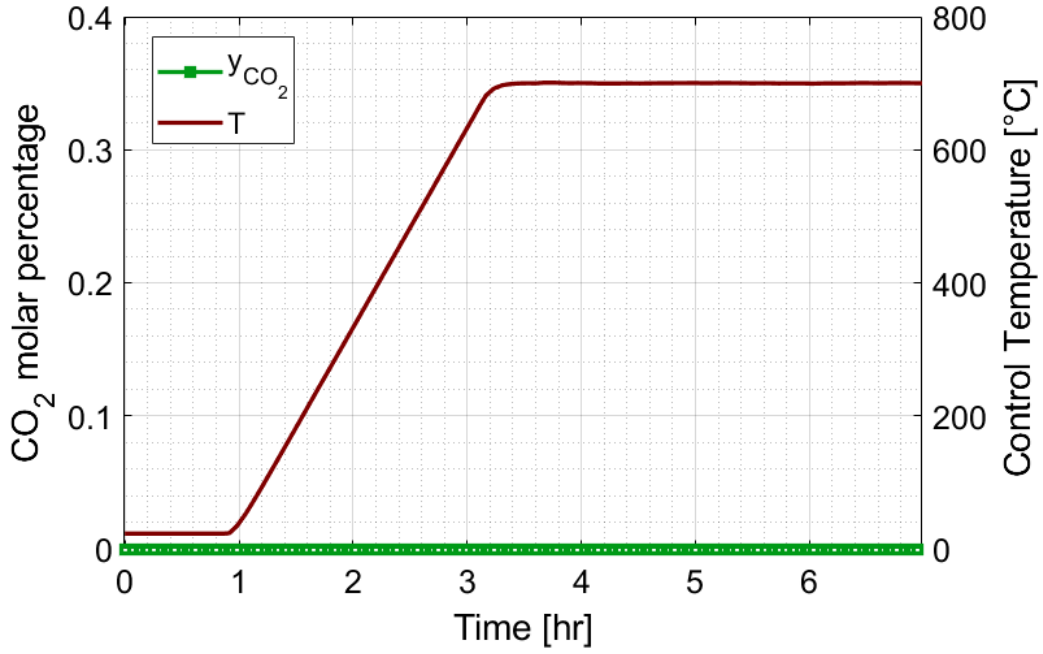

Figure 4.10: *CO_2 molar percentage as a function of the catalytic bed temperature obtained with TPO after stress test at atmospheric pressure. P = 1 bar. Catalyst EX11914. Experimental conditions as reported in Table 4.2.*

Table 4.6: *Mass of solid carbon formed during the stress-test and coking rate.*

Carbon formed [mg]	Carbon expected at equilibrium [mg]	Coking rate [$mg_C/(g_{cat}h)$]
0	12220	0

4.1.3 Conclusions

According to the campaign at atmospheric pressure with the quartz reactor, three main results have been achieved, particularly:

1. The procedure of temperature programmed reduction for catalyst activation is capable of completely activate the catalysts even after the complete oxidation obtained during the TPO;
2. The procedure of temperature programmed oxidation allows the evaluation of the coke produced, without leading to any irreversible deactivation of the catalyst related to the presence of oxygen at high temperatures (up to 700°C);
3. No solid carbon has formed, even after 5 days of continuous operation;

4. The activity of the catalyst does not have any significant decrease even after 5 days of continuous operation, leading to a methane enrichment up to 91.0%.
5. However, the product mixture does not respect the Italian grid injection requirements, even though it is in-line with the experimentation made by Snam (Società nazionale Metanodotti) in December 2019 [41]. Therefore, further improvements are required.

4.2 Experimental campaign at 6 bar

After the tests at atmospheric pressure, an experimental campaign at 6 bar has been carried out. The pressure is chosen according to the norms about the Italian biomethane distribution line, where the injection pressure must be of 5 bar. Also, from previous thesis work [21], it is known that a larger methane enrichment is achieved when operating at pressures larger than the atmospheric, according to equilibrium calculations.

For the tests at 6 bar, the setup has changed since the quartz reactor cannot operate under pressure. Therefore, an Inconel reactor is used. Its design has already been reported in Chapter 3, Table 3.1. As in the atmospheric tests, two K-type thermocouples have been used: one placed within the catalysts and used for temperature control; the other placed below the catalytic bed for temperature monitoring. It is important to notice that the thermocouples layout is the opposite of that used in atmospheric tests, being the control temperature within the catalytic bed. The layout was changed to ensure the same temperature within the catalyst bed in different test, since the heat generated by the reaction depends on the conversion (i.e., CO_2 conversion), therefore controlling the temperature below the catalytic bed at different test conditions could lead to different temperature within the bed. Moreover, all the reactor volume below the catalyst bed was filled with quartz wool, to provide better support. The catalyst is always EX11914 type and also the particle granulometry is the same of that used for atmospheric tests. The reactor is schematized in Figure 4.11.

To avoid ambiguities due to the bulk density and to allow comparisons with results obtained in the atmospheric campaign, WHSV is used instead of GHSV, as shown in Chapter 3.

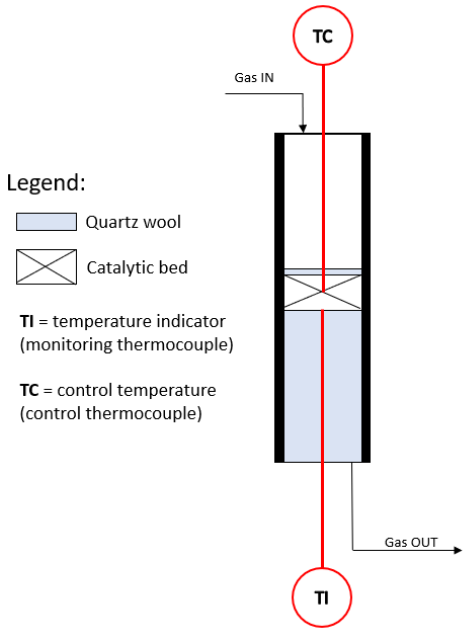

Figure 4.11: *Scheme of the reactor used for the experimental tests at 6 bar. Catalyst EX11914.*

A specific test at atmospheric pressure has been done to verify the consistency between the two experimental set-ups. Test conditions are reported in Table 4.7. Particularly, the gas inlet flowrate is chosen to operate at the same WHSV, equal to 14.27 ml/(mg_{cat}h). Moreover, set-up 1 indicates that used for the atmospheric pressure tests represented in Figure 4.1 whereas set-up 2 indicates that used for the campaign at high pressure, represented in Figure 4.11.

Table 4.7: *Experimental conditions of the tests. WHSV = 14.27 ml/mg/h. Inlet molar percentages as in Table 3.6. P = 1 bar.*

Set-up [-]	Reactor [-]	$\dot{V}$ [ml/min]	Temperature Range [°C]	Heating Rate [°C/min]
1	Quartz	153	RT-280°C	10
2	Inconel	236	RT-305°C	10

In Figure 4.12 the CH_4 molar percentage and the temperature within the catalytic bed for the two tests are reported. Particularly, for set-up 1 the bed temperature is just monitored whereas for set-up 2 it is also used for control. For both the setups, the compositions are plotted as a function of the catalytic bed temperature.

Except for some difference related to experimental error, it is possible to notice that the catalyst activates in the same temperature range (about 160-170°C) and the correspondence between molar fraction of methane in the two tests, confirming that the results obtained with the two set-ups are comparable.

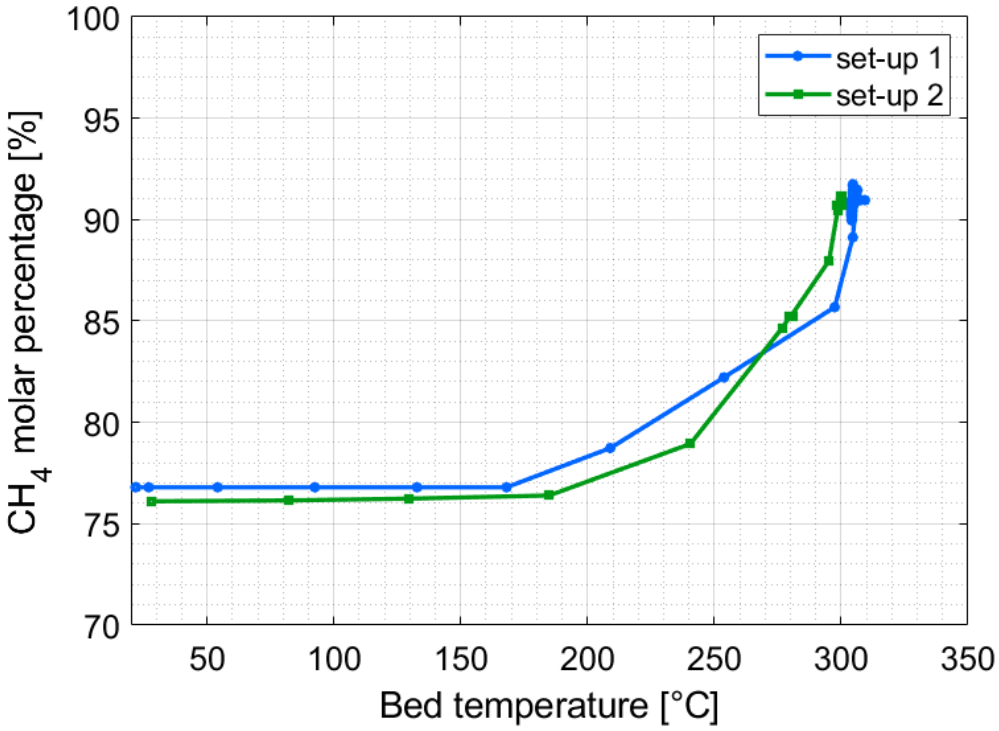

Figure 4.12: *Comparison of methane molar percentage as a function of the bed temperature, for the two different set-ups and same test conditions, reported in Table 4.5. P = 1 bar. Catalyst EX11914.*

The purpose of this campaign is to quantify coke formation rate also during stress-test at 6 bar. Particularly, three test have been performed:

1. A blank test without catalysts, to understand whether the Ni present in the Inconel tube could catalyze coke formation (via methane cracking) or produce it via steel carburation;
2. A coke-formation stress test at 6 bar, to have a reference in terms of molar percentages and solid carbon formed;
3. Another stress-test but with 20% of H_2O in the inlet mixture, to study its effect on solid carbon formation.

4.2.1 Inconel tube blank test

For this test, the Inconel tube was empty, except for a layer of quartz wool, placed at the reactor bottom, in order to collect solid carbon, if formed. The thermocouples configuration is the same as shown in Figure 4.11.

The experimental conditions of the test are reported in Table 4.8.

Table 4.8: Experimental conditions of the blank coke formation stress-tests. WHSV not defined (catalyst not present). Inlet molar percentages as in Table 3.6.

$\dot{V}$ [ml/min]	Temperature Range [°C]	Heating Rate [°C/min]
236	RT-305°C for 5 days	10

The molar flowrates of each component, represented in Figure 4.13, do not vary along time. Therefore, up to 305°C, the nickel of the Inconel tube does not catalyze either the Sabatier reaction or other side reactions such as methane cracking, over a reasonable long testing period of 5 days. Also, no homogeneous phase reaction occurs at a significant rate capable of changing the dry molar percentages of the different species by a variation detectable by the micro-GC, even with a larger residence time due to the absence of the catalyst reducing the flow section. Therefore, no coke formation is expected, notwithstanding the high quantity of nickel in the Inconel tube and the high methane partial pressure.

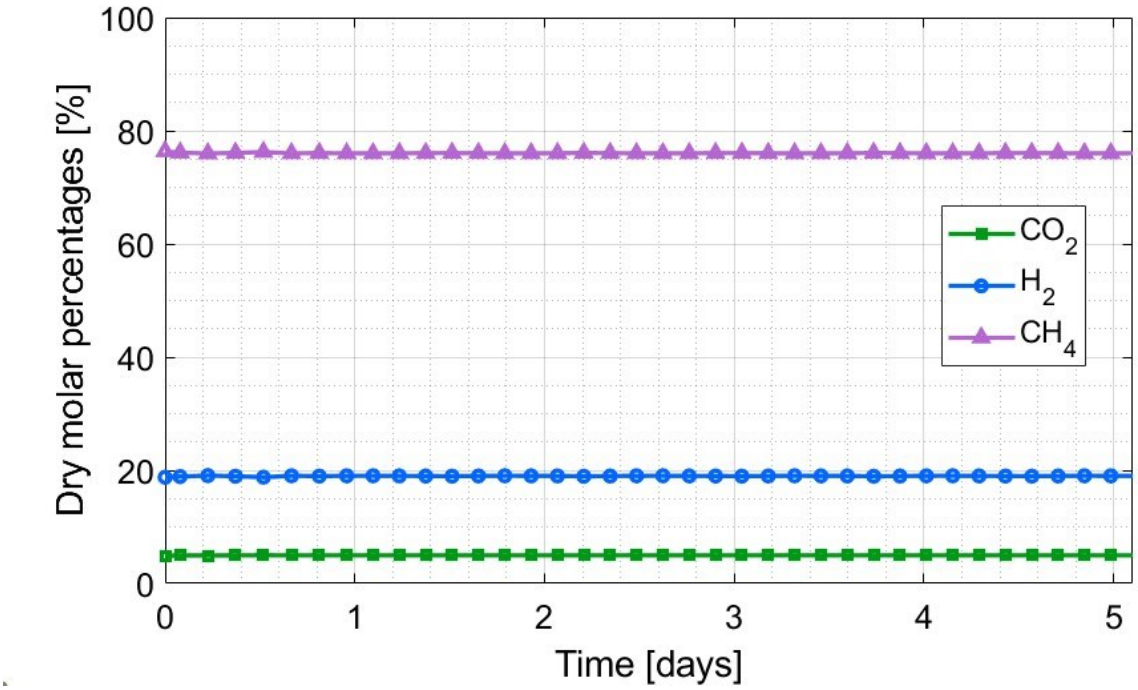

***Figure 4.13**: Dry gas molar percentages as a function of time. P = 6 bar. Catalysts absent. Experimental conditions reported in Table 4.6.*

Furthermore, the profile of the pressure, reported in Figure 4.14, does not suggest any solid carbon formation, since after pressure stabilization its value remains constant. However, the catalytic bed is not present in the system, therefore the coke can only be deposited on the quartz wool layer. Thus, no macropores clogging can occur and a relevant pressure increase is not

expected, even in the case carbon could forms. Accordingly, the pressure drop without a packing is not a representative method to measure carbon formation.

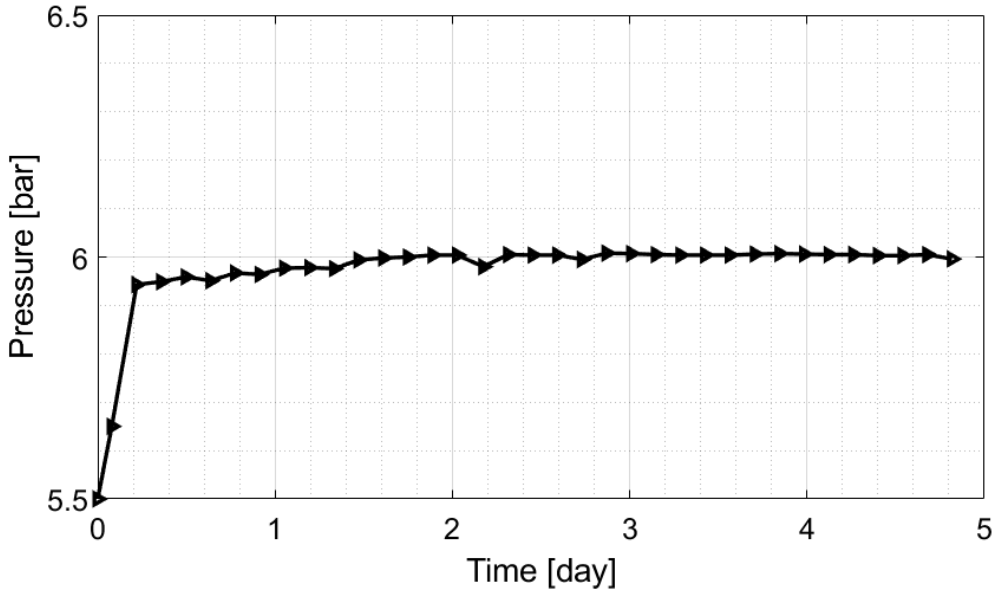

Figure 4.14: *Pressure at the top of the reactor. P = 6 bar. Catalyst absents. Experimental conditions as reported in Table 4.6.*

From the CO_2 profile obtained with the TPO, represented in Figure 4.15, we see that some carbon formed indeed during the blank test. Particularly, carbon oxidation starts at about 490°C. Coke formation could be a consequence of methane cracking catalyzed by the nickel in the Inconel tube, however its production rate is not high enough to induce a change in molar fraction detectable by the analytical instrument.

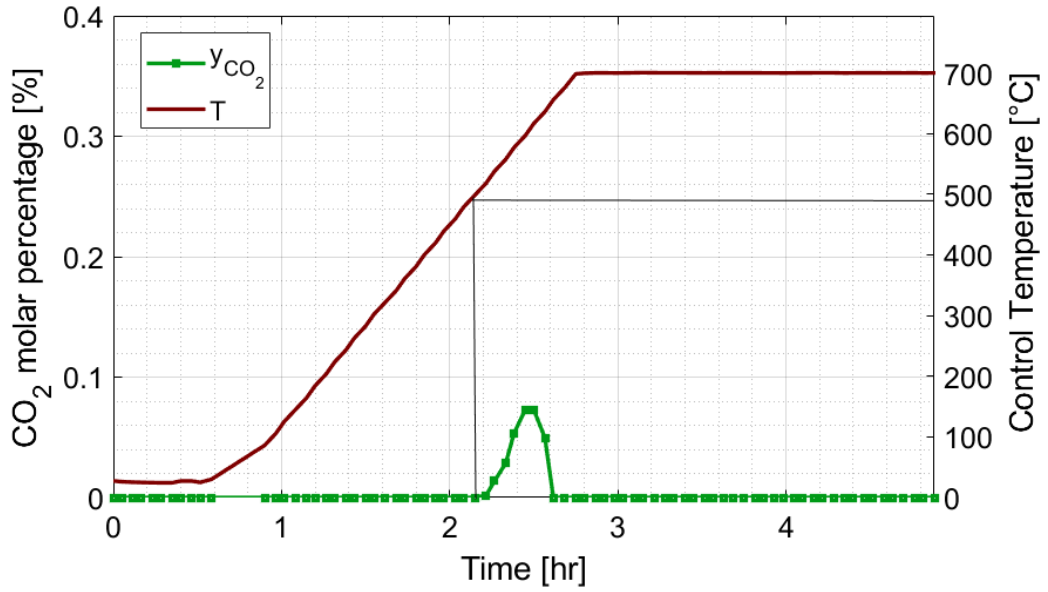

Figure 4.15: *CO_2 molar percentage and control temperature as a function of time. P = 1 bar. Catalyst EX11914. Experimental conditions as reported in Table 4.2.*

The quantity of carbon formed in the blank tests is indeed very small, as shown in Table 4.9, reporting the quantity of coke formed but also the carbon formation rate, or coking rate, which is an index commonly used in industries, as already explained in Chapter 1.2.3.1. Particularly, the quantity of solid produced is three orders of magnitude lower than that expected at equilibrium, strengthening the hypothesis of a really low methane cracking rate.

For this test the coking rate cannot be defined, since catalyst is not present within the reactor.

Table 4.9: *Mass of solid carbon formed during the stress-test and coking rate.*

Carbon formed [mg]	Carbon expected at equilibrium [mg]	Coking rate [$mg_C/(g_{cat}h)$]
1.01	4534	Not defined

4.2.2 Coke formation stress test

The purpose of this test is to assess the stability of catalyst activity over 5 days of continuous operation at 6 bar, as done with the coke-formation stress test at atmospheric pressure. It also aims at evaluating the quantity of carbon produced via methane cracking, when the methane composition at steady state is expected to be higher than that obtained at atmospheric pressure, according to chemical equilibrium calculation.

The experimental conditions of the test are reported in Table 4.10.

Table 4.10: Experimental conditions of the coke formation stress-tests at 6 bar. WHSV = 14.27. Catalyst EX11914. Inlet molar percentages as in Table 3.6.

$\dot{V}$ [ml/min]	Temperature Range [°C]	Heating Rate [°C/min]
236	RT-305°C for 5 days	10

From Figure 4.15, we see that the experimental composition approaches that obtained with equilibrium for all species, when solid carbon is not included in the calculation. Moreover, the H_2 dry molar percentage is lower than that obtained from chemical equilibrium where solid carbon is included in the calculation, enlightening how the effect of methane cracking is less relevant than expected. This is likely due to anti-coking additives present in the EX11914 catalyst.

From Figure 4.16 is also possible to observe that the product mixture is enriched in methane from 75.8% to 96.4%, against the 91% obtained at atmospheric pressure. Moreover, the CO_2 molar percentage is about 1% and no CO is observed, therefore its concentration, if not zero, is very small, since it is not detected by the micro-GC. Therefore, a comparison with equilibrium calculations will be meaningless. However, its composition respects the requirements for the Italian biomethane grid injection. However, H_2 molar fraction in the product mixture at steady state is 2.6%, so it does not respect the grid requirements, even though it is in line with the experimentation done by Snam (Società Nazionale Metanodotti) [41] in April 2019 to allow 5% of H_2 in the biomethane.

Also, no relevant activity loss is detected in time, suggesting that the coke, if formed, is not a quantity large enough to cause catalysts deactivation, according to the possible deactivation mechanisms discussed in Chapter 1.2.3.1.

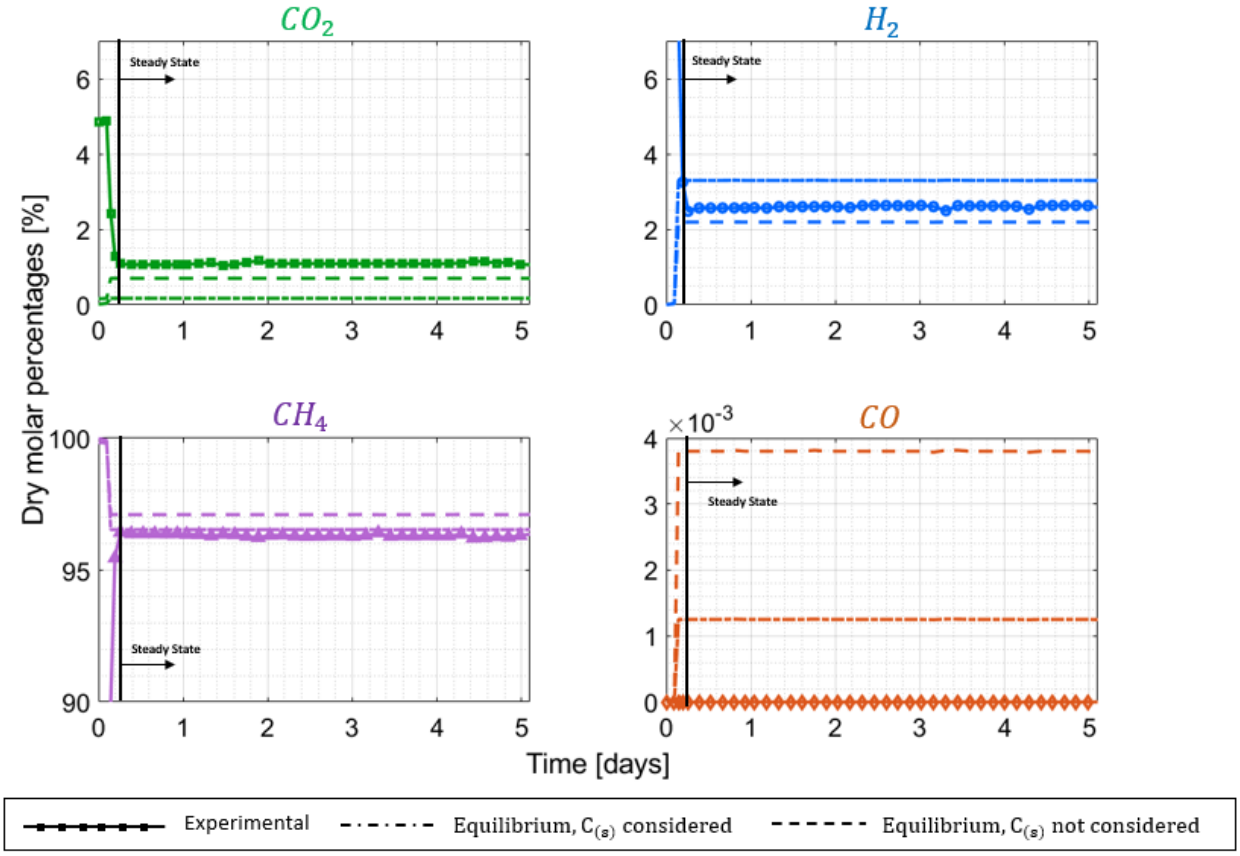

Figure 4.16: *Dry gas molar percentages as a function of time, compared to equilibrium where solid carbon formation is considered in the calculation and with equilibrium where solid carbon formation is not considered in the calculation, both calculated at 6 bar with the experimental y^0. P = 6 bar. Catalysts EX11914. Experimental conditions reported in Table 4.10.*

The CO_2 conversion, represented in Figure 4.17, confirms that experimental measurements are closer to the equilibrium predictions obtained without considering solid carbon: the average experimental CO_2 conversion achieved at steady state is equal to 81.92% against the 88.34% predicted by equilibrium, neglecting $C_{(s)}$. The variability of the CO_2 experimental values seen in Figure 4.7 has been solved, improving the integration of the peak of He used as tracker.

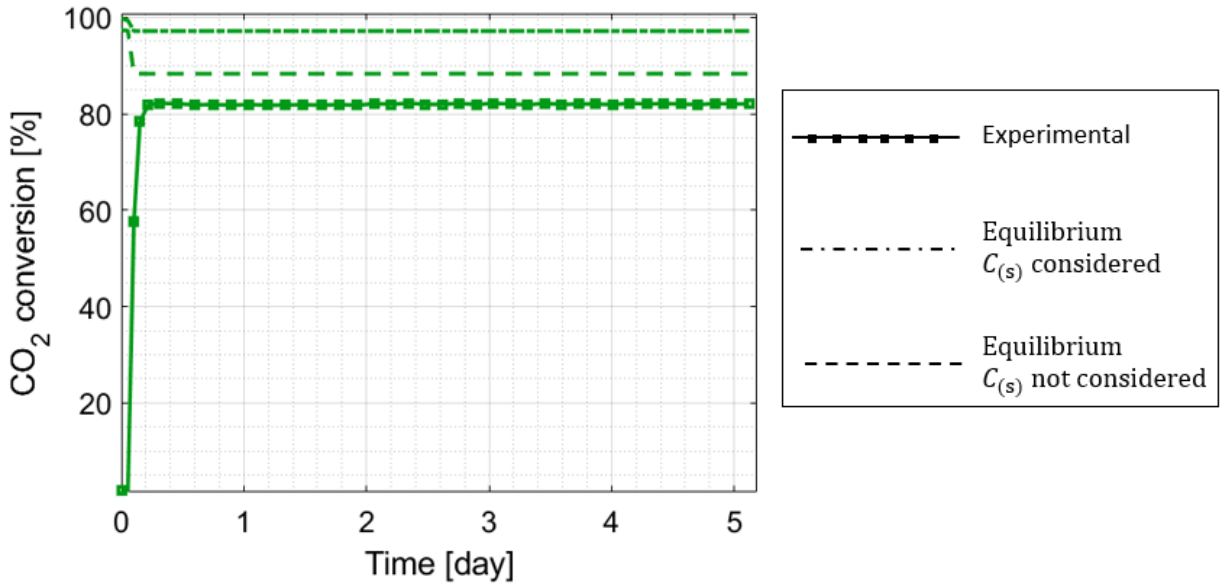

Figure 4.17: *CO_2 conversion as a function of time, compared to equilibrium where solid carbon formation is considered in the calculation and with equilibrium where solid carbon formation is not considered in the calculation, both calculated at 6 bar with the experimental y^0_i. P = 6 bar. Catalysts EX11914. No water addition. Experimental conditions reported in Table 4.10.*

Figure 4.18 shows that the pressure at the reactor top after 2.5 days at a constant value of 6 bar, starts to increase. This can be a consequence of macropores clogging, however, the catalyst does not show activity losses and the macropores clogging is anticipated by other deactivation phenomena (e.g., nickel encapsulation and detachment, as explained in Chapter 1.2.3.1), since it is the result of a higher quantity of carbon deposited than that required for other deactivation mechanisms. Therefore, the progressive increase of the pressure at the reactor top could be due to combined effects of coke deposition and condenser filling. Thus, we believe that the pressure increase measured is not a direct indicator of coke formation.

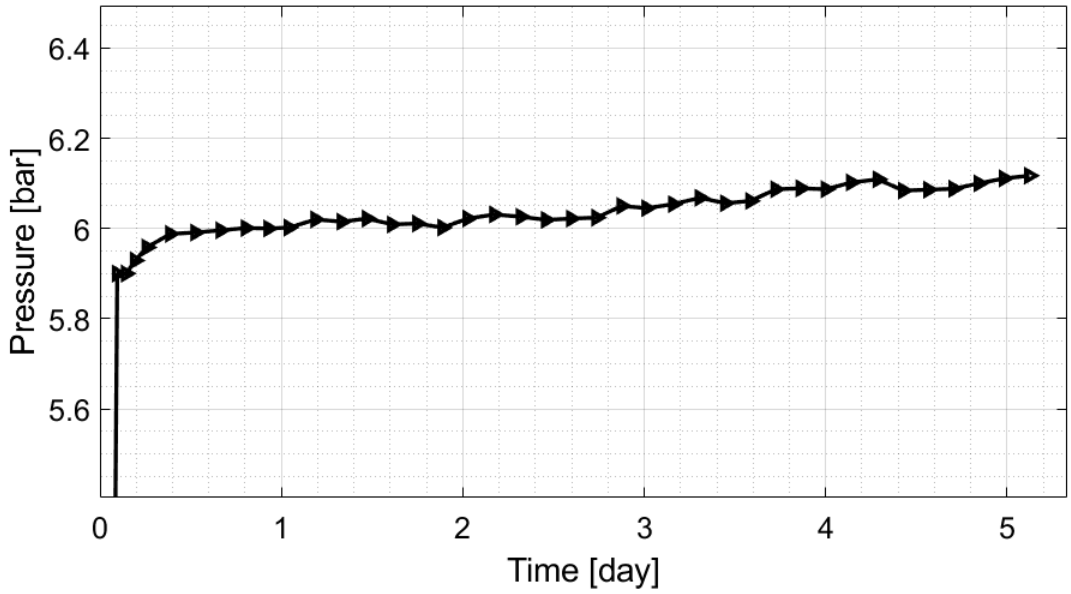

Figure 4.18: *Pressure at the top of the reactor. P = 6 bar. Catalyst EX11914. Experimental conditions as reported in Table 4.8.*

The trend of the error on the closure on carbon balance, shown in Figure 4.19, underlines how some carbon is missing in the product mixture, suggesting that some carbon remains within the reactor as coke. The progressive mean shows an increasing trend, since until steady state is reached the error on carbon balance oscillates around 0% and when steady state is reached it stabilizes at a value of about 0.7%. Such values of errC lower than 1% in absolute values suggests that, except for some carbon lack in the product mixture due to coking, the experimental error is low and confirms the accuracy of the data.

The value of the statistical parameters computed at the end of the coke-formation stress test at 6 bar, are shown in Table 4.11. The value of the coefficient of variation suggests a high data variability (since it is larger than 0.5) but is mainly due to the oscillations around 0% at the beginning of the test, during the transitory regime. This is enlightened by the confidence bands, which progressively shrink over time.

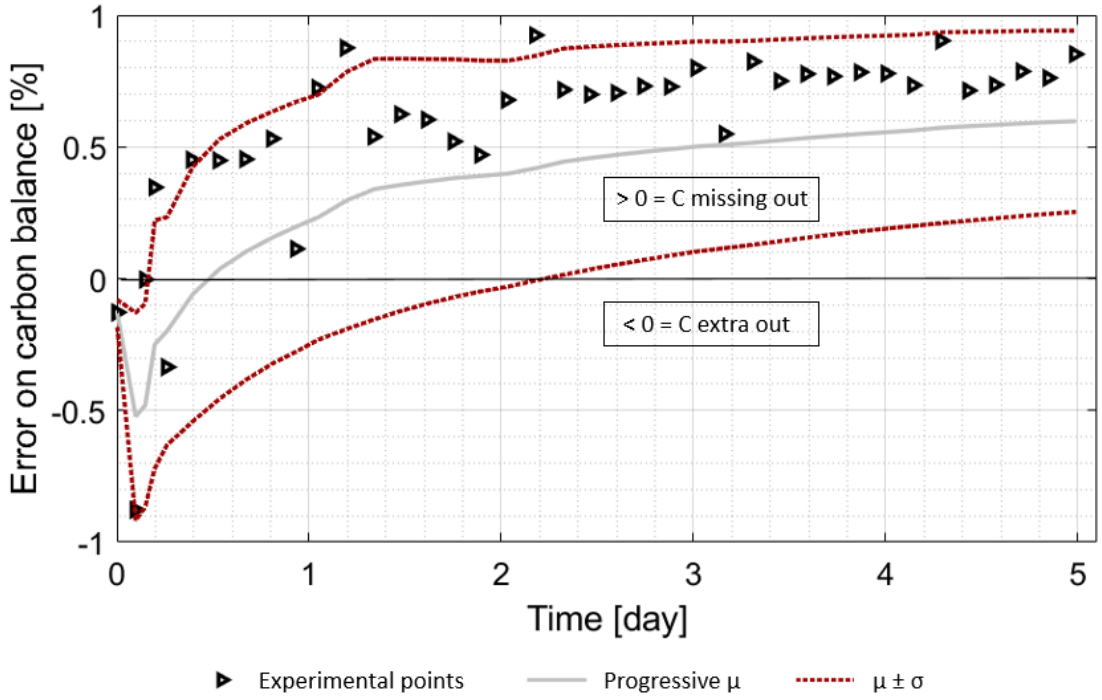

Figure 4.19: *Error on the closure of carbon balance (errC), progressive mean, and confidence intervals as a function of time. P = 6 bar. Catalyst EX11914. No water addition.*

Table 4.11: *Statistical parameters for the coke formation stress tests at 6 bar.*

Mean μ [%]	Standard Deviation σ [%]	Coefficient of Variation σ/μ [-]
0.5957	0.3403	0.5713

From the results of the TPO following the coke-formation stress at 6 bar, represented in Figure 4.20, we see that that some CO_2 has formed. Therefore, carbon has certainly been produced during the stress-test, as expected from the error on carbon balance. The temperature at which CO_2 starts producing from solid carbon is about 490°C, suggesting that the type of carbon produced is the same of that produced during the blank test, since their oxidation temperature is the same.

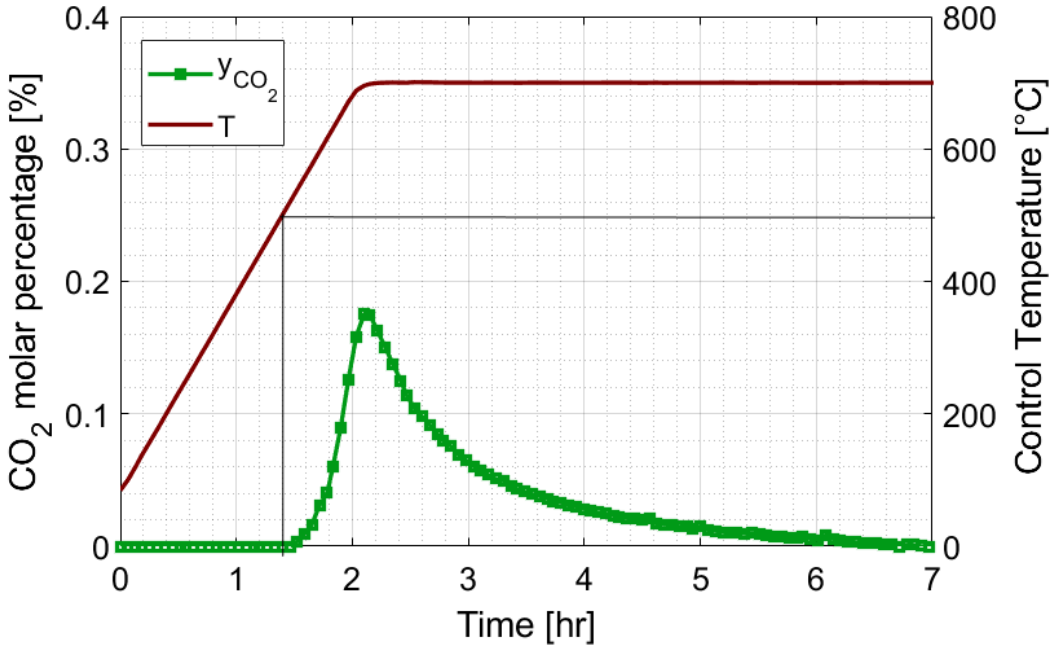

Figure 4.20: *CO_2 molar percentage and control temperature as a function of time. P = 1 bar. Catalyst EX11914. Experimental conditions as reported in Table 4.2.*

The quantity of carbon produced in the stress test and the coking rate are reported in Table 4.12, also with the mass of carbon expected at equilibrium. As in the blank test, the quantity of coke produced is much lower than that expected at equilibrium (about two orders of magnitude less in this case), giving an additional confirmation of the slow rate of methane cracking.

Table 4.12: *Mass of solid carbon formed during the stress-test and expected at equilibrium and coking rate.*

Carbon formed [mg]	Carbon expected at equilibrium [mg]	Coking rate [$mg_C/(g_{cat}h)$]
12.68	4560	0.1022

4.2.2.1 Comparison with test at atmospheric pressure

In Figure 4.21, a comparison between the experimental dry molar percentages obtained with the stress tests at atmospheric pressure and at 6 bar is reported. Only the first day of operation has been reported, since in both the tests the compositions were stable for the whole test duration. Particularly, as expected from equilibrium calculation, the pressure enhances the Sabatier reaction (2.1), leading to a larger methane dry molar percentage (96.4% at 6 bar, 91.3% at atmospheric pressure) and lower H_2 and CO_2 molar percentages (2.57% and 1.06% at 6 bar and

6.35% and 2.33% at atmospheric pressure respectively). In both cases, no CO is detected, since the temperature is not high enough to activate side reactions such as RWGS and DR. However, in both cases H_2 molar percentage is not low enough to satisfy the requirements of the biomethane grid injection, but in line with the experimentation done by Snam respectively in April 2019 and December 2019 [41].

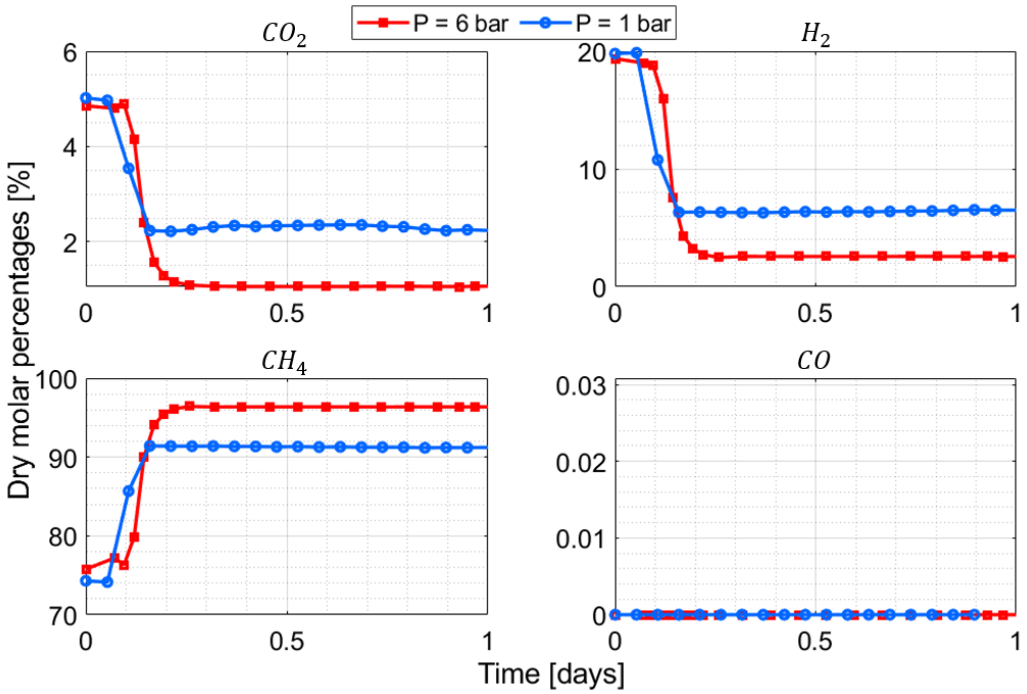

Figure 4.21: *Comparison of dry molar percentages as a function of time, for the two stress tests at different pressure. Catalyst EX11914. Experimental conditions reported in Table 4.4 and 4.10.*

The CO_2 conversion profiles for the two tests, shown in Figure 4.22, confirm the best performance of the stress test at 6 bar, particularly, an increase of 14.8 percentage points (from 67.6% to 82.4%) is observed.

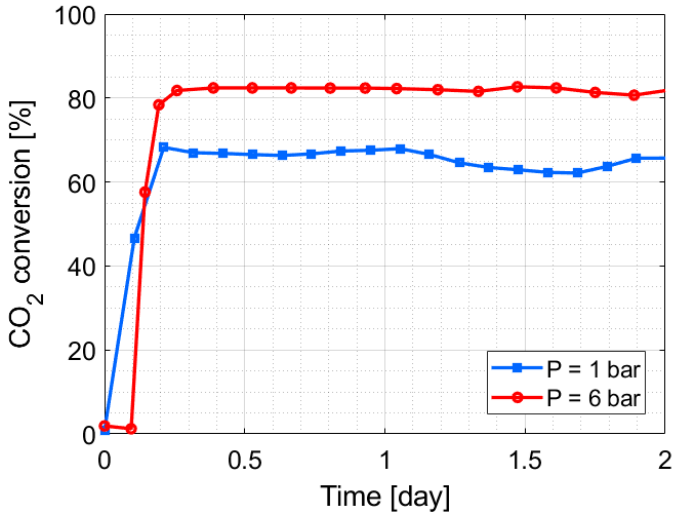

Figure 4.22: *Comparison of CO_2 conversion as a function of time, for the two stress tests at different pressure. Catalyst EX11914. Experimental conditions reported in Table 4.4 and 4.10.*

4.2.3 Coke-formation stress test with addition of H_2O in the reactant mixture

The purpose of this test is to understand the effect of H_2O addition to the reactant mixture, both on dry molar percentages of the product mixture and more specifically the coke formed during the stress test. Moreover, it also aims at assessing the catalyst stability under 5 days of continuous operation, as done with the coke-formation stress test without water addition.

From equilibrium calculations, the Sabatier reaction (2.1) is limited by water addition, since it is a rection product, but a reduction of coke is also expected, mainly due to solid carbon gasification (2.7). It is also important to notice that equilibrium obtained considering and not considering solid carbon formation in the calculation coincides, since with the inlet water composition used for the experimental tests (20% on molar basis), no C formation is predicted.

The experimental conditions of the test are reported in Table 4.13.

Table 4.13: *Experimental conditions of the coke formation stress-tests at 6 bar with water. WHSV = 14.27 (obtained considering the dry inlet mixture). Catalyst EX11914.*

$\dot{V}$ [ml/min]	y^0 [%]	Temperature Range [°C]	Heating Rate [°C/min]
295	CH_4 = 57.31 H_2 = 14.49 CO_2 = 3.76 He = 4.02 H_2O = 20	RT-305°C for 5 days	10

From Figure 4.23, where the dry molar percentages of the species are shown, is possible to notice that all the experimental compositions approach that obtained with chemical equilibrium. However, they are not equal to the equilibrium predictions, therefore kinetics limits the Sabatier reaction (2.1) at 305°C. This can also be related to the addition of water, being a product of the Sabatier reaction and reducing the partial pressures of reactants in the inlet mixture. Particularly, the product mixture is enriched in methane from 75.8% up to 93.1%, whereas the H_2 and CO_2 molar percentages are 5.20% and 1.68% respectively. CO is never detected in the product mixture. Therefore, as in all the other coke-formation stress test, CO_2 and CO dry molar percentages respect the Italian biomethane grid injection requirements, whereas H_2 molar percentage is larger than that allowed, but in line with Snam experimentations [41] of December 2019.

Also, no relevant activity loss is detected in all the test, suggesting that the coke, if formed, is not a quantity large enough to cause catalysts deactivation, according to the possible deactivation mechanisms discussed in Chapter 1.2.3.1.

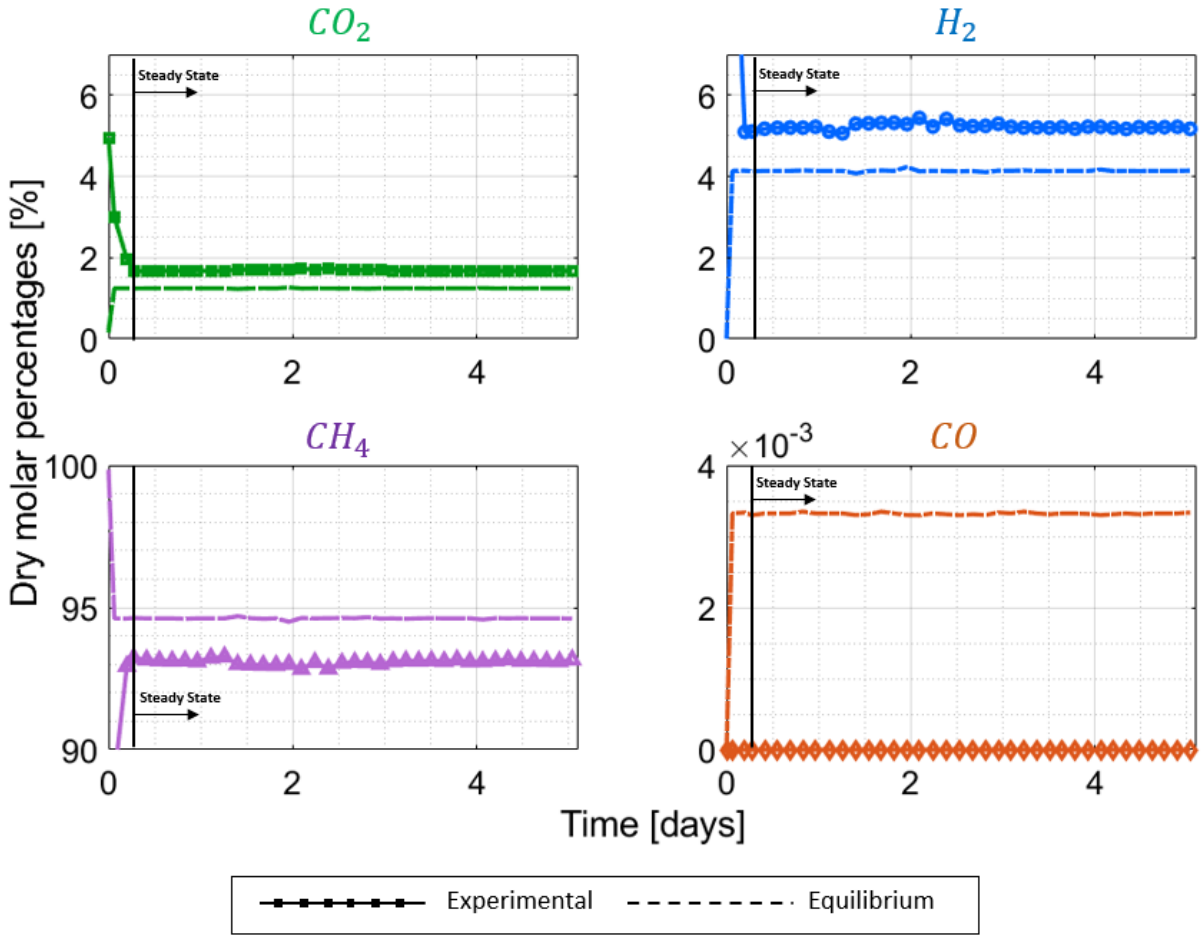

Figure 4.23: *Dry gas molar percentages as a function of time, compared to equilibrium calculation, calculated at 6 bar with the experimental y^0. P = 6 bar. Catalysts EX11914. Experimental conditions reported in Table 4.13.*

The CO_2 conversion, represented in Figure 4.24, confirms that experimental points only approach the equilibrium predictions: the average experimental CO_2 conversion achieved at steady state is equal to 71.45% against the 78.79% expected at equilibrium.

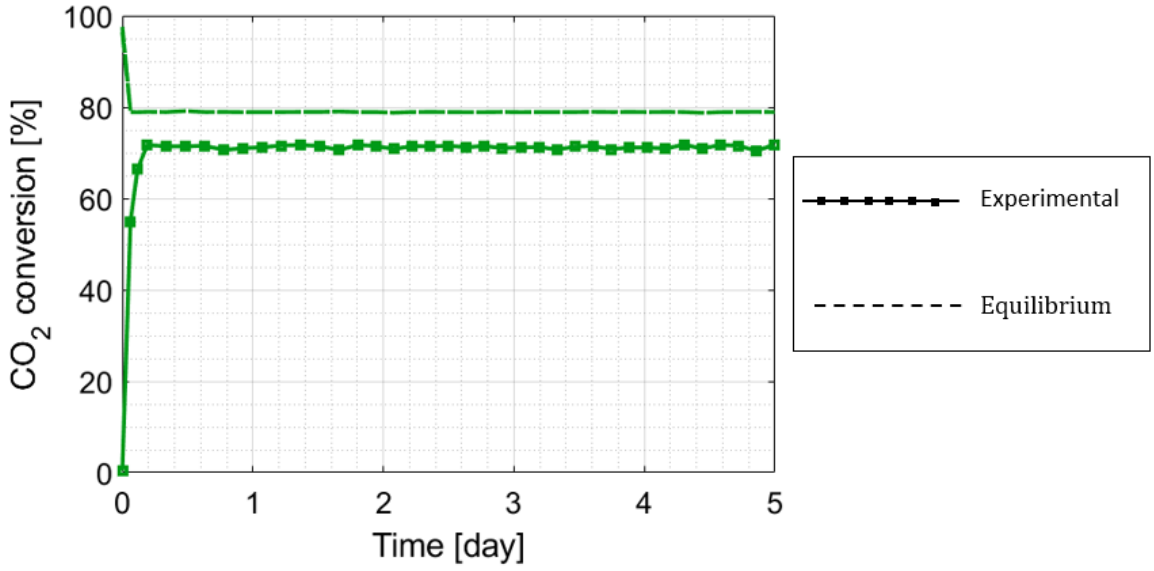

Figure 4.24: *CO_2 conversion as a function of time, compared to equilibrium where solid carbon formation is considered in the calculation and with equilibrium where solid carbon formation is not considered in the calculation, both calculated at 6 bar with the experimental y^0_i. P = 6 bar. Catalysts EX11914. 20% water added to reactant mixture. Experimental conditions reported in Table 4.13.*

The trend of the pressure at reactor top, represented in Figure 4.25, shows a gradual increase of pressure starting from the second day of continuous operation. This is anticipated by half a day with respect to the test without water addition (see Figure 4.18). This apparently confirm that the increase in pressure is related more to the condenser filling than to any solid carbon formation and macropores clogging, strengthening the idea that pressure could not be simply a consequence of coke formation within the catalyst bed.

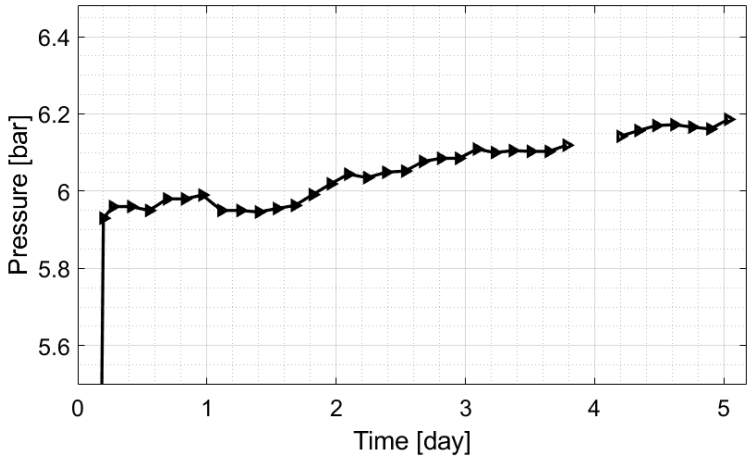

Figure 4.25: *Pressure at the top of the reactor. P = 6 bar. Catalyst EX11914. Experimental conditions as reported in Table 4.13.*

The trend of the error on the closure on carbon balance, shown in Figure 4.26, underlines how some carbon is missing in the product mixture, being always positive, suggesting that actually some carbon remains within the reactor as coke.

Values of errC lower than 2% in absolute value underlines that the experimental error is very low and confirms the accuracy of the data. The value of the statistical parameters computed at the end of the coke-formation stress test at 6 bar with H_2O addition are reported in Table 4.14. It is important to notice that mean and standard deviation are expressed as percentage since it is also the unit of measure of the error on the closure on carbon balance. With respect to the stress test with no water addition, the mean value is higher (0.9565% in this test against 0.5957% of the test without water addition) suggesting a larger carbon formation therefore going against chemical equilibrium calculations. However, only the TPO can provide a direct and precise quantification of solid carbon produced. Also, a smaller variability is shown in this test, being the coefficient of variation lower than a half of that obtained in the stress test without water addition.

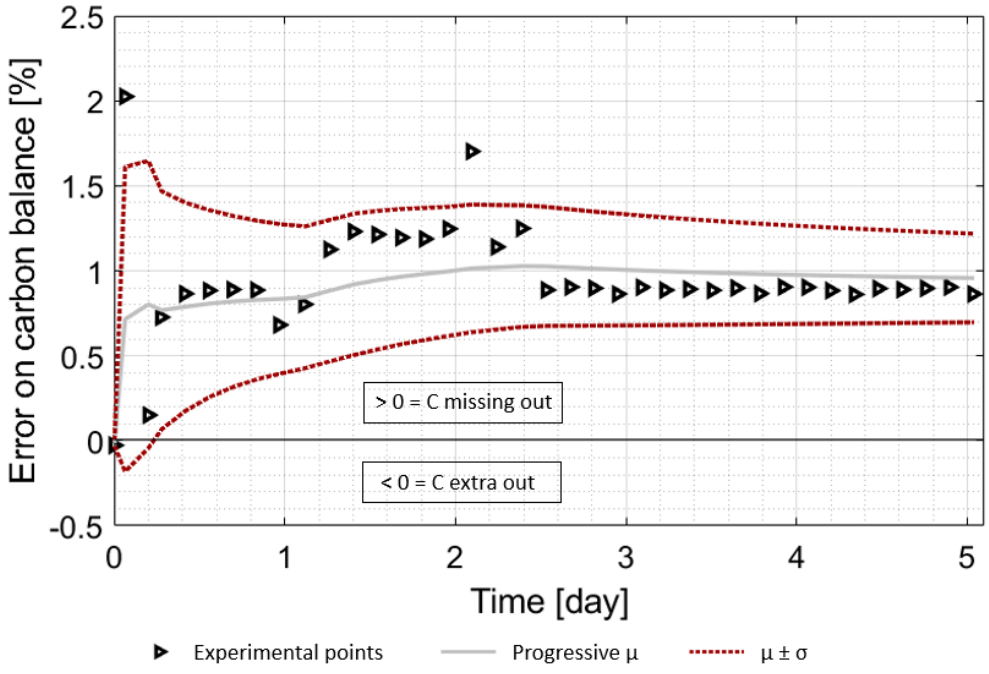

Figure 4.26: *Error on the closure of carbon balance (errC), progressive mean, and confidence intervals as a function of time. P = 6 bar. Catalyst EX11914. 20% water added to reactant mixture.*

Table 4.14: *Statistical parameters for the coke formation stress tests at 6 bar.*

Mean μ [%]	Standard Deviation σ [%]	Coefficient of Variation σ/μ [-]
0.9565	0.2591	0.2709

From the results of the TPO following the coke-formation stress at 6 bar with water addition, represented in Figure 4.27, is possible to notice that some CO_2 has formed. Therefore, a certain quantity of carbon has been produced during the stress-test, as expected from the error on carbon balance. The temperature at which CO_2 starts producing from solid carbon is about 490°C, suggesting that the type of carbon produced is the same of that produced during the blank test and the coke-formation stress test at 6 bar, since their oxidation temperature is the same. The quantity of carbon produced in the stress test and the coking rate are reported in Table 4.15. In this case no coke formation is expected at equilibrium, therefore, it can be concluded that equilibrium calculation does not provide an accurate estimation of solid carbon production in the reactive system considered, since kinetics should limit coke production, likely as a consequence of the anti-coking additives of the catalyst used.

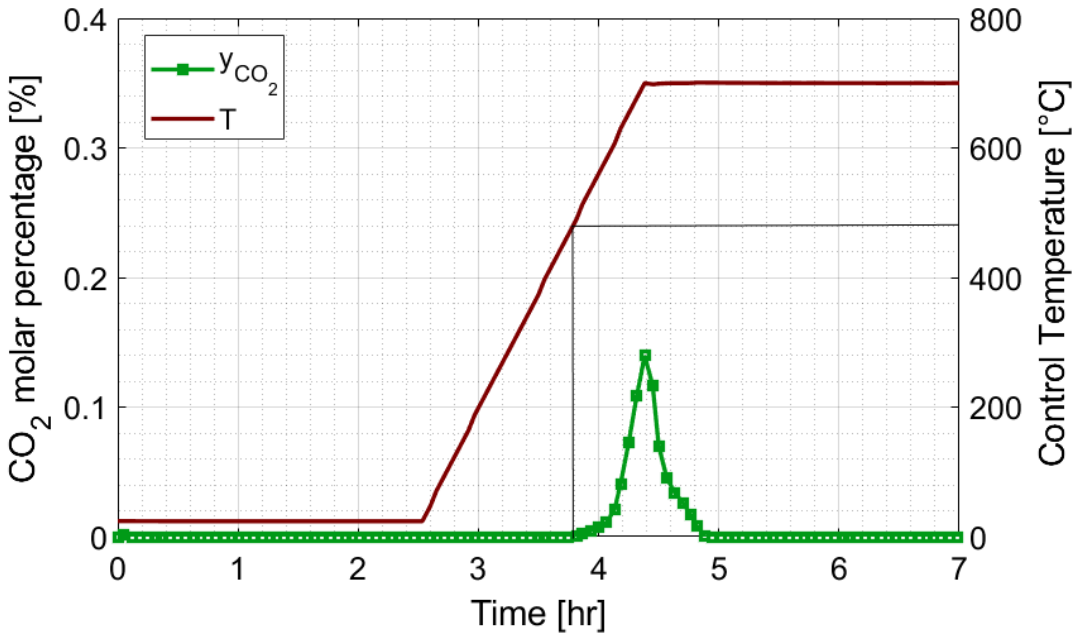

Figure 4.27: *CO_2 molar percentage and control temperature as a function of time. P = 1 bar. Catalyst EX11914. Experimental conditions as reported in Table 4.2.*

Table 4.15: *Mass of solid carbon formed during the stress-test and expected at equilibrium and coking rate.*

Carbon formed [mg]	Carbon expected at equilibrium [mg]	Coking rate [$mg_C/(g_{cat}h)$]
2.75	0	0.0224

4.2.4 Comparison between stress tests at 6 bar

Figure 4.28 compares the dry molar percentages obtained during the stress tests at 6 bar with and without water addition, enlightening the limitation to Sabatier reaction (2.1) caused by addition of a reaction product. Particularly, the CH_4 molar percentage decrease is of 3.3 percentage points (from 96.4% without water addition to 93.1% with 20% water inlet molar percentage), H_2 almost doubles (from 2.54% to 5.27%) and similarly the residual CO_2 (from 1.08% to 1.72%). However, in both cases CO_2 and CO compositions fulfil the Italian biomethane grid injection requirements, whereas H_2 is above the limit allowed even though it is in-line with Snam experimentations. Particularly, in the case of dry reactant mixture it is below the 5% of the experimentation of April 2019 whereas in the case of 20% H_2O inlet molar percentage it is below the 10% of the experimentations of December 2019. A small reduction of the water inlet molar percentage should be considered to keep the H_2 molar fraction (and according to the ideal gas law also the volumetric fraction) below 5%.

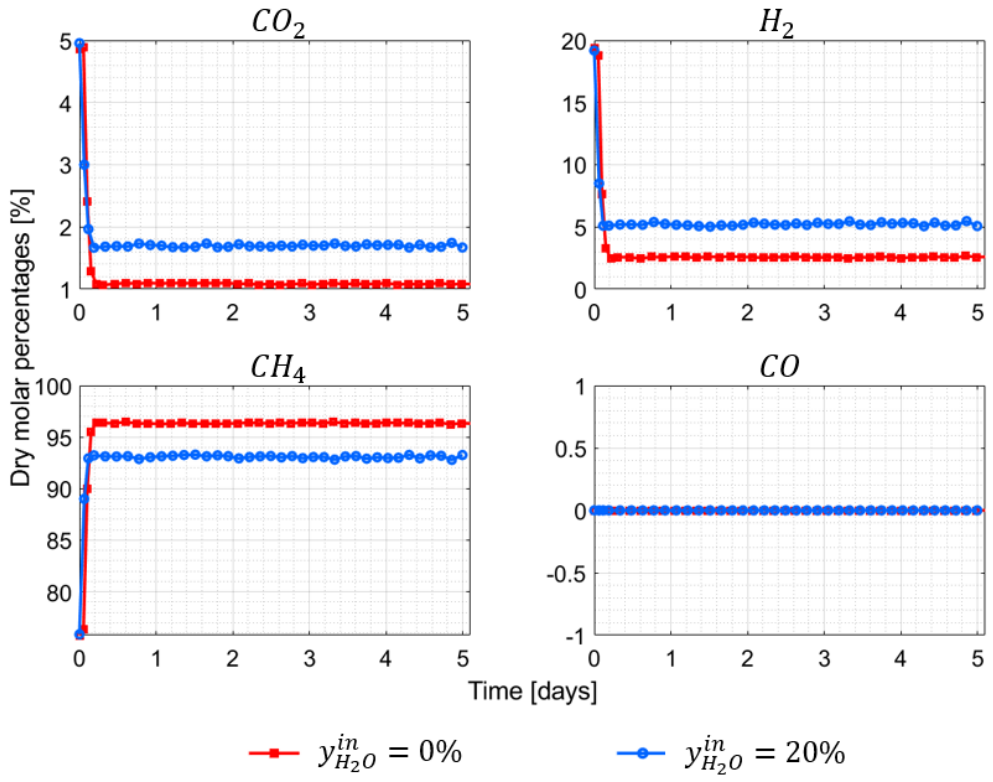

Figure 4.28: *Comparison of dry molar percentages as a function of time, for the two stress tests at 6 bar with and without water addition in the reactant mixture. Catalyst EX11914. Experimental conditions reported in Table 4.10 and 4.13.*

The CO_2 conversion, reported in Figure 4.29, confirms what was just explained about the limitations of Sabatier reaction (2.1) caused by water addition. Particularly, a CO_2 conversion of 11.1 percentage point occurs, from 82.4% with the dry reactant mixture to 71.3% with 20% H_2O inlet molar percentage.

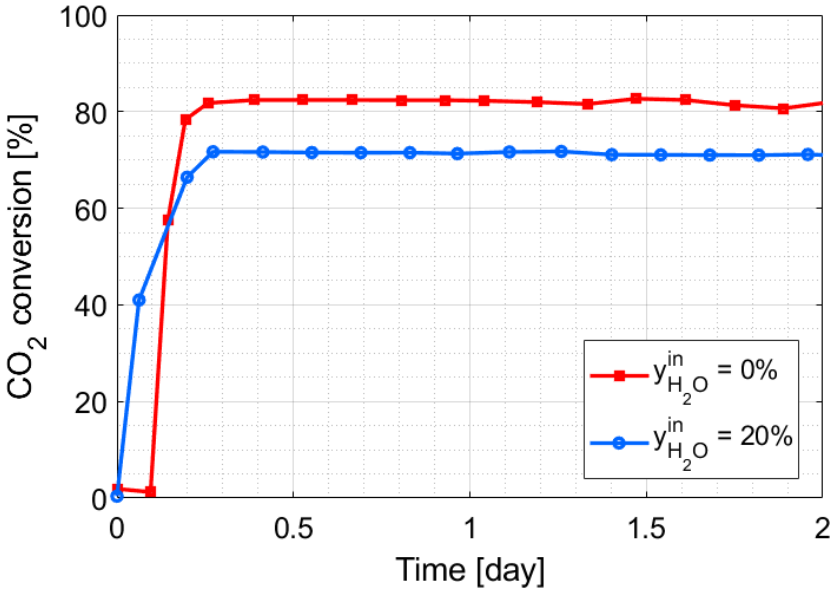

Figure 4.29: *Comparison of CO_2 conversion as a function of time, for the two stress tests at different pressures. Catalyst EX11914. Experimental conditions reported in Table 4.10 and 4.13.*

On the other hand, H_2O addition has a positive effect on carbon deposition, as shown in Figure 4.30 representing the CO_2 molar percentages as a function of time for the three coke-formation stress tests at 6 bar (also including the blank test). Particularly, as explained in Chapter 3 the solid carbon is obtained by integration over time of the CO_2 molar flowrate leaving the reactor during TPO and this flowrate is directly related to molar percentage of CO_2 according to equation 4.1, where the total molar flowrate is constant at reactor inlet and outlet since the only reaction occurring during is TPO is C complete oxidation to CO_2, characterized by constant number of moles in the gas phase (C partial oxidation to CO occurs with increasing number of moles, thus leading to an increase in the total molar flowrate, but no CO is produced during TPO).

$$\dot{n}_{CO_2}^{out} = \dot{n}_{TOT}^{out} y_{CO_2} \tag{4.2}$$

Therefore, since the flowrate fed to the reactor is the same for all the temperature programmed oxidations, according to the area below the CO_2 molar percentage is possible to speculate, semiquantitatively, that the solid carbon produced during the stress test with water is less than that obtained without water addition. This can be related to the effect of carbon gasification (2.7) but also to the fact that the partial pressure of methane is reduced by the presence of water within the reactor, leading to a decrease of the methane cracking reaction rate, or, in general, to lower methane molar percentages both during transitory regime and when steady state is reached. Moreover, the quantity of coke produced in the stress-test is larger than that obtained in the blank test. This is due to a higher methane percentage due to Sabatier reaction and the combined effect of methane cracking, favored at high methane percentages and catalyzed by the active nickel of the catalyst and of the Inconel reactor.

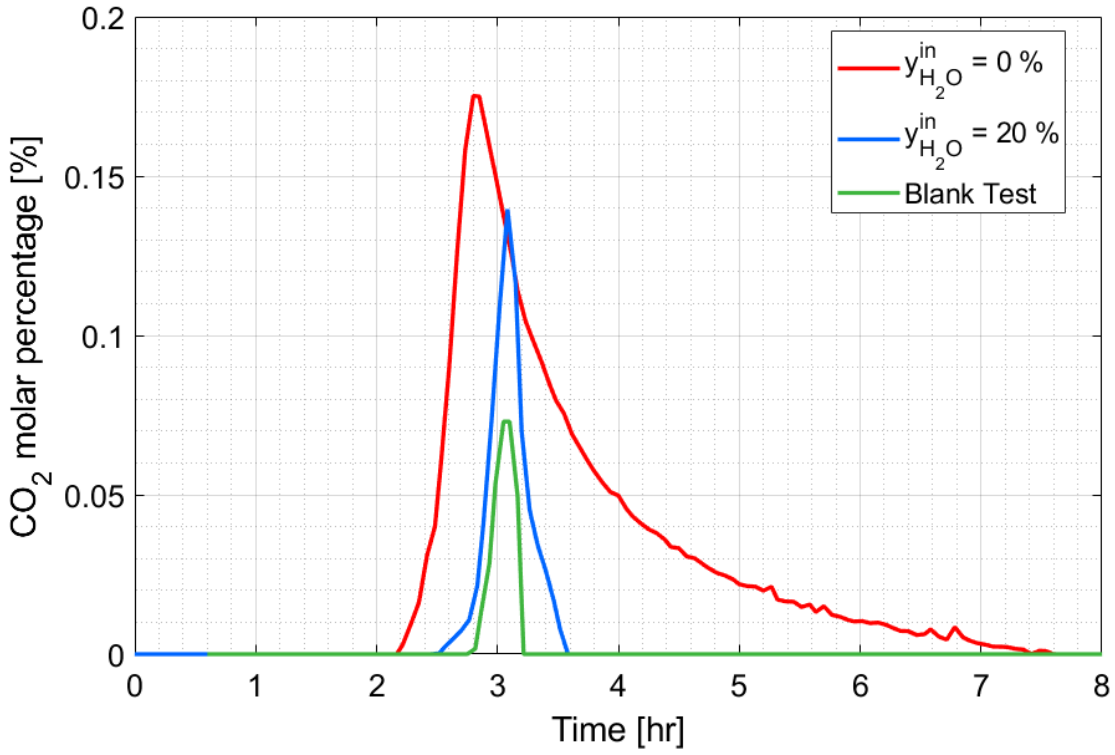

Figure 4.30: *Comparison of the TPO results for the blank tests (green line, test 160), stress-test without water (red line, test 158) and stress test with water addition (blue line, test 155).*

Table 4.16, where the quantity of carbon formed and the coking rate for the three tests, allows a quantitative discussion. Particularly, by adding 20% H_2O in the reactant mixture, the coking rate decreases by about 80% with respect to the stress-test without water addition. However, in both

cases the solid carbon production rate is much higher than in the blank tests, according to the reasons already explained, particularly is about one order of magnitude and two order of magnitude higher respectively for the stress test without and with water addition.

Table 4.16: *Comparison between mass of solid carbon formed and coking rates for the three coke-formation tests at 6 bar.*

Test [-]	Carbon formed [mg]	Coking rate [$mg_C/(g_{cat}h)$]
Blank	1.01	Not defined (no catalyst)
Stress-test, no water addition	12.68	0.1022
Stress-test, with water	2.75	0.0224

4.2.5 Conclusions

According to the campaign at 6 bar with the Inconel reactor, the main results achieved are:

- The Inconel reactor is responsible of some solid carbon formation, since it was produced during the blank test when no catalyst was present;
- Equilibrium calculations are not capable of predicting the precise quantity of coke formed during the stress test, providing an estimation of two-three order of magnitude larger than the experimental result, due to an overestimation of the relevance of methane cracking, practically limited by low reaction rate, also because of the effect of anti-coking additives present in EX11914 catalyst;
- The catalyst is able to operate continuously for 5 days without any relevant activity loss. Moreover, the quantity of carbon produced within this time is not enough to deactivate via nickel encapsulation and detachment or via macropores clogging;
- In both the stress-test both CO_2 and CO molar percentages respected the Italian grid injection requirements. However, H2 molar percentage was always above the 1% allowed for the grid injection, but always in-line with the experimentations done by Snam (at least that of December 2019 [41]);
- Water addition to the reactant mixture has a negative on the Sabatier reaction but allows to reduce the coking rate by 80%. Therefore, the effect of the water molar percentage should be further investigated to find the best compromise, to also ensure a H_2 molar percentage below the 5% tested by Snam in the experimentation of April 2019 [41];

- For the experimental set-up adopted for this experimental campaign, pressure is not a direct measure of catalyst deactivation by macropores clogging as shown by an increasing trend of pressure in the two stress test with and without water addition, where no relevant activity loss was detected.

Conclusions

The experimental campaigns collected different information, regarding the EX11914 catalyst stability under long-duration tests, the coking but also the activity toward the methanation reaction, translated in the methane dry molar percentage in the outlet mixture or, similarly, in the CO_2 conversion.

A summary of the results, depending on the test conditions (such as pressure and water inlet molar percentage), is reported in Table 5.1.

Table 5.1: *Main results obtained. WHSV = 14.27 ml/mg/h except for the blank test where catalyst is absent.*

Catalyst [-]	CH_4 inlet (dry) [%]	H_2O inlet [%]	Pressure [bar]	Catalyst stable after 5 days [-]	CH_4 outlet [%]	CO_2 conversion [%]	Coking rate [$mg_C/(g_{cat}h)$]
EX11914	75.8	0	1	Yes	91.0	67.6	0
Absent	75.8	0	6	-	75.8	0	Not defined
EX11914	75.8	0	6	Yes	96.4	81.9	0.1022
EX11914	75.8	20	6	Yes	93.1	71.5	0.0224

For all the stress tests performed during the experimental campaigns, the catalysts were capable of maintaining its activity toward methanation, since no significant variation of the species molar percentages were detected. This implies that the rate of solid carbon production is not high enough to lead to catalysts deactivation via nickel encapsulation and subsequent detachment, macropores clogging or other mechanisms due to the presence of solid carbon. This is also enlightened by the coking rate, assuming a value much lower than that obtained in industrial plants of methane cracking, i.e., equal to 2400 $mg_C/(g_{cat}h)$ (obtained at 500°C, with $p_{H_2} = 0.2$ bar and $p_{CH_4} = 5$ bar). Even though the tests conditions are different, the order of magnitude obtained for the second methanation stage is always at least 4 orders of magnitude lower.

Particularly, using a quartz reactor no solid carbon has formed, however this is not a material used at pilot or real plant scale and this data is useful only to have a reference, when compared to results obtained with the Inconel reactor. Particularly, the blank tests without catalysts allow to demonstrate that, using this material, some carbon is produced because of the nickel present in this type of steel, and provide an additional reference for the coke-formation stress tests at 6 bar. Indeed, more solid carbon has formed because of the effect of the active nickel of EX11914

catalyst also combined with the effect of larger methane molar percentages due to the effect of the Sabatier reaction. However, the coking rate is still small, being only about a 0.1mg of solid carbon produced per gram of catalyst and hour of continuous operation at the desired steady state. Furthermore, the addition of a certain quantity of water allows to reduce the coking rate by 80% (in the stress-test conditions), leading to a decrease of methane dry percentage in the product mixture of 3.3% only (from 96.4% to 93.1%), always ensuring a higher CO_2 conversion and methane enrichment than that obtained at atmospheric pressure. However, by adding 20% of water vapor, the H_2 molar percentage is not in line with the experimentations done by Snam in April 2019, to allow a 5% of H_2 in the biomethane. Therefore, further studies should be done to understand the quantity of water optimizing the H_2 conversion and the reduction of the coking rate.

In the real two-stage methanation process, keeping a certain inlet molar percentage of water in the second-stage reactor means reducing the degree of H_2O condensation in the interstage condenser, allowing to use water from tower as refrigerant fuel instead of a mixture of water and glycol, but also, depending on the water inlet molar percentage decided, also an external loop could be required. This is the case of 20% of H_2O leaving a condenser operating at 6 bar, where the temperature required will be 110°C, thus reducing the pre-heating duty required before the second-stage and improving the process in terms of heat integration.

To conclude, also the procedures for TPR – coke formation stress tests – TPO cycles should be improved, particularly, instead of oxidizing the solid carbon feeding diluted O_2 the reactor, a TPSR (Temperature Programmed Surface Reaction) procedure should be used, feeding H_2 instead of O_2. This procedure allows to avoid the catalyst activation required after the TPO but also permits to identify the type of solid carbon produced during the stress test.

Bibliography

[1] Kristian Stangeland, Dori Kalai, Hailong Li, Zhixin Yu “CO2 Methanation: The Effect of Catalysts and Reaction Conditions”, Energy Procedia, Volume 105, 2017, Pages 2022-2027, ISSN 1876-6102
https://doi.org/10.1016/j.egypro.2017.03.577.

[2] Awe, Olumide Wesley and Zhao, Yaqian and Nzihou, Ange and Minh, Doan Pham and Lyczko, Nathalie “A review of biogas utilisation, purification and upgrading technologies”, Waste and Biomass Valorization, Volume 8, 2017, Pages 267-283

[3] Pierre Collet, Eglantine Flottes, Alain Favre, Ludovic Raynal, Hélène Pierre, Sandra Capela, Carlos Peregrina “Techno-economic and Life Cycle Assessment of methane production via biogas upgrading and power to gas technology”, Applied Energy, Volume 192, 2017, Pages 282-295, ISSN 0306-2619
https://doi.org/10.1016/j.apenergy.2016.08.181.

[4] Rosa M. Cuéllar-Franca, Adisa Azapagic “Carbon capture, storage and utilisation technologies: A critical analysis and comparison of their life cycle environmental impacts”, Journal of CO2 Utilization, Volume 9, 2015, Pages 82-102, ISSN 2212-9820
https://doi.org/10.1016/j.jcou.2014.12.001.

[5] Dannesboe, C., Hansen, J.B. & Johannsen, I. Removal of sulfur contaminants from biogas to enable direct catalytic methanation. Biomass Conv. Bioref. 11, 1823–1834 (2021)
https://doi.org/10.1007/s13399-019-00570-7

[6] Götz, Manuel, Amy McDaniel Koch, and Frank Graf. "State of the art and perspectives of CO2 methanation process concepts for power-to-gas applications." International Gas Union Research Conference. Vol. 13. Fornebu, Norway: International Gas Union, 2014.

[7] Chalachew Mebrahtu, Florian Krebs, Salvatore Abate, Siglinda Perathoner, Gabriele Centi, Regina Palkovits “Chapter 5 - CO2 Methanation: Principles and Challenges”, Editor(s): Stefania Albonetti, Siglinda Perathoner, Elsje Alessandra Quadrelli, Studies in Surface Science and Catalysis, Elsevier, Volume 178, 2019, Pages 85-103, ISSN 0167-2991, ISBN 9780444641274
https://doi.org/10.1016/B978-0-444-64127-4.00005-7.

[8] Stefan Rönsch, Jens Schneider, Steffi Matthischke, Michael Schlüter, Manuel Götz, Jonathan Lefebvre, Praseeth Prabhakaran, Siegfried Bajohr "Review on methanation – From fundamentals to current projects", Fuel, Volume 166, 2016, Pages 276-296, ISSN 0016-2361 https://doi.org/10.1016/j.fuel.2015.10.111.

[9] E. Ryckebosch, M. Drouillon, H. Vervaeren "Techniques for transformation of biogas to biomethane", Biomass and Bioenergy, Volume 35, Issue 5, 2011, Pages 1633-1645, ISSN 0961-9534 https://doi.org/10.1016/j.biombioe.2011.02.033.

[10] Qie Sun, Hailong Li, Jinying Yan, Longcheng Liu, Zhixin Yu, Xinhai Yu "Selection of appropriate biogas upgrading technology-a review of biogas cleaning, upgrading and utilization", Renewable and Sustainable Energy Reviews, Volume 51, 2015, Pages 521-532, ISSN 1364-0321 https://doi.org/10.1016/j.rser.2015.06.029.

[11] Ruggia Marisa (2013). "Silossani nel biogas di discarica". Master's degree thesis in chemistry. University of Pisa.

[12] Davide Papurello, Vitaliano Chiodo, Susanna Maisano, Andrea Lanzini, Massimo Santarelli "Catalytic stability of a Ni-Catalyst towards biogas reforming in the presence of deactivating trace compounds", Renewable Energy, Volume 127, 2018, Pages 481-494, ISSN 0960-1481 https://doi.org/10.1016/j.renene.2018.05.006.

[13] M.A.A. Aziz, A.A. Jalil, S. Triwahyono, R.R. Mukti, Y.H. Taufiq-Yap, M.R. Sazegar "Highly active Ni-promoted mesostructured silica nanoparticles for CO2 methanation", Applied Catalysis B: Environmental, Volume 147, 2014, Pages 359-368, ISSN 0926-3373 https://doi.org/10.1016/j.apcatb.2013.09.015.

[14] Bai, X., Wang, S., Sun, T. et al. The sintering of Ni/Al_2O_3 methanation catalyst for substitute natural gas production. Reac Kinet Mech Cat 112, 437–451 (2014). https://doi.org/10.1007/s11144-014-0700-8

[15] Vincenzo Barbarossa, "Conversione di CO2 in metano", 2012-09-01 https://iris.enea.it/retrieve/dd11e37c-d70c-5d97-e053-d805fe0a6f04/Report%20RdS%202012-203.pdf

[16] Vincenzo Barbarossa, Giuseppina Vanga, Rosanna Viscardi, Daniele Mirabile Gattia "CO2 as Carbon Source for Fuel Synthesis", Energy Procedia, Volume 45, 2014, Pages 1325-1329, ISSN 1876-6102

https://doi.org/10.1016/j.egypro.2014.01.138.
[17] P. Canu, M. Pagin, “Biogas upgrading by 2-steps methanation of its CO2 – Thermodynamics analysis”, Journal of CO2 Utilization, Volume 63, 2022, 102123, ISSN 2212-9820
https://doi.org/10.1016/j.jcou.2022.102123.
[18] G. C. Bond, G. Webb, J. R. H. Ross “Metal catalysed methanation and steam reforming”, SPR Catalisys, volume 7, 1982, ISBN 78-1-84755-319-5
https://doi.org/10.1039/9781847553195
[19] Manuel Götz, Jonathan Lefebvre, Friedemann Mörs, Amy McDaniel Koch, Frank Graf, Siegfried Bajohr, Rainer Reimert, Thomas Kolb “Renewable Power-to-Gas: A technological and economic review”, Renewable Energy, Volume 85, 2016, Pages 1371-1390, ISSN 0960-1481
https://doi.org/10.1016/j.renene.2015.07.066.
[20] Jehng, JM., Chen, CM. Amination of Polyethylene Glycol to Polyetheramine over the Supported Nickel Catalysts. Catalysis Letters 77, 147–154 (2001).
https://doi.org/10.1023/A:1012782927451
[21] Pagin Mattia (2019). “Catalytic upgrading of biogas to biomethane by high pressure CO_2 methanation”. Master’s degree thesis in chemical and process engineering. University of Padova.
[22] Scarpa Marco (2022). “Two-steps methanation of CO_2 in cleaned biogas”. Master’s degree thesis in chemical and process engineering. University of Padova.
[23] Calvin H Bartholomew, “Mechanisms of catalyst deactivation”, Applied Catalysis A: General, Volume 212, Issues 1–2, 2001, Pages 17-60, ISSN 0926-860X
https://doi.org/10.1016/S0926-860X(00)00843-7.
[24] Ashraf M. Amin, Eric Croiset, William Epling, “Review of methane catalytic cracking for hydrogen production”, International Journal of Hydrogen Energy, Volume 36, Issue 4, 2011, Pages 2904-2935, ISSN 0360-3199
https://doi.org/10.1016/j.ijhydene.2010.11.035.
[25] Michael Neubert, Alexander Hauser, Babak Pourhossein, Marius Dillig, Juergen Karl “Experimental evaluation of a heat pipe cooled structured reactor as part of a two-stage catalytic methanation process in power-to-gas applications”, Applied Energy, Volume 229, 2018, Pages 289-298, ISSN 0306-2619
https://doi.org/10.1016/j.apenergy.2018.08.002.

[26] Dannesboe, Christian, John Bøgild Hansen, and Ib Johannsen "Catalytic methanation of CO 2 in biogas: Experimental results from a reactor at full scale." Reaction Chemistry & Engineering 5.1 (2020): 183-189.

[27] Shogo Sayama, Seiji Yamamoto “A 6-kW thermally self-sustained two-stage CO2 methanation reactor: design and experimental evaluation of steady-state performance under full-load conditions”, Applied Energy, Volume 325, 2022, 119773, ISSN 0306-2619 https://doi.org/10.1016/j.apenergy.2022.119773.

[28] Manuel Gruber, Petra Weinbrecht, Linus Biffar, Stefan Harth, Dimosthenis Trimis, Jörg Brabandt, Oliver Posdziech, Robert Blumentritt “Power-to-Gas through thermal integration of high-temperature steam electrolysis and carbon dioxide methanation - Experimental results”, Fuel Processing Technology, Volume 181, 2018, Pages 61-74, ISSN 0378-3820 https://doi.org/10.1016/j.fuproc.2018.09.003.

[29] Kopyscinski, Jan. "Production of synthetic natural gas in a fluidized bed reactor." Disseration ETH Zurich (2010).

[30] Benjamin Mutz, Paul Sprenger, Wu Wang, Di Wang, Wolfgang Kleist, Jan-Dierk Grunwaldt “Operando Raman spectroscopy on CO2 methanation over alumina-supported Ni, Ni3Fe and NiRh0.1 catalysts: Role of carbon formation as possible deactivation pathway”, Applied Catalysis A: General, Volume 556, 2018, Pages 160-171, ISSN 0926-860X https://doi.org/10.1016/j.apcata.2018.01.026.

[31] D.L. Trimm, David L. "The formation and removal of coke from nickel catalyst." Catalysis Reviews Science and Engineering 16.1 (1977): 155-189. https://doi.org/10.1080/03602457708079636

[32] D.L. Trimm “Coke formation and minimisation during steam reforming reactions”, Catalysis Today, Volume 37, Issue 3, 1997, Pages 233-238, ISSN 0920-5861 https://doi.org/10.1016/S0920-5861(97)00014-X.

[33] https://yearbook.enerdata.net/totalenergy/world-energy-production.html. (Last access: 06/01/2023)

[34] https://www.climate.gov

[35] Daily metals price at: https://www.dailymetalprice.com/metalprices.php. (Last access: 10/05/2023).

[36] http://www.montello-spa.it/nuovo-impianto-di-biometano/

[37] Marc-Antoine, Eyl-Mazzega and Carol Mathieu. “Biogas and biomethane in Europe: Lessons from Denmark, Germany and Italy”. Etudes de l’ifri. Ifri,April 2019.
[38] Workshop on conformity assessment of biomethane. “Gas quality situation in Italy – gas (natural gas and biomethane) quality specifications, laws and hoe it is controlled”. [online]. Available: http://empir.npl.co.uk/biomethane/wpcontent/uploads/sites/28/2019/02/Workshop-Delft-Alejandra-Casola.pdf
[39] https://infobiogas-bts.it/procedure-applicative-decreto-biometano/
[40] https://www.assogasmetano.it/biometano-mappa-impianti-italia-e-europa/
[41] https://www.snam.it/it/transizione_energetica/idrogeno/snam_e_idrogeno/
[42] Conference on biomethane 10/03/2023: “Biometano sinonimo di sostenibilità, la ripartenza del settore dopo il nuovo DM 15 settembre 2023”
[43] Bronkhorst® HIGH-TECH. General instructions digital Mass Flow/Pressure instruments laboratory style/ In-Flow. “Instruction manual”
[44] Perry Chemical Handbook, 8th edition, pag. 2-433

Appendix

Experimental test conditions

	Catalyst	Mass of cat	HR	$\dot{V}$	P	y_{Ar}	y_{He}	y_{CO2}	y_{H2O}	y_{CO}	y_{H2}	y_{CH4}	y_{O2}	WHSV	Associated figures
	[-]	[mg]	[°C/min]	[ml/min]	[bar]	[%]	[%]	[%]	[%]	[%]	[%]	[%]	[%]	[ml/mgh]	[-]
130	EX11914	639,7	5	200	1	0,000%	95,000%	0,000%	0,000%	0,000%	5,000%	0,000%	0,000%	-	4.2
131	EX11914	639,7	10	152,59	1	4,971%	0,000%	4,747%	0,000%	0,000%	18,038%	72,244%	0,000%	14,27	4.4
132	EX11914	639,7	3	100	1	0,000%	95,025%	0,000%	0,000%	0,000%	0,000%	0,000%	4,975%	-	
133	EX11914	639,7	10	200	1	0,000%	95,000%	0,000%	0,000%	0,000%	5,000%	0,000%	0,000%	-	
134	EX11914	639,7	5	152,53	1	4,990%	0,000%	4,740%	0,000%	0,000%	18,070%	72,200%	0,000%	14,27	4.4
135	EX11914	639,7	10	200	1	0,000%	95,000%	0,000%	0,000%	0,000%	5,000%	0,000%	0,000%	-	
136	EX11914	639,7	5	152,33	1	5,000%	0,000%	4,600%	0,000%	0,000%	18,400%	72,000%	0,000%	14,27	4.5, 4.6, 4.7, 4.8, 4.9, 4.12
137	EX11914	639,7	5	200	1	0,000%	95,000%	0,000%	0,000%	0,000%	0,000%	0,000%	5,000%	-	4.10
138	EX11914	993,4	10	200	1	95,000%	0,000%	0,000%	0,000%	0,000%	5,000%	0,000%	0,000%	-	
139	EX11914	993,4	5	236	6	0,000%	5,000%	4,600%	0,000%	0,000%	18,400%	72,000%	0,000%	14,27	
140	EX11914	993,4	5	200	1	0,000%	95,000%	0,000%	0,000%	0,000%	0,000%	0,000%	5,000%	-	
146	EX11914	993,4	5	200	1	95,000%	0,000%	0,000%	0,000%	0,000%	5,000%	0,000%	0,000%	-	
147	EX11914	993,4	10	236	6	0,000%	5,000%	4,600%	0,000%	0,000%	18,400%	72,000%	0,000%	14,27	
148	EX11914	993,4	5	200	1	95,000%	0,000%	0,000%	0,000%	0,000%	0,000%	0,000%	5,000%	-	
153	EX11914	993,4	5	200	1	95,000%	0,000%	0,000%	0,000%	0,000%	5,000%	0,000%	0,000%	-	
154	EX11914	993,4	10	237	6	0,000%	5,000%	4,600%	0,000%	0,000%	18,400%	72,000%	0,000%	14,27	4.16, 4.17, 4.18, 4.19, 4.21, 4.22, 4.28, 4.29
155	EX11914	993,4	5	200	4.221	95,000%	0,000%	0,000%	0,000%	0,000%	0,000%	0,000%	5,000%	-	4.20, 4.30
156	EX11914	993,4	10	200	1	95,000%	5,000%	0,000%	0,000%	0,000%	0,000%	0,000%	0,000%	-	

157	EX11914	993,4	10	236	6	0,000%	5,000%	4,600%	0,000%	0,000%	18,400%	72,000%	0,000%	14,27	4.23, 4.24, 4.25, 4.26, 4.28, 4.29
158	EX11914	993,4	5	200	1	95,000%	0,000%	0,000%	0,000%	0,000%	0,000%	0,000%	5,000%	-	4.27, 4.30
159	-	-	10	236	6	0,000%	5,000%	4,600%	0,000%	0,000%	18,400%	72,000%	0,000%	-	4.13, 4.14
160	-	-	5	200	1	95,000%	0,000%	0,000%	0,000%	0,000%	0,000%	0,000%	5,000%	-	4.15, 4.30